



**NAVAL
POSTGRADUATE
SCHOOL**

MONTEREY, CALIFORNIA

THESIS

**STALL ANALYSIS IN A TRANSONIC COMPRESSOR
STAGE AND ROTOR**

by

William Lee Davis

June 2009

Thesis Advisor:
Second Reader:

Anthony Gannon
Garth Hobson

Approved for public release; distribution is unlimited.

THIS PAGE INTENTIONALLY LEFT BLANK

REPORT DOCUMENTATION PAGE			<i>Form Approved OMB No. 0704-0188</i>
Public reporting burden for this collection of information is estimated to average 1 hour per response, including the time for reviewing instruction, searching existing data sources, gathering and maintaining the data needed, and completing and reviewing the collection of information. Send comments regarding this burden estimate or any other aspect of this collection of information, including suggestions for reducing this burden, to Washington headquarters Services, Directorate for Information Operations and Reports, 1215 Jefferson Davis Highway, Suite 1204, Arlington, VA 22202-4302, and to the Office of Management and Budget, Paperwork Reduction Project (0704-0188) Washington DC 20503.			
1. AGENCY USE ONLY (Leave blank)	2. REPORT DATE June 2009	3. REPORT TYPE AND DATES COVERED Master's Thesis	
4. TITLE AND SUBTITLE Stall Analysis in a Transonic Compressor Stage and Rotor		5. FUNDING NUMBERS	
6. AUTHOR(S) William Lee Davis		8. PERFORMING ORGANIZATION REPORT NUMBER	
7. PERFORMING ORGANIZATION NAME(S) AND ADDRESS(ES) Naval Postgraduate School Monterey, CA 93943-5000		10. SPONSORING/MONITORING AGENCY REPORT NUMBER	
9. SPONSORING /MONITORING AGENCY NAME(S) AND ADDRESS(ES) N/A		11. SUPPLEMENTARY NOTES The views expressed in this thesis are those of the author and do not reflect the official policy or position of the Department of Defense or the U.S. Government.	
12a. DISTRIBUTION / AVAILABILITY STATEMENT Approved for public release; distribution is unlimited.		12b. DISTRIBUTION CODE	
13. ABSTRACT (maximum 200 words) Gas turbine engine design is based on simplifying assumptions, including axi-symmetric flow. These assumptions break down in the real machines especially when operating near to stall. The reduction in operating surge margin associated with current trends to develop high performance military fighter aircraft further highlights the need to develop a thorough understanding of the flow in rotor blade passages and especially when operating close to stall. This research investigates the behavior of a Transonic Compressor Rig (TCR) as it approaches stall in the rotor-only and full-stage configuration using combinations of frequency and time domain analysis in the subsonic (70% rated speed), sonic (80% rated speed) and transonic operating ranges (90%, 95%, and 100% rated speed). A steady-state analysis of the pressure measurements across a rotor passage of the TCR was conducted to identify potential pre-stall indicators, the structure of the flow field within the blade passages, and to correlate changes in flow structure with changes in pressure measurements. Further investigation using flow visualization techniques within the blade passages demonstrated how the TCR rotor departed from an idealized rotor when the axi-symmetric assumption holds when operating at steady-state and near stall conditions. This identification of potential stall indicators and characterization of the time variant flow field within the passages will impact future compressor design to enable operation closer to stall and increased performance across an operating spectrum.			
14. SUBJECT TERMS Compressor, Transonic, Stall, Surge		15. NUMBER OF PAGES 141	
		16. PRICE CODE	
17. SECURITY CLASSIFICATION OF REPORT Unclassified	18. SECURITY CLASSIFICATION OF THIS PAGE Unclassified	19. SECURITY CLASSIFICATION OF ABSTRACT Unclassified	20. LIMITATION OF ABSTRACT UU

THIS PAGE INTENTIONALLY LEFT BLANK

Approved for public release; distribution is unlimited

STALL ANALYSIS IN A TRANSONIC COMPRESSOR STAGE AND ROTOR

William L. Davis
Lieutenant, United States Coast Guard
B.S., Virginia Military Institute, 2000

Submitted in partial fulfillment of the
requirements for the degree of

MASTER OF SCIENCE IN MECHANICAL ENGINEERING

from the

**NAVAL POSTGRADUATE SCHOOL
June 2009**

Author: William Lee Davis

Approved by: Professor Anthony J. Gannon
Thesis Advisor

Professor Garth V. Hobson
Second Reader

Knox T. Millsaps, PhD
Chairman, Department of Mechanical and Aeronautical
Engineering

THIS PAGE INTENTIONALLY LEFT BLANK

ABSTRACT

Gas turbine engine design is based on simplifying assumptions, including axisymmetric flow. These assumptions break down in the real machines especially when operating near to stall. The reduction in operating surge margin associated with current trends to develop high performance military fighter aircraft further highlights the need to develop a thorough understanding of the flow in rotor blade passages and especially when operating close to stall. This research investigates the behavior of a Transonic Compressor Rig (TCR) as it approaches stall in the rotor-only and full-stage configuration using combinations of frequency and time domain analysis in the subsonic (70% rated speed), sonic (80% rated speed) and transonic operating ranges (90%, 95%, and 100% rated speed). A steady-state analysis of the pressure measurements across a rotor passage of the TCR was conducted to identify potential pre-stall indicators, the structure of the flow field within the blade passages, and to correlate changes in flow structure with changes in pressure measurements. Further investigation using flow visualization techniques within the blade passages demonstrated how the TCR rotor departed from an idealized rotor when the axisymmetric assumption holds when operating at steady-state and near stall conditions. This identification of potential stall indicators and characterization of the time variant flow field within the passages will impact future compressor design to enable operation closer to stall and increased performance across an operating spectrum.

THIS PAGE INTENTIONALLY LEFT BLANK

TABLE OF CONTENTS

I.	INTRODUCTION.....	1
II.	COMPRESSORS STALL THEORY.....	3
	A. TYPES OF STALL.....	4
	1. Rotating Stall.....	4
	2. Compressor Surge.....	5
	B. IMPACT OF COMPRESSOR STALL OR SURGE ON GAS TURBINES ENGINES.....	6
	1. Performance Reduction.....	6
	2. Mechanical Damage.....	7
	3. Recovery.....	7
III.	OVERVIEW OF PREVIOUS RESEARCH.....	9
	A. ROTOR ONLY ANALYSIS.....	9
	B. FULL STAGE ANALYSIS.....	16
IV.	EXPERIMENTAL APPARATUS.....	19
	A. TRANSONIC COMPRESSOR RIG.....	19
	B. DATA ACQUISITION SYSTEM.....	21
	1. Slow-Speed Data Collection.....	21
	2. High-Speed Data Collection.....	22
V.	EXPERIMENTAL PROCEDURE.....	25
VI.	DATA ANALYSIS DESCRIPTION.....	27
	A. USER INTERFACE FUNCTIONALITY.....	27
	B. RAW DATA CALIBRATION.....	28
	1. MATLAB Code Overview.....	28
	2. Calibration Description.....	28
	C. STEADY STATE ANALYSIS ROUTINE.....	29
	1. MATLAB Code Overview.....	29
	2. Analysis Description.....	30
	D. STEADY STATE CONTOUR ROUTINE.....	33
	1. MATLAB Code Overview.....	33
	2. Analysis Description.....	33
	E. TRANSIENT CONTOUR ROUTINE.....	34
	1. MATLAB Code Overview.....	34
	2. Analysis Description.....	35
	F. TRANSIENT CONTOUR ANALYSIS ROUTINE.....	35
	1. MATLAB Code Overview.....	35
	2. Analysis Description.....	36
VII.	ANALYSIS AND RESULTS.....	37
	A. FREQUENCY DOMAIN.....	37
	B. TIME DOMAIN ANALYSIS.....	45
	C. PRESSURE CONTOUR ANALYSIS.....	54

D.	CORRELATION OF FREQUENCY AND TIME DOMAIN ANALYSIS	59
E.	STALL INVESTIGATION.....	62
	1. Rotor Only Configuration.....	62
	2. Full Stage Configuration	65
VIII.	CONCLUSIONS	69
A.	INTEGRATED DATA ANALYSIS TOOL.....	69
B.	STEADY-STATE OPERATION.....	69
C.	STALL INCEPTION ANALYSIS.....	70
IX.	RECOMMENDATIONS.....	71
	LIST OF REFERENCES	73
	APPENDIX A: ROTOR-ONLY KULITE DATA	75
	APPENDIX B: FULL STAGE KULITE DATA.....	95
	APPENDIX C: MATLAB INTERFACE.....	119
	INITIAL DISTRIBUTION LIST	127

LIST OF FIGURES

Figure 1.	Steam Induced Stall of F-18D during steam catapult assisted takeoff at NAWC Patuxent River	1
Figure 2.	Angle of Incidence.....	3
Figure 3.	Rotating Progressive Stall Cell	4
Figure 4.	Compressor Surge Cycle.....	6
Figure 5.	Surge Cycle Showing Reverse Flow and Hysteresis, After [12].....	8
Figure 6.	Established Stall Margin and Pressure Mapping, From [5].....	9
Figure 7.	Diffusion Factor at Near Stall, From [3].....	10
Figure 8.	Inlet (Left) and Exit (Right) Mach Number at 100% Rotor Speed, From [3].....	10
Figure 9.	Inlet Flow Angle Measurements at 100% Rotor Speed, From [3]	11
Figure 10.	Magnitude of Flow Pitch Toward the Center Line, From [4].....	11
Figure 11.	Computation Fluid Dynamics Model of Compressor Inlet, From [4]	12
Figure 12.	Inlet Mach Number Experimental Data and CFD Comparison, From [4]	12
Figure 13.	Power Spectrum at 90% Speed Near Stall, From [5].....	13
Figure 14.	Power Contour Plot of Kulite Data at 70%, From [5]	13
Figure 15.	Turbulence Intensity vs. Mass Flow Rate, From [5]	14
Figure 16.	Computation Fluid Dynamics Model of Compressor Rotor, From [6]	14
Figure 17.	CFD to Experimental Results Comparison of Pressure Ratio, From [6].....	15
Figure 18.	Steam Stall Compressor Map, From [8]	15
Figure 19.	Compressor Stage Performance Map, From [11]	16
Figure 20.	Compressor Stage and Rotor-Only Performance Comparison, From [11].....	17
Figure 21.	Rotor-Only Pressure Contour Mapping, From [11].....	17
Figure 22.	Sanger Test Stage in Rotor-only and Full Stage Configuration	19
Figure 23.	Transonic Test Rig Schematic, After [11]	21
Figure 24.	Schematic of High Speed Data Capture System, After [11].....	22
Figure 25.	Kulite Probe Locations Relative to Rotor Cross Section.....	23
Figure 26.	Full Stage Compressor Performance Maps.....	25
Figure 27.	Top Level GUI Functionality.....	27
Figure 28.	Data Load and Calibrate Workflow	28
Figure 29.	Generic Raw Kulite Voltage Conversion to Pressure Ratio Data Sets.....	29
Figure 30.	Steady State Analysis Workflow	30
Figure 31.	Fast Fourier Transform of Pressure Signal at 100% Rotor Speed.....	31
Figure 32.	Generic Blackman Window Employed in Analysis	31
Figure 33.	Signal with Band-Pass Filtering Applied.....	32
Figure 34.	Steady State Pressure Contour Workflow.....	33
Figure 35.	Steady State Pressure Contour Plot Showing Interpolation Regions.....	34
Figure 36.	Transient Pressure Contour Workflow	35
Figure 37.	Transient Contour Analysis Workflow.....	36
Figure 38.	Full Stage Waterfall Plot of Filtered Frequency Data at 80% Speed, Near Stall	38

Figure 39.	Rotor Only Waterfall Plots of Filtered Frequency Data at 100% Rotor Speed.....	39
Figure 40.	Waterfall Plots of Filtered Frequency Data Showed Forward Transport	40
Figure 41.	Full Stage Waterfall Plots of Filtered Frequency Data at 95% Rotor Speed...	41
Figure 42.	RMS Power of Rotor and Stage in Low Frequency Band.....	42
Figure 43.	RMS Power of Rotor and Stage in Full Frequency Spectrum.....	43
Figure 44.	Non-Dimensional RMS Power for Rotor and Stage.....	44
Figure 45.	Raw Bulk Mach Number Data at 100% Rotor Speed.....	46
Figure 46.	Inlet Mach of Bulk Flow in Rotor-only and Full Stage	47
Figure 47.	Peak-to-Peak Mach Variation of Bulk Flow in Rotor-only and Full Stage.....	48
Figure 48.	Raw Bulk Inlet Angle at 100% Rotor Speed	50
Figure 49.	Mean Relative Inlet Angle of Bulk Flow in Rotor-only and Full Stage.....	51
Figure 50.	Peak-to-Peak Variation of Relative Inlet Angle in Rotor-only and Full Stage.....	52
Figure 51.	Instantaneous Maximum Relative Inlet Angle in Rotor-only and Full Stage..	53
Figure 52.	Rotor Only Pressure Contour Plot at 100% Rotor Speed	55
Figure 53.	Rotor Only Steady State Pressure Contour Plots at 100% Rotor Speed.....	56
Figure 54.	Full Stage Steady State Pressure Contour Plots at 95% Rotor Speed.....	58
Figure 55.	Rotor Only Pressure Contour and Frequency Data Comparison at 100% Rotor Speed.....	59
Figure 56.	Rotor-Only Standard Deviation Pressure Contours at 100% Rotor Speed.....	60
Figure 57.	Full Stage Pressure Contour and Frequency Data Comparison at 95% Rotor Speed.....	61
Figure 58.	Full Stage Standard Deviation Pressure Contours at 95% Rotor Speed.....	62
Figure 59.	Full stage RPM Entering Stall Event at 95% Rotor Speed.....	63
Figure 60.	Full Stage Bulk Inlet Angle Entering Stall Event at 95% Rotor Speed.....	63
Figure 61.	Full Stage Entering Stall at 95% Rotor Speed.....	64
Figure 62.	Full Stage Steady State Blade Passage Instabilities at 95% Rotor Speed.....	65
Figure 63.	Rotor Only RPM Entering Stall Event at 100% Rotor Speed	66
Figure 64.	Rotor Only Bulk Inlet Angle Entering Stall Event at 100% Rotor Speed.....	66
Figure 65.	Rotor Only Entering Stall at 100% Rotor Speed	67
Figure 66.	Rotor Only Steady State Blade Passage Instabilities at 100% Rotor Speed....	68

LIST OF TABLES

Table 1.	Sanger Test Stage Design Parameters.....	20
Table 2.	Rotor Speed Profile.....	25
Table 3.	RMS Power Comparison	45
Table 4.	Inlet Bulk Mach Number Comparison.....	49
Table 5.	Relative Inlet Angle Comparison.....	54

THIS PAGE INTENTIONALLY LEFT BLANK

I. INTRODUCTION

Rotational stall and axi-symmetric stall and compressor surge in modern aircraft gas turbines can result in engine efficiency losses, total loss of thrust, and mechanical failure due to high cyclical loading of the relatively thin compressor blades. Both stall modes are commonly referred to as “pop stall” because of the flame ejected from the engine exhaust, Figure 1. This is often caused by blade wear and damage, intake of high-temperature gases, and extreme flight maneuvers. Carrier-based aircraft are particularly susceptible to this type of engine failure because of their extreme operational requirements and the likelihood of steam ingestion during launch from the carrier’s steam catapult system. Because of the reduced stall margin associated with the wear and age of the Navy’s current fleet of fighter aircraft, and the lack of engine redundancy introduced by any future single engine aircraft, a thorough understanding of compressor stall and its effects is critical to mitigate the risks associated with takeoff and operation.



Figure 1. Steam Induced Stall of F-18D during steam catapult assisted takeoff at NAWC Patuxent River

Current research completed at the Turbopropulsion Laboratory (TPL) at the Naval Postgraduate School (NPS) has focused on the steady-state analysis of steam-induced

stall of a transonic compressor rotor. The stage (rotor and stator) components implemented in this study were designed specifically for use in the TPL transonic compressor rig by Sanger at the NASA Glenn Research Center [1]. Rogers [2], Villescas [3], Brunner [4], Payne [5], Zarro [6], Gannon et al. [7] induced compressor stall by injecting low pressure steam through the rotor, without stator, through the full power range (70% - 100%) The compressor performance was then compared to pure throttle induced stall to identify a reduction in stall margin throughout the given power band. Koessler [8] and Gannon et al. [9] furthered this research using high-pressure steam and identified stall precursors, their modal oscillations, and an additional stall margin reduction. These works resulted in a complete performance map in the subsonic (70% rated speed) and transonic ranges (90%, 95%, and 100% rated speed). Gannon et al. further extended this research into an analysis of the transient stall effects of the rotor in the full power range [10]. Using these previously identified performance characteristics a mapping and analysis of the performance of the full stage (rotor and stator) was accomplished by Hurley [11]. A reduction in stall margin, when compared to the rotor-only configuration, was identified. This indicated that the stator is possibly more susceptible to stall than the rotor.

This paper continues the full stage analysis into the steady state and transient phenomenon present in the subsonic (70% rated speed), transonic (80% rated speed) and supersonic operating ranges (90%, 95%, and 100% rated speed). Additional analysis of the test rig in its rotor only configuration was also accomplished using an updated instrumentation array and procedure when compared to previous rotor-only research. Using combinations of frequency and time-based analysis an attempt to correlate results across methods in an effort to validate assumptions and interpretation of results is also presented.

II. COMPRESSORS STALL THEORY

Critical to a compressor's ability to affect an increase in pressure is the angle with which the fluid makes relative to the camberline of the rotor and stator blades. Any angular departure that the fluid makes with respect to the tangent of the camberline is defined as the incidence angle, Figure 2.

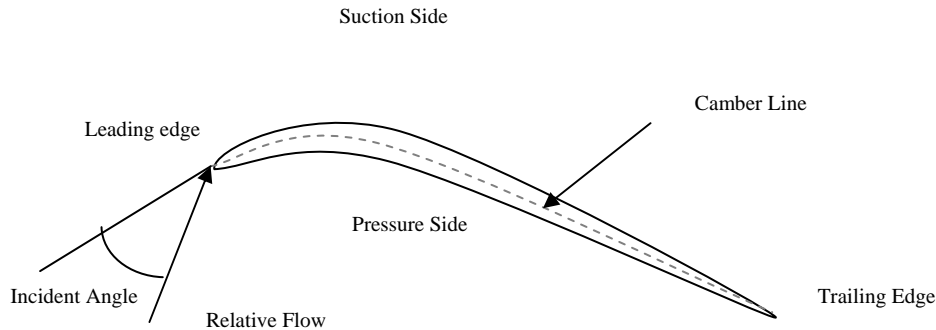


Figure 2. Angle of Incidence

As the incidence angle increases areas of low pressure can form on the suction side of the blade, Figure 2. The rapid acceleration of the flow around the leading edge must, at some point, begin to decelerate. During this deceleration, the boundary layer will begin to grow and may eventually separate resulting in a region of reversed flow.

Since a boundary layer often acts like a physical boundary, the sudden increase in layer thickness creates an effective decrease in the passage area between the blades. This area reduction can result in a localized mass flow reduction. While local separation is usually present on the blades of a compressor, the extent to which it covers a blade row only becomes relevant if there is a corresponding reduction in flow or a coalescence of many adjacent localized separation zones into a stall cell which leads to full compressor stall.

A. TYPES OF STALL

The stall phenomenon discussed in this document can be separated into two major categories: Rotating Stall and Compressor Surge. While both major categories can trace their roots to deviation in flow properties from design (Angle of Attack, Density, Temperature, etc.) their manifestation and effect on the operation of a compressor can be markedly different.

1. Rotating Stall

Rotating Stall is caused by the coalescence of a few adjacent locally stalled blade passages into a cell(s) that rotates in the same direction as the rotor but at a slower speed, Figure 3. This rotation is caused because of the reduction in flow rate associated with a stall cell(s). As blades immediately adjacent to a stall cell begin to increase their flow rate to accommodate the cells local reduction, they experience a change in angle of attack that directly leads to separation and stall. In this way, a stall cell can “walk” around the annulus of a compressor rotor.

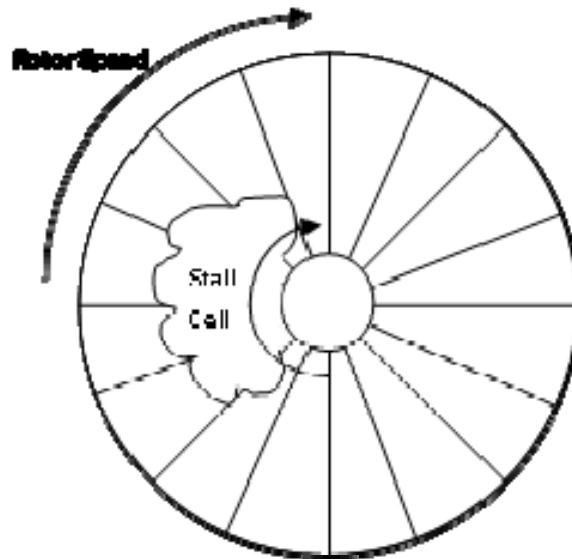


Figure 3. Rotating Progressive Stall Cell

Rotating Stall can manifest itself as a stalled region extending the full span of the blade (abrupt stall) or only a partial span of the blades (progressive stall). In both cases, the stall cell(s) generally rotate between 50-70% of the blade speed and are characterized by excess noise, vibration, and a reduction in performance. The primary difference is in the magnitude of the disturbance to the system. In the case of progressive stall performance, degradation is usually minor and the only external indication of stall is an increase in noise levels and vibration. In abrupt stall, all of these symptoms are magnified with the potential of the stall cell(s) extending through multiple compressor stages and a significant reduction or total loss of pressure rise across the compressor resulting in surge.

2. Compressor Surge

While Rotating Stall is a phenomenon associated with the interaction of adjacent blades on a rotor, Compressor Surge is due to an unstable fluid coupling of the rotor and stator. This is often characterized by a violent oscillation in rotor speed.

The unstable interaction between the rotor and stator is due to variation in fluid flow properties from design parameters. Similar to rotating stall a cell(s) is formed; however, in the case of the Sanger Stage, it is thought to that the stator blades are first affected. The stalled stator chokes the flow locally and reduces mass flow through the rotor blades, stalling and choking the flow through the rotor, and reducing mass flow to the stator. This in-turn allows the stator to recover and operate normally. If the underlying cause of the stall is not corrected then this stall-recovery cycle will repeat, Figure 4.

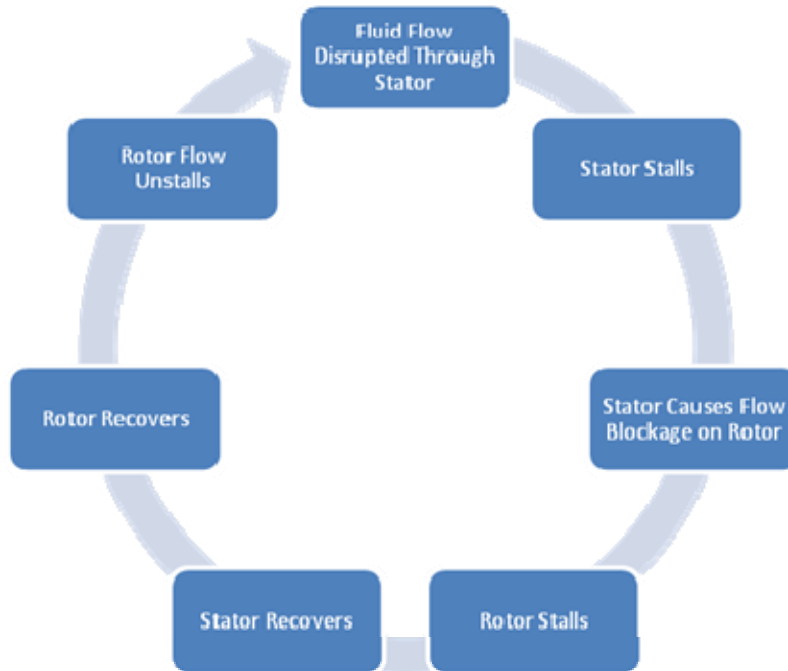


Figure 4. Compressor Surge Cycle

B. IMPACT OF COMPRESSOR STALL OR SURGE ON GAS TURBINES ENGINES

Gas turbine engines are high-precision machines designed to run at steady-state conditions around predetermined operating points. Since blade stall manifests itself as highly disturbed flow (generating rapid changes in pressure, velocity, and fluid density) it can impact the performance of a turbine in numerous ways ranging from minor degradation in thrust and power to a complete mechanical engine failure.

1. Performance Reduction

Compressor stall at its most basic level represents a reduction in intake airflow through a gas turbine. This reduction in flow through the engine, depending on its severity, can result in a measureable performance reduction manifesting as reduction, or loss, in thrust and/or a reduction in fuel economy.

If the stall cell grows into a surge cycle it may effectively stop the flow of high-pressure air to the burner section. The resulting inability of the compressor blades to impart mechanical work to the fluid can allow the high-pressure fluid in the burner

section to reverse direction and exit the intake section of the engine or allow excess unburned fuel to be expelled from the exhaust section. In both cases, when fuel rich air is allowed to exit the turbine, it may result in secondary burning of the fuel or an explosion when it is allowed to mix with oxygen-rich air (as shown in Figure 1).

2. Mechanical Damage

The cyclical nature of the stall cell, as it “walks” around the compressor annulus or progressively stalls and recovers, results in fatigue loading well in excess of engine design specifications. The asymmetrical nature of the compressor loading under stall also imparts unsteady loads to the bearings and support structures designed primarily for thrust loads. Both effects work to decrease engine life and increase lifecycle maintenance costs.

3. Recovery

Once a compressor has entered surge it will not recover unless there is a change in airflow properties (generally produced by a change in throttle). The change in throttle required to effect recovery is called compressor hysteresis. Figure 5 shows compressor surge taken at a constant throttle setting. The level of throttle reduction, hysteresis, required to return to steady state conditions is shown. Once corrective action is taken, the compressor returns to a state that is not the same as the point where the compressor entered the surge cycle.

The magnitude of the hysteresis is highly dependent on compressor design increasing as the pressure ratio across stages increases; however, large pressure ratios are extremely desirable because they represent an increase in engine efficiency and performance as well as a reduction in weight and size for a given compressor. These competing design requirements can manifest in lower pressure ratios or in higher control system costs to help reduce the amount of time required to restart a stalled engine in flight.

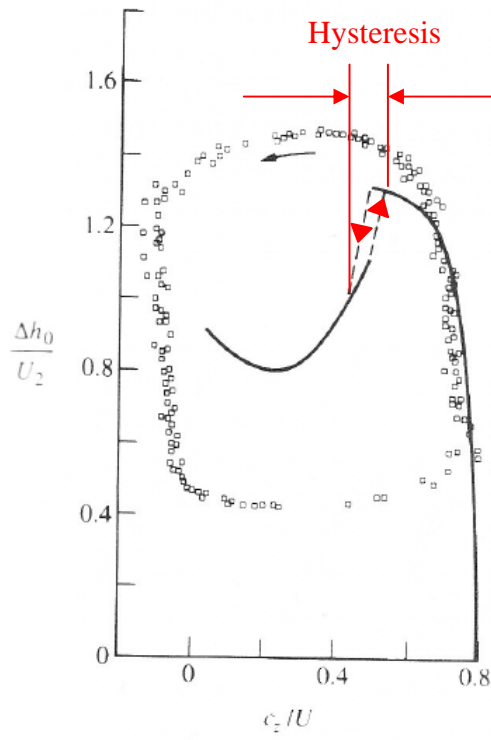


Figure 5. Surge Cycle Showing Reverse Flow and Hysteresis, After [12]

III. OVERVIEW OF PREVIOUS RESEARCH

Initial research conducted on the transonic compressor rig focused on establishing the stall margins at various speed (Table 2) and air only inlet flow conditions. Steady State and Transient analysis of the rig in its rotor-only configuration led to the verification of these parameters as well as identification of low frequency instabilities prior to and during stall. Later on additional rotor-only analysis, to identify reductions in stall margin, with high and low pressure steam ingestion was also conducted.

Research using the full stage, rotor and stator, was conducted to identify changes in performance characteristics and stall margin when compared to the rotor only configuration in both throttle and steam induced stall.

A. ROTOR ONLY ANALYSIS

Rodgers reestablished measurements and testing procedures at 60%, 70%, and 80% for the Sanger developed transonic compressor rig at the TPL [2]. This research was expanded by Villescas [3], Brunner [4], and Payne [5] to include full pressure measurements at 60%, 70%, 80%, 90%, 95%, and 100% of rotor speed, Figure 6. Steady and unsteady analysis of pressure measurements and identification of stall margins prior to steam introduction were presented.

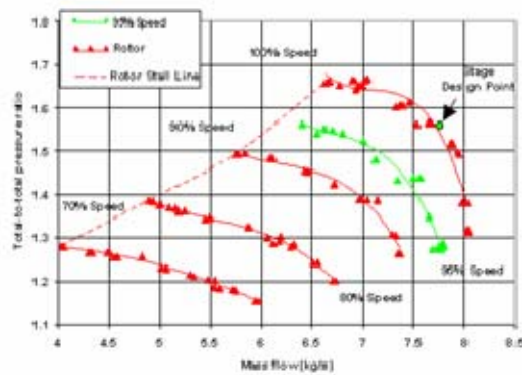


Figure 6. Established Stall Margin and Pressure Mapping, From [5]

Villescas [3] further investigated rotor diffusion factors at choke, peak efficiency, and stall as a means to predict compressor stall. Direct measurement and analysis showed a clear correlation between diffusion factor and the onset of compressor stall, Figure 7.

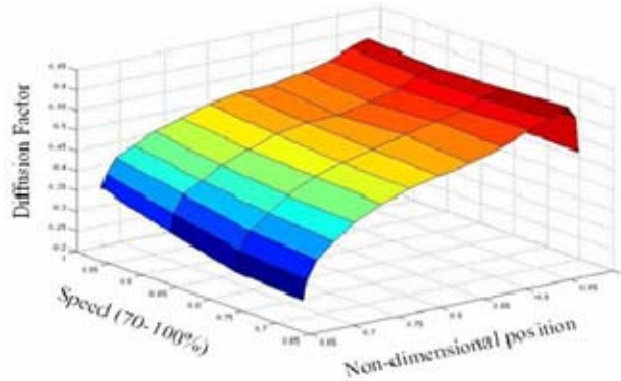


Figure 7. Diffusion Factor at Near Stall, From [3]

Flow field properties were also characterized to facilitate future Computation Fluid Dynamics (CFD) modeling with measurements of inlet and outlet Mach number (Figure 8) and Flow Angle (Figure 9) as a function of the hub-tip radius ratio, Villescas [3] and Brunner [4].

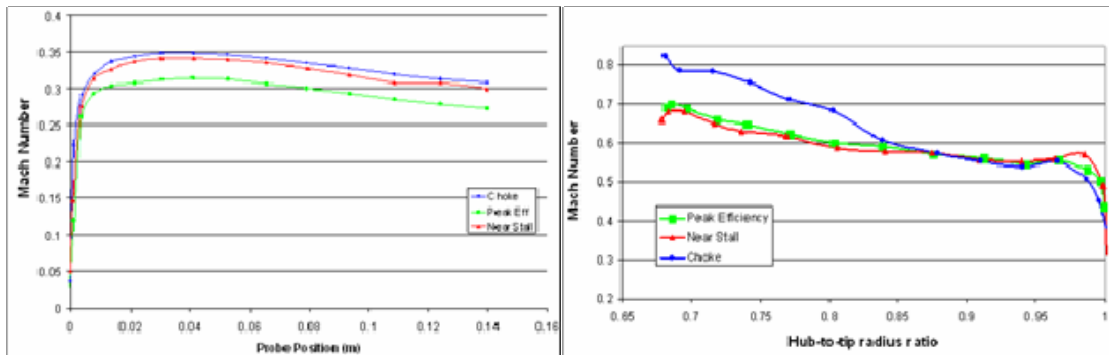


Figure 8. Inlet (Left) and Exit (Right) Mach Number at 100% Rotor Speed, From [3]

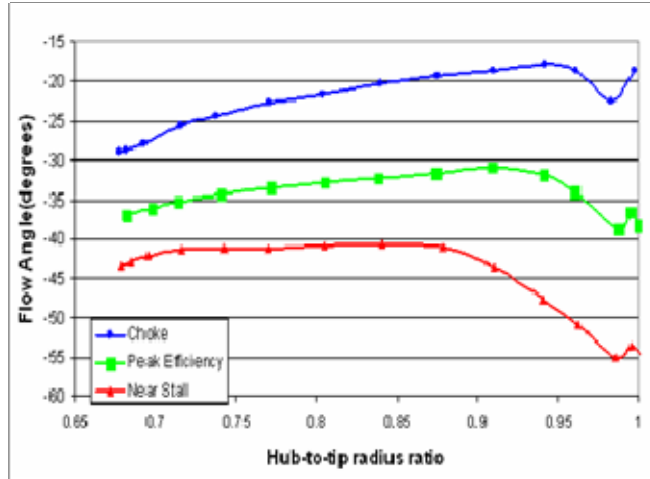


Figure 9. Inlet Flow Angle Measurements at 100% Rotor Speed, From [3]

The Pitch Angle at the compressor inlet was measured at the peak efficiency points at 70%, 80%, and 90% rotor speeds, Figure 10. This data identified inlet flow swirl at the inlet of the compressor further characterizing the flow for CFD analysis.

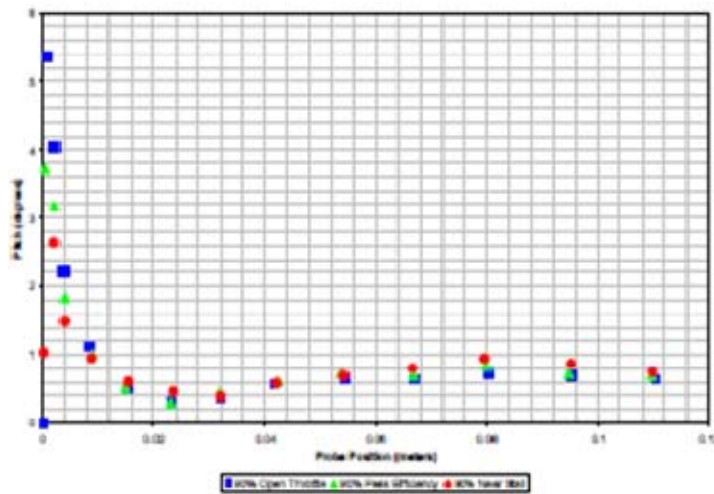


Figure 10. Magnitude of Flow Pitch Toward the Center Line, From [4]

A CFD model of the flow inlet ducting and bell-mouth were generated using the Ansys CFX-5 software package, Figure 11.

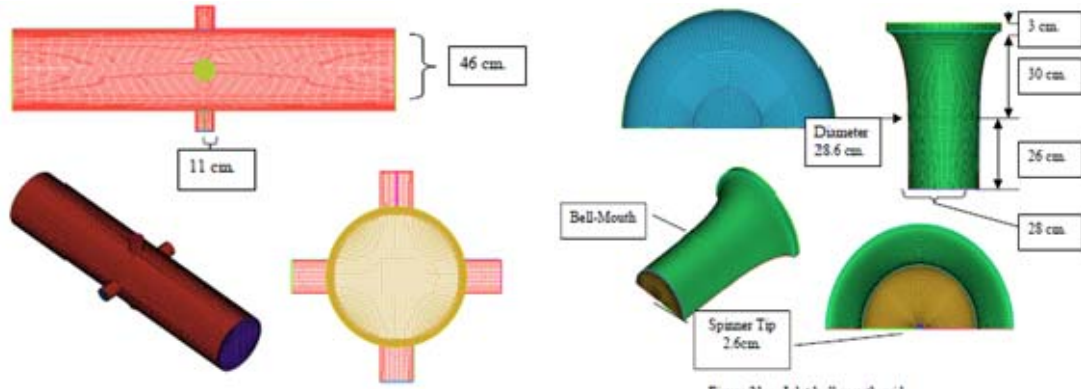


Figure 21. Inlet bell-mouth grid

Figure 11. Computation Fluid Dynamics Model of Compressor Inlet, From [4]

Computational results were then compared to the experimental data as a means of validating the model for future redesign and analysis, Figure 12. A strong correlation between the numerical and experimental results allowed for future modification of the experimental apparatus prior to steam induction testing.

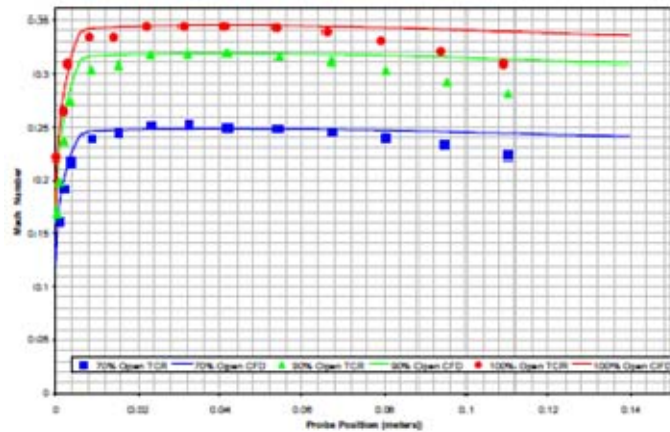


Figure 12. Inlet Mach Number Experimental Data and CFD Comparison, From [4]

A full analysis of efficiency and pressure ratio under varying rotor speeds was presented by Payne [5]. Using Fast Fourier Transform (FFT) Techniques to determine the dominant frequencies and their magnitudes stall precursors were identified in the pre-stall condition, Figure 13.

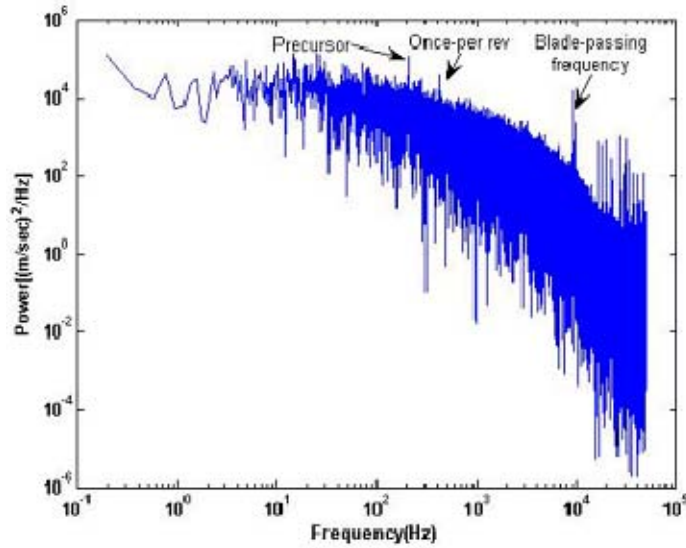


Figure 13. Power Spectrum at 90% Speed Near Stall, From [5]

Evaluating the power spectrum data at fixed intervals in time verified that the precursor modal instabilities were stable and present throughout the sampling period, Figure 14. This plot also displayed a clear boundary between the flow properties immediately preceding and following stall. The location of the stall cell at roughly 60% of the blade passage frequency with no indication of instability at any frequency harmonics indicates a single stall cell rotating around the compressor face.

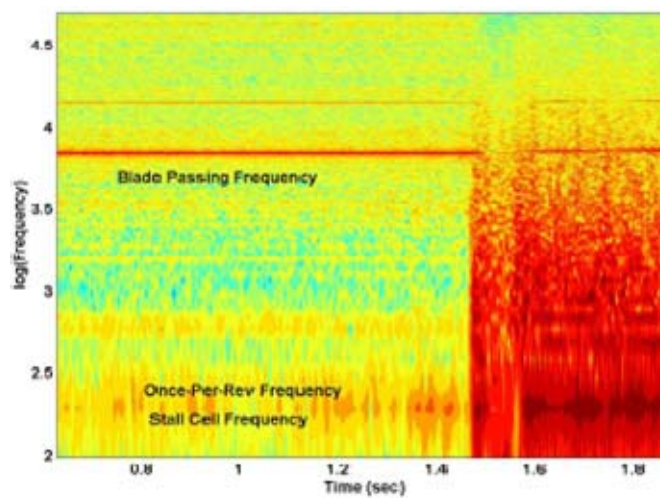


Figure 14. Power Contour Plot of Kulite Data at 70%, From [5]

Using hotfilm data at varying speeds and mass flow rates, an average turbulence intensity was calculated and plotted. While no clear correlation has found between the rotor speeds, mass flow rate, or turbulence intensity, an average intensity of 2.26% was determined, Figure 15. This further characterization assisted future CFD modeling.

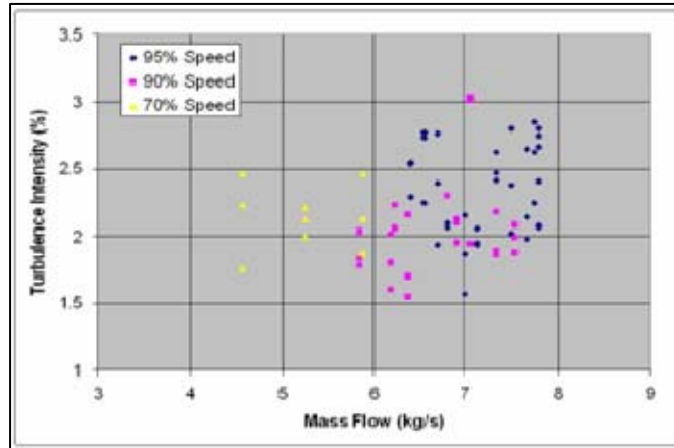


Figure 15. Turbulence Intensity vs. Mass Flow Rate, From [5]

A CFD model of the compressor rotor was then generated using Ansys CFX-5, Figure 16. To reduce the computational requirements, a single blade passage was modeled with periodic boundary conditions to simulate a full rotor.

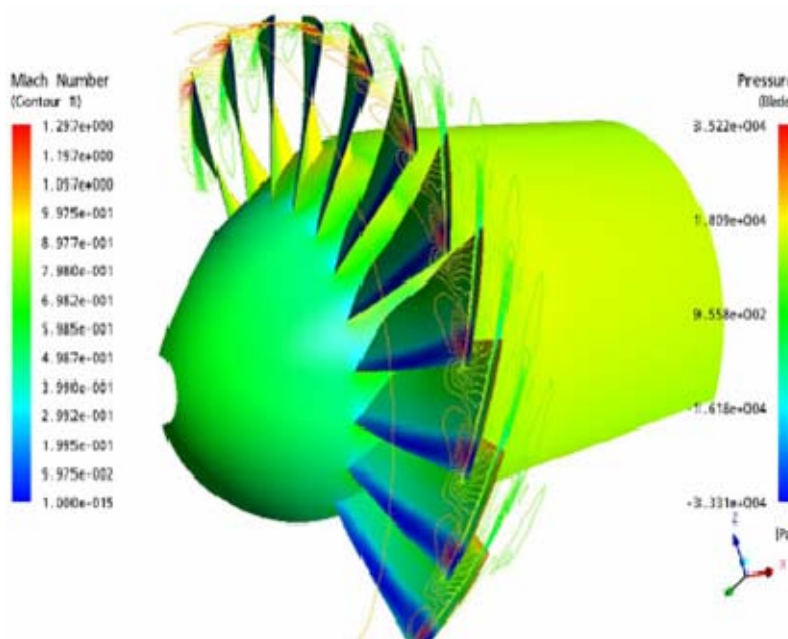


Figure 16. Computation Fluid Dynamics Model of Compressor Rotor, From [6]

This model was run at varying speeds and inlet conditions, and the results were compared to the experimentally derived results, Figure 17. The model successfully approximated the rotor performance characteristics with an underestimation of the pressure ratio and overestimation of the efficiency. This minor discrepancy indicated that a more complete understanding of inlet conditions was required prior to the generation of a new CFD model.

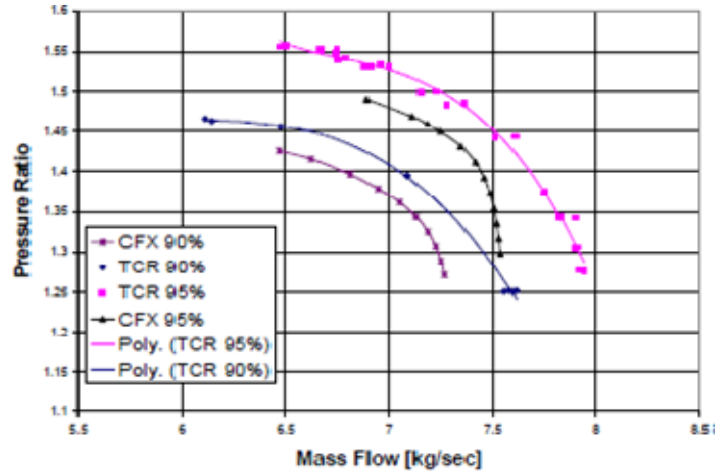


Figure 17. CFD to Experimental Results Comparison of Pressure Ratio, From [6]

Work accomplished by Koessler adjusted the compressor stall margin using low- and high-pressure steam ingestion, Figure 18. An adjustment of the stall margin of up to 30% was identified.

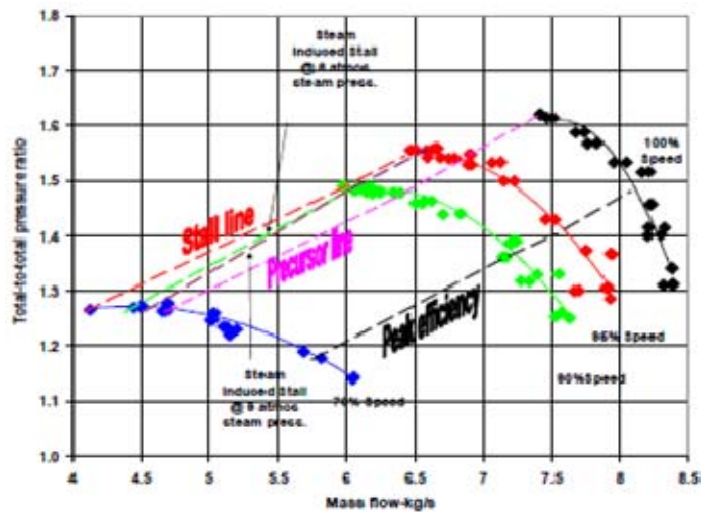


Figure 18. Steam Stall Compressor Map, From [8]

B. FULL STAGE ANALYSIS

Hurley established the performance map for the full compressor stage at 70%, 80%, 90%, 95%, and 100% of rated speed using throttle and steam stall procedures, Figure 19. He identified a reduction in stall margin for the throttled stage when compared to a steam induced stall from 3-5%.

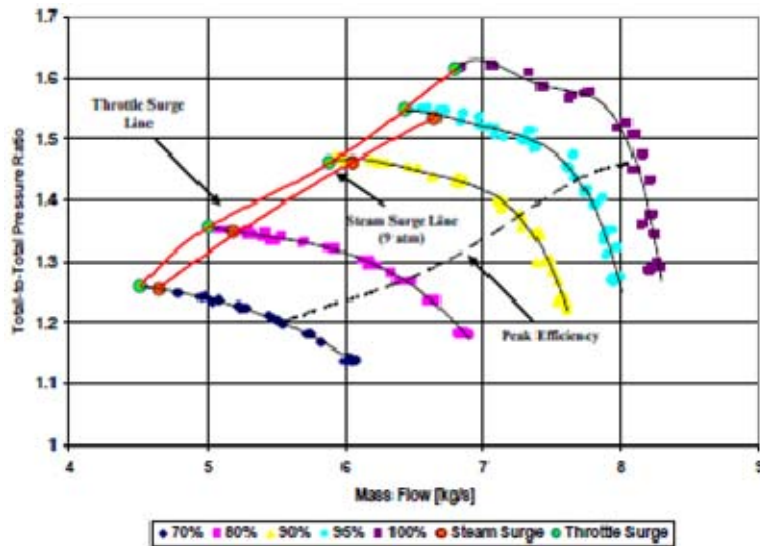


Figure 19. Compressor Stage Performance Map, From [11]

A comparison of the stall margins of the rotor-only and stage configurations identified a significant reduction in margin of 10-14% under steam and throttle induced stall, Figure 20. This overall reduction in performance across all rotor speeds and throttle settings indicated that the stator was entering stall prior to the rotor.

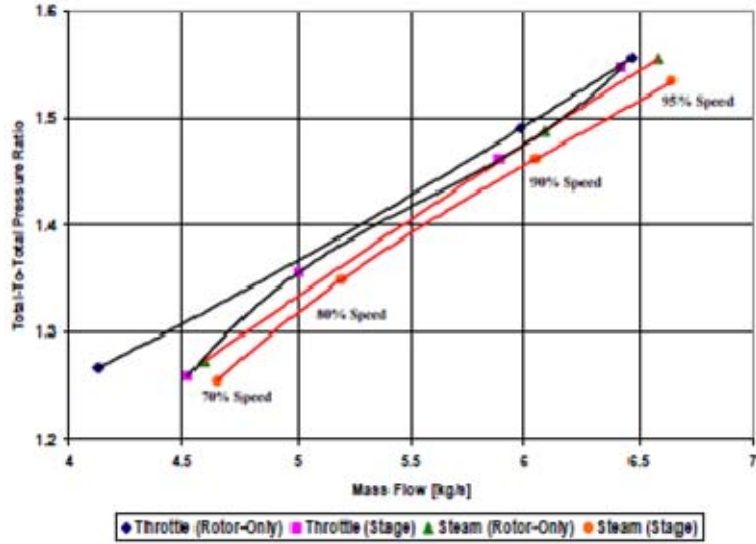


Figure 20. Compressor Stage and Rotor-Only Performance Comparison, From [11]

An interpolation of this pressure data resulted in pressure contour plots that clearly showed oblique shocks at the leading edge of the rotor blades, Figure 21. This visual representation of the flow field allows a refinement and validation of past CFD models.

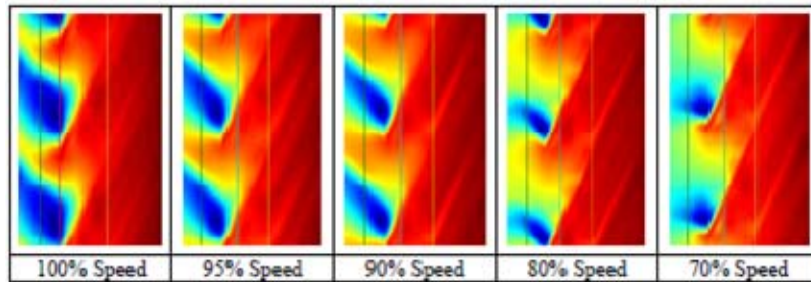


Figure 21. Rotor-Only Pressure Contour Mapping, From [11]

A continuation of this research will be presented in the following chapters.

THIS PAGE INTENTIONALLY LEFT BLANK

IV. EXPERIMENTAL APPARATUS

A. TRANSONIC COMPRESSOR RIG

Unlike previous work that focused only on one test rig configuration, this research employed data collected from test runs in the rotor-only and full stage configuration of the Sanger test stage [1]. This experimental apparatus has been described in detail in previous research and is only briefly summarized below.

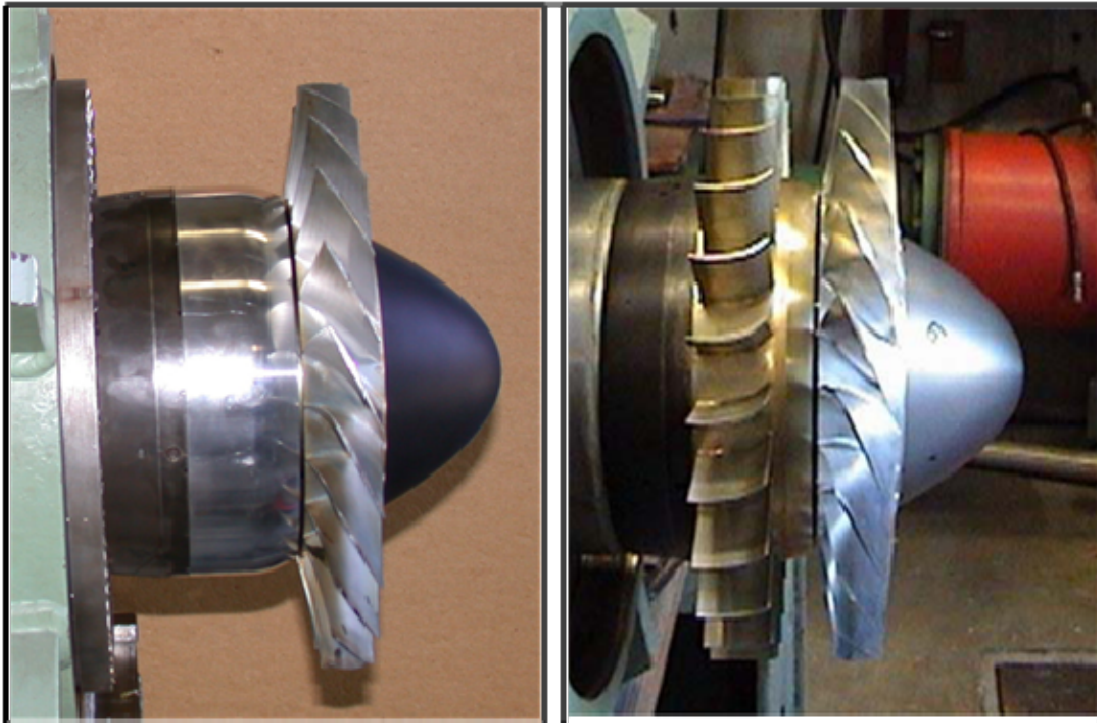


Figure 22. Sanger Test Stage in Rotor-only and Full Stage Configuration

The full stage employed at the NPS Turbo Propulsion Laboratory consisted of a 22-blade rotor and a 27-blade stator, Figure 22. Both were manufactured from T7075-T6 Aluminum alloy because of its lightweight and durability. The later was particularly important because of the strong vibration and high possibility of mechanical damage during the stall events that culminated each speed run. A detailed description of the critical design parameters is shown in Table 1.

Rotor Pressure Ratio	1.61
Stage Pressure Ratio	1.56
Tip Speed	396.2 m/sec
Design Speed	27,085 rpm
Design Mass Flow	7.75 kg/sec
Specific Mass Flow	170.9 kg/sec-m ²
Specific Head Rise	0.246
Tip Inlet Relative Mach Number	1.6
Aspect Ratio	1.2
Hub/Tip Radius Ratio	0.51
Number of Rotor Blades	22
Number of Stator Blades	27
Tip Solidity (Rotor)	1.3
Tip Solidity (Stator)	1.0
Outside Diameter	0.2794 m (11")
Rotor Diffusion Factor (Tip)	0.40
Rotor Diffusion Factor (Hub)	0.47
Stator Diffusion Factor (Tip)	0.52
Stator Diffusion Factor (Hub)	0.58

Table 1. Sanger Test Stage Design Parameters

Rotor speed was controlled through two single-stage power turbines, on a common shaft, that received air from a 12-stage Allis-Chalmers Axial compressor that took air directly from the atmosphere and delivered it directly to the TCR at the required flow rate. The compressed air used to drive the axial turbine was throttled to the flow rate needed to maintain the desired rotor speed and was exhausted back to atmospheric radially. Flow through the compressor stage was controlled by an upstream throttle plate that receives electrical command from the test control station.

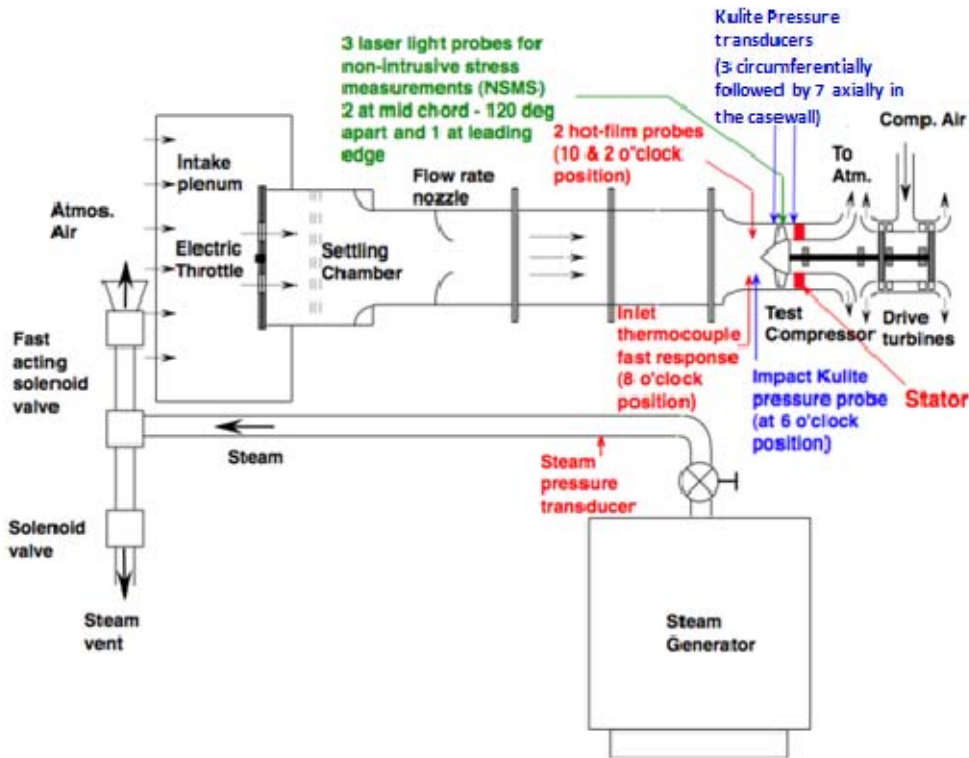


Figure 23. Transonic Test Rig Schematic, After [11]

As discussed by Hurley the test rig differs from previous research due to the removal of a honeycomb flow straightener located behind the fan and the introduction of ceramic high temperature ball bearings [11].

B. DATA ACQUISITION SYSTEM

Data collection was accomplished using a high-speed and low-speed system for recording pressure and temperature measurements across the rotor as well as rotor speed measurements.

1. Slow-Speed Data Collection

Steady-state measurements were taken using pressure probes positioned upstream of the rotor and at the same axial position of the Kulite probes so stagnation pressure measurements could be taken for each variation of rotor speed and throttle position. Additional measurements were also made via 11 stagnation temperature probes

positioned downstream of the rotor. Using these probes isentropic efficiency and mass averaged temperature/pressure ratios were calculated and use to determine the compressor performance maps.

2. High-Speed Data Collection

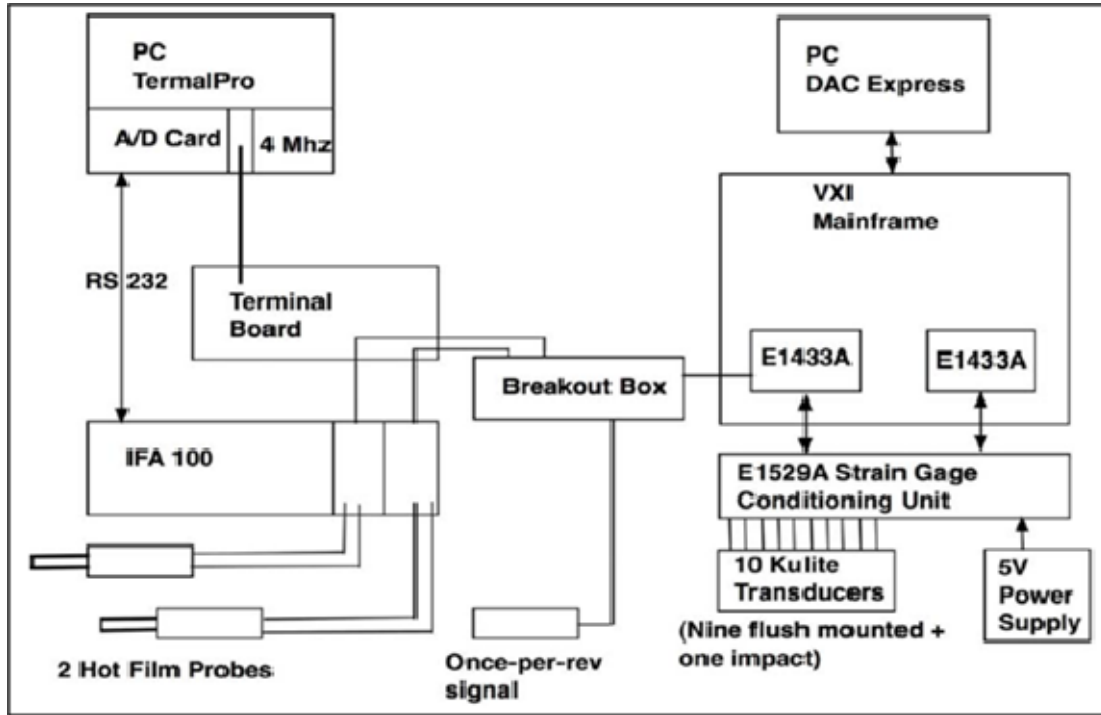


Figure 24. Schematic of High Speed Data Capture System, After [11]

As shown in Figure 23 and Figure 24, the high-speed system consists of ten Kulite pressure probes in the casewall across the rotor blades, one Kulite impact probe upstream, and two hot film probes. The Kulite probes are capable of sampling at 300 kHz and the hotwire probes can respond to changes in velocity at 400 Hz. They are sampled and stored via a VXI Mainframe at its maximum sampling frequency of 196.6 kHz to reduce the aliasing of high-frequency signals into the lower frequency regions of interest. Data is stored in a binary format internally on the VXI Mainframe but can be exported to PC in a delimited text file for analysis. This file format is used to ensure portability of data regardless of system type or post processing software.

As shown in Figure 25 the Kulite probes are positioned on the casewall so that static pressure measurements can be taken across the chord of the rotor blades starting at a position well upstream (Probes 1, 7 and 8) and ending at a position well downstream (Probe 6). The upstream probes are positioned 120-degrees around the casewall at the same axial location so that the speed of any stall cells can more accurately be determined.

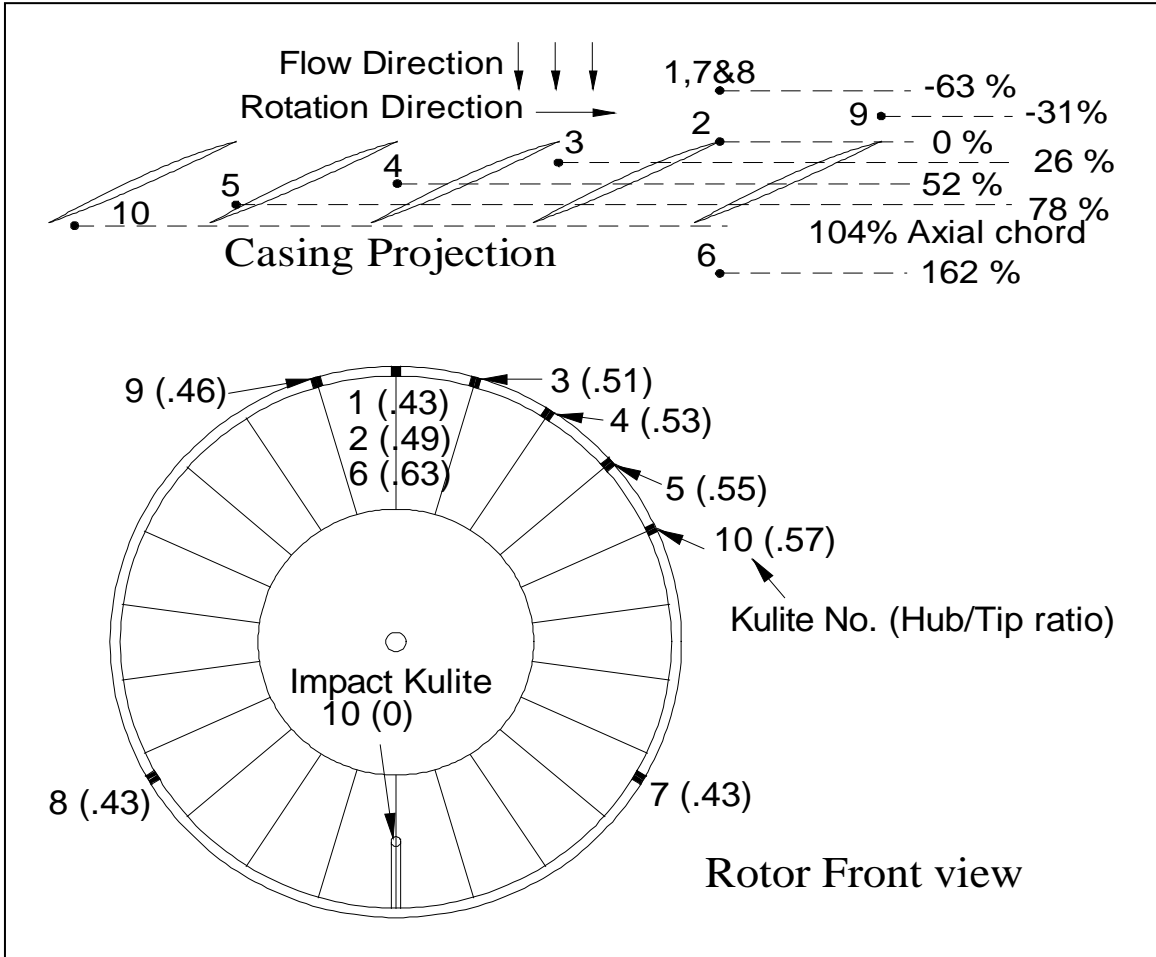


Figure 25. Kulite Probe Locations Relative to Rotor Cross Section

THIS PAGE INTENTIONALLY LEFT BLANK

V. EXPERIMENTAL PROCEDURE

As in previous research conducted on the Transonic Compressor Rig (TCR) steady state reading were recorded using the high and low speed data so that a compressor performance map could be generated. This was accomplished by running the compressor at a constant RPM and varying throttle position so that the progression of pressure ratio and efficiency could be recorded and plotted, Figure 26.

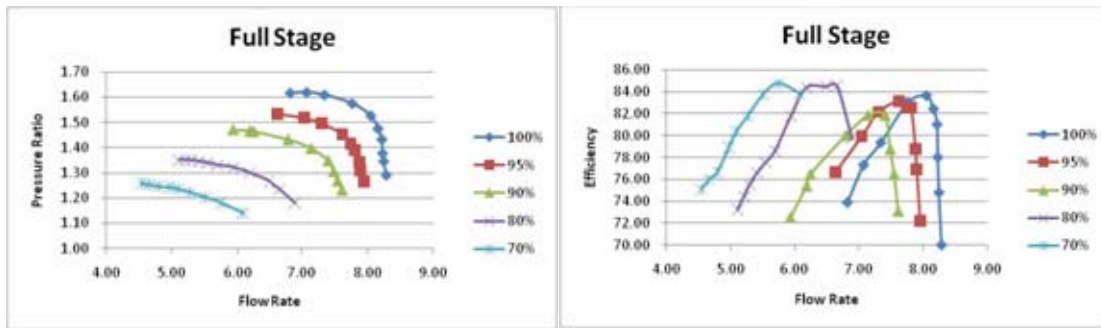


Figure 26. Full Stage Compressor Performance Maps

To obtain the data from the low- and high-speed data acquisition system, the compressor rig was operated in steady state condition at one of the speeds identified in Table 2. This speed was then corrected for local variation in temperature and pressure so that the inlet Mach number for any given run would be the same regardless of daily atmospheric variation.

% Rotor Speed	RPM
100%	27,085
95%	25,730
90%	24,375
80%	21,670
70%	18,960

Table 2. Rotor Speed Profile

A generic test procedure consists of the following:

- The rotor RPM is stabilized around the corrected RPM for the desired speed using the Allis-Chalmers Controls.
- The slow-speed data from the stagnation pressure and temperature probes are recorded via a PC based data acquisition system.
- The high-speed data is recorded using varying back pressures on the Kulite Probes (0, 5, 10 and 15psi). This is done so that the data can be accurately calibrated and analyzed. For steady state operation, a 2-second recording is taken using the high-speed system; for a stall run, a 60-second recording is taken to ensure that the full stall event is captured.
- The throttle is then set to a new position in preparation of the next run.

VI. DATA ANALYSIS DESCRIPTION

The underlying MATLAB code used in this research represents a revision of the code primarily developed by A. J. Gannon and has been used in most previous theses on the TCR. The contribution of this research was an improved implementation of the data loading and calibration routines and the filter construction and application algorithm. A simple-to-use graphical user interface (GUI) was also developed to enable rapid data analysis.

A. USER INTERFACE FUNCTIONALITY

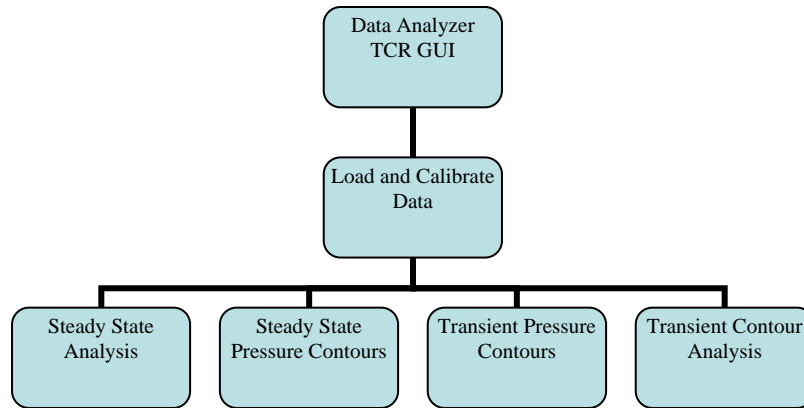


Figure 27. Top Level GUI Functionality

The **Data Analyzer GUI** was used to accomplish five primary tasks, Figure 27:

- 1) **Load and calibrate** raw voltage signals from the Kulite pressure transducers.
- 2) Perform a **steady-state analysis** of the pressure signals, in the time and frequency domains, to identify precursor frequencies and bulk inlet flow properties.
- 3) Generate a time-averaged **steady-state pressure contour** of the blade passages. This enables the identification of flow field structure within a typical blade passage.

- 4) Generate a **Transient Pressure Contour** plot of all the rotor blades over a given set of rotations to visualize the flow field as it changes in the passages over time.
- 5) Perform a **Transient Contour Analysis** of the pressure data at discrete locations within a blade passage. Information regarding magnitude and frequency and standard deviation of the locations are presented.

B. RAW DATA CALIBRATION

1. MATLAB Code Overview

This Data Loading and Calibration subroutine used the m-files briefly described below (Figure 28) to generate the binary files used in all subsequent analysis.

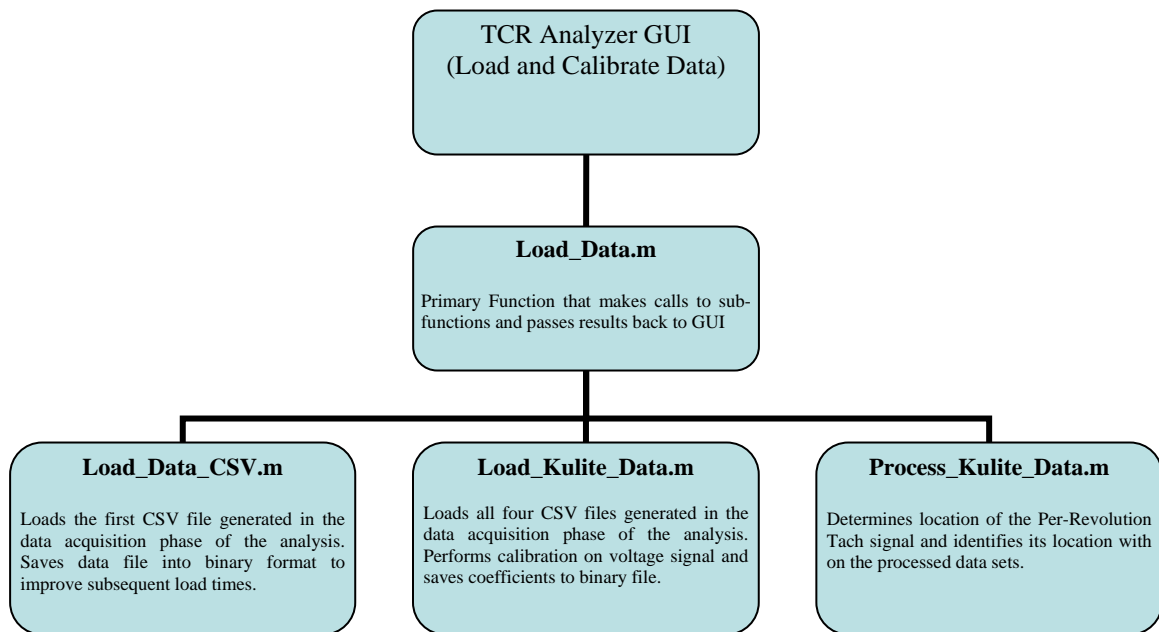


Figure 28. Data Load and Calibrate Workflow

2. Calibration Description

The raw Kulite data, recorded using varying back pressures, was processed using the load_kulite_data.m script so that it could be accurately converted from voltages to pressure ratios with regard to the recorded atmospheric pressure for that particular run.

The average of the raw voltage for each Kulite, the static pressures recorded from probes at the same axial location on the compressor casing, and the pressure taken from the impact Kulite positioned upstream of the rotor were processed. These calibration curves, uniquely determined for each Kulite, were then applied to all voltages recorded during a given series of test runs and were used to develop all the experimental results discussed in subsequent chapters, Figure 29.

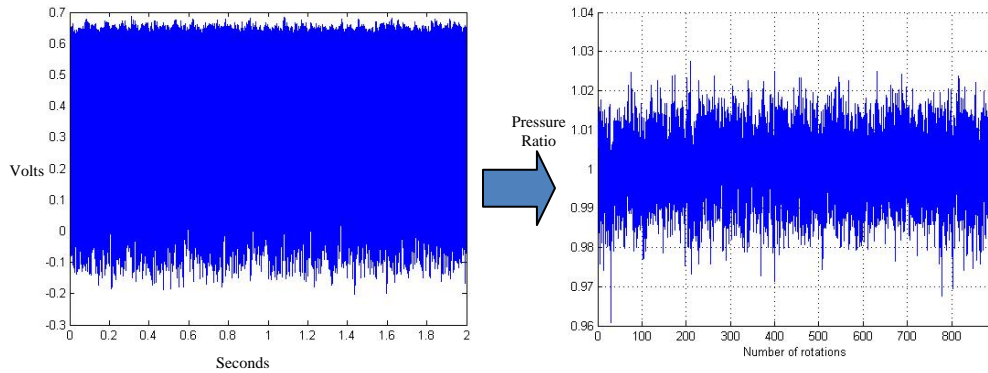


Figure 29. Generic Raw Kulite Voltage Conversion to Pressure Ratio Data Sets

C. STEADY STATE ANALYSIS ROUTINE

1. MATLAB Code Overview

This Steady-State Analysis subroutine used the m-files briefly described below (Figure 30) to perform the analysis and generate the data plots.

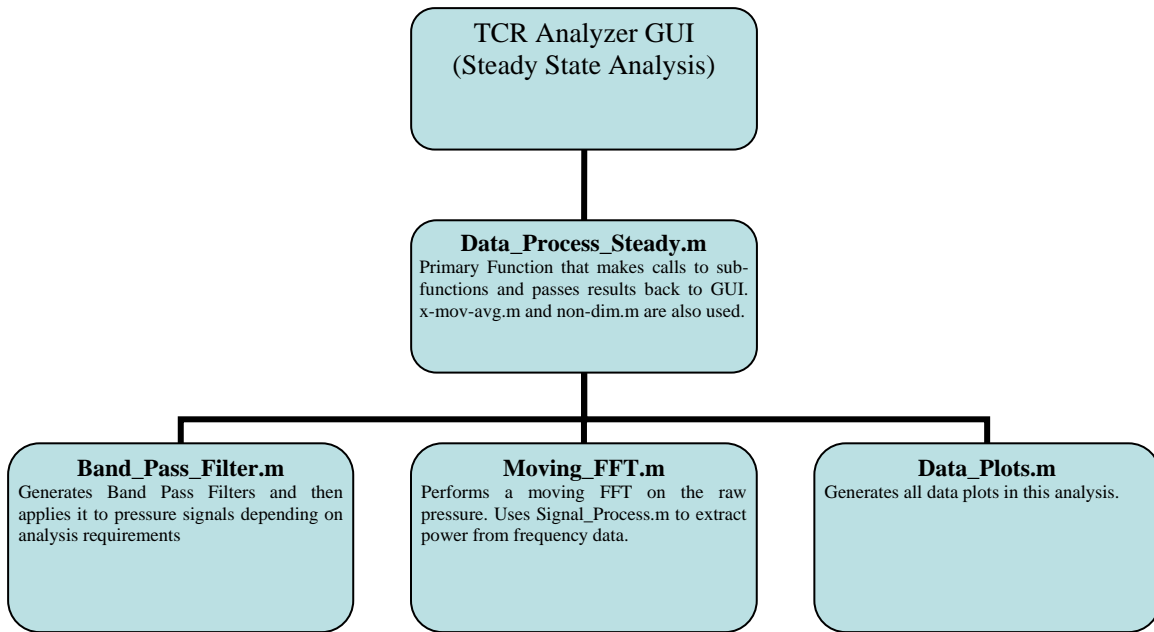


Figure 30. Steady State Analysis Workflow

2. Analysis Description

The steady-state analysis was conducted by transferring the pressure data into the frequency domain so that frequency regions of interest could be located and data processing methods could be better targeted, Figure 31. All frequencies were normalized with the blade passage frequency at the given rotor speed so that the dominant blade passing frequencies could be more easily identified at their integer locations. Primary areas of interest were frequencies lying below and just above the blade passing frequency (10^0) because these regions were known locations of low-frequency oscillation at all rotor speeds. However, the relative magnitude of the multiples of the blade passing required that a filter be developed so that the relatively small peaks within the regions of interest could be more easily identified.

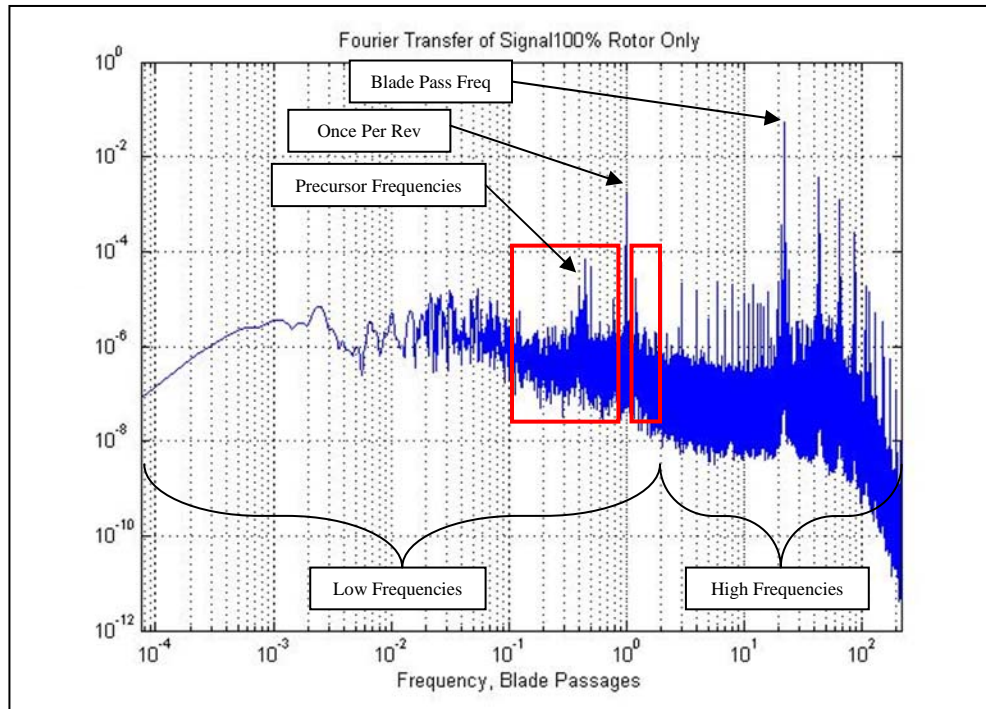


Figure 31. Fast Fourier Transform of Pressure Signal at 100% Rotor Speed

To construct the filter built-in MATLAB Fast Fourier Transform and filtering functions were employed. A Blackman Window was selected as the base filter because of its high roll-off and low ripple, Figure 32.

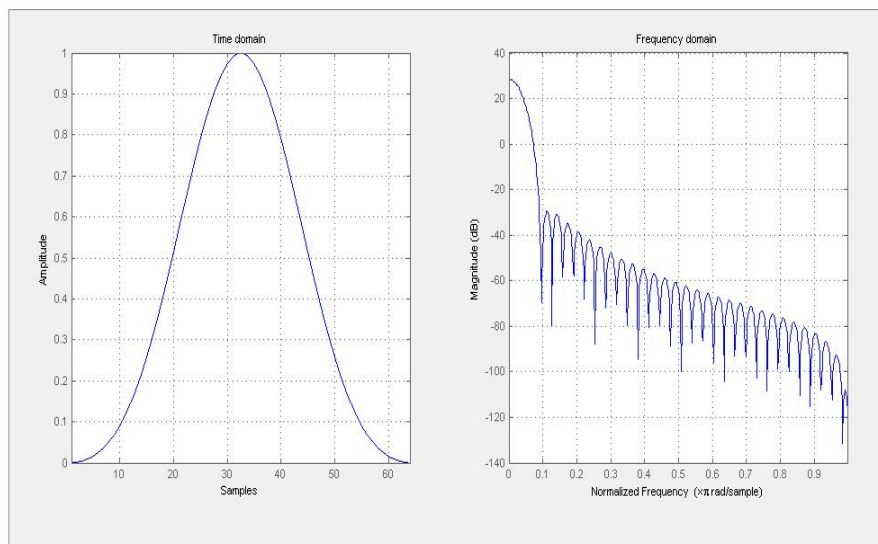


Figure 32. Generic Blackman Window Employed in Analysis

The Blackman window was sized so that the signal would be attenuated as quickly as possible outside of the regions of interest without adversely impacting the raw signal in the frequency range of interest. The exact size was determined using the sampling frequency (f_s) and the desired roll-off.

$$\text{Windows Length} = \frac{4}{\text{Band Width}} = 4 \left(\frac{\text{Roll Off}}{f_s} \right)^{-1}$$

A roll-off of 1-Decade was ultimately chosen because of the quick attenuation it provided to signals immediately outside of the analysis region and because it limited the window size to a manageable length. The filter elements were added together to generate arbitrary band pass filters allowing an analysis across any frequency range, Figure 33. This also had the benefit of providing a reduction of high frequency sensor noise and low frequency sampling error.

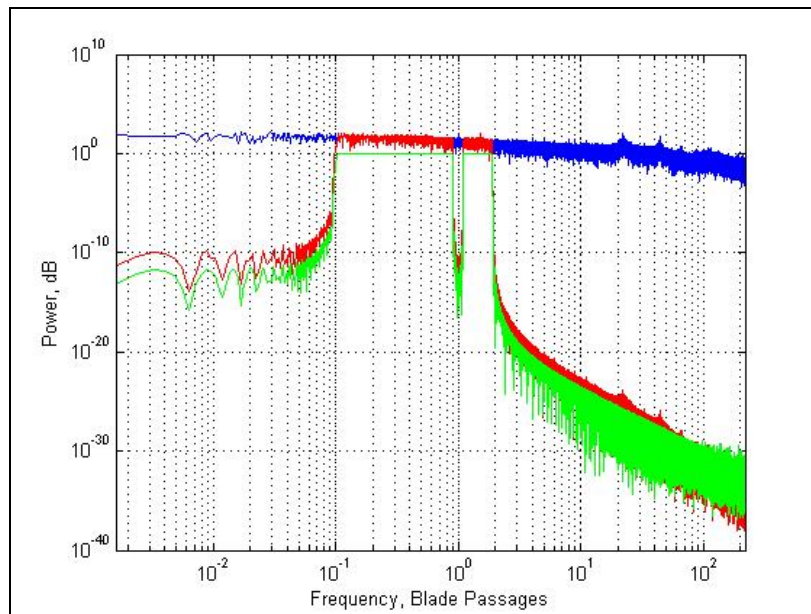


Figure 33. Signal with Band-Pass Filtering Applied

This frequency data was then used to generate the waterfall plots of the oscillations across the blade passage as a function of frequency and percent of chord.

The data is then transferred back into the time domain using MATLAB's inverse Fourier Transform function so that bulk inlet properties can be calculated.

D. STEADY STATE CONTOUR ROUTINE

1. MATLAB Code Overview

This Steady-State Pressure Contour subroutine used the m-files briefly described below (Figure 34) to perform the analysis and generate the data plots.

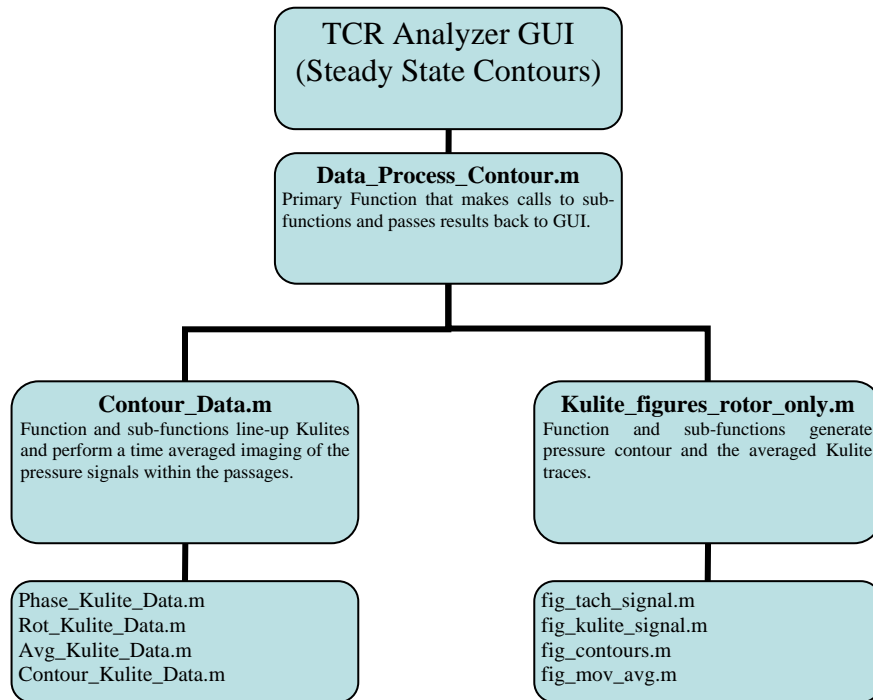


Figure 34. Steady State Pressure Contour Workflow

2. Analysis Description

The Steady-State Contour program used the unfiltered Kulite data to generate a snapshot of a time-averaged typical blade passage. Due to the fact that pressure data only exists at the angular Kulite positions (The vertical lines from Figure 35) the axial pressure data had to be interpolated using MATLAB. This required that all Kulite data be lined up as if they existed along a single angular location. The data was then interpolated in three

distinct regions to reduce the interpolation error in locations of known high gradient (Along the shock (R1), horizontally through the blade passage (R2), and along the blade (R3).) These regions were then stitched together using modified cosine functions so that the transitions were seamless.

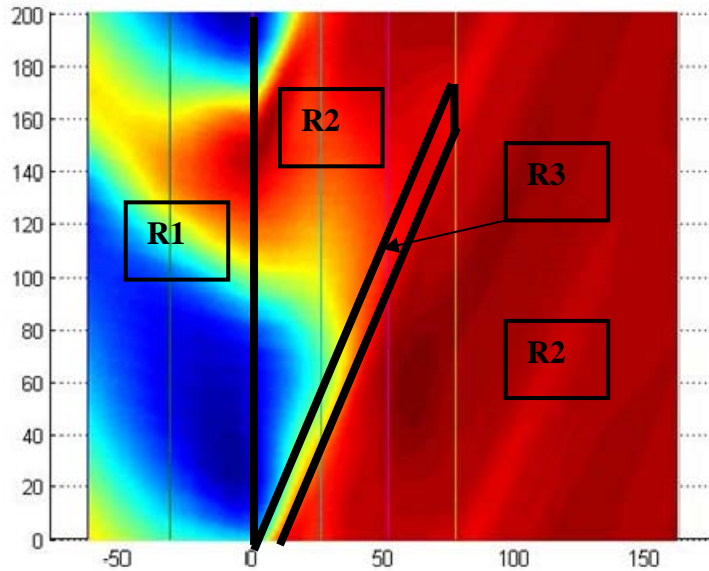


Figure 35. Steady State Pressure Contour Plot Showing Interpolation Regions

E. TRANSIENT CONTOUR ROUTINE

1. MATLAB Code Overview

This Transient Pressure Contour subroutine used the m-files briefly described below (Figure 36) to perform the analysis and generate the data plots.

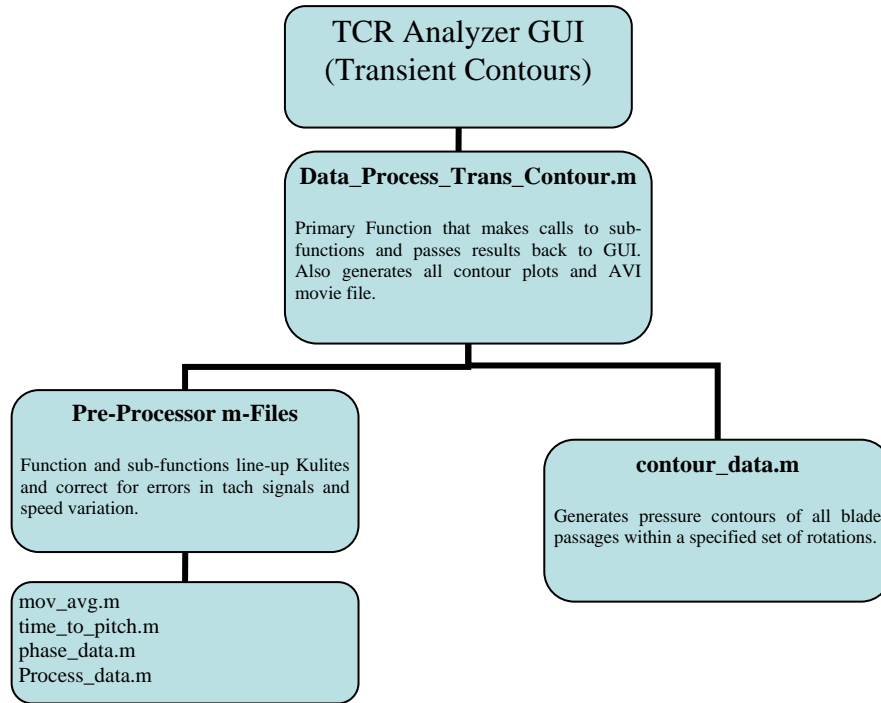


Figure 36. Transient Pressure Contour Workflow

2. Analysis Description

This program performed the contouring interpolation in the same manner as the Steady-State Contour sub-routine with the exception that it did not perform the time averaging. It used the high-pressure point at the leading edge of the blade to identify the blade tip and assumed a constant pitch length to correctly interpolate the shock and blade angle. In addition to the time strip plots of the identified rotations the program also generated a video file by using individual blade passages as still frames. The file was then saved as a compressed AVI file or a high-quality uncompressed AVI file.

F. TRANSIENT CONTOUR ANALYSIS ROUTINE

1. MATLAB Code Overview

This Transient Contour Analysis subroutine used the m-files briefly described below (Figure 37) to perform the analysis and generate the data plots.

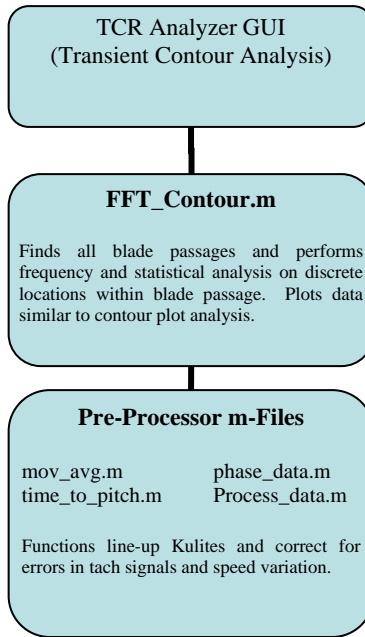


Figure 37. Transient Contour Analysis Workflow

2. Analysis Description

The underlying code implemented in this analysis routine was based on the same methods employed in the transient contour generation. This method differed in that it used the tach signal and pressure signal to locate the blade tip and pitch length in the pressure data. Because the sampled pressure data did not sample the same position in the passage at each blade passing the data was interpolate at regular positions so that the frequency analysis and statistical analysis were being used properly. The pressure at each discrete location was the processed using MATLAB's Fourier Transfer and Standard Deviation functions so that the regions of highest change would be identified.

VII. ANALYSIS AND RESULTS

This research represents an analysis of the Transonic Compressor Rig at 70%, 80%, 90% and, 100% of rated speeds in both the rotor-only and full stage configuration to better quantify the differences between both operating conditions. For the steady-state operating mode, an analysis of the raw pressure data was conducted in the frequency domain with the intent of determining dominant frequencies and the effect that the addition of a stator had on the dynamic of the system when compared to previous rotor-only research. A separate analysis was conducted in the time domain with the intent of correlating the physical structure of the flow field (Shocks, Boundary Layers, etc.) with the localized the frequency domain data. A transient analysis of the TCR as it entered stall was then conducted using many of the same tools and methods developed for steady state operation.

A. FREQUENCY DOMAIN

Using the filtered Kulite pressure signals described in Chapter IV, it became possible to display the power-frequency data across the compressor blade so that the relative values and frequencies could be used to identify frequency-spatial regions of interest for further analysis in the time domain. The previously described frequency normalization was used in these plots; however, the Axial Location was also normalized against the blade chord so that “0” denotes the leading edge and “100” denotes the trailing edge, Figure 38.

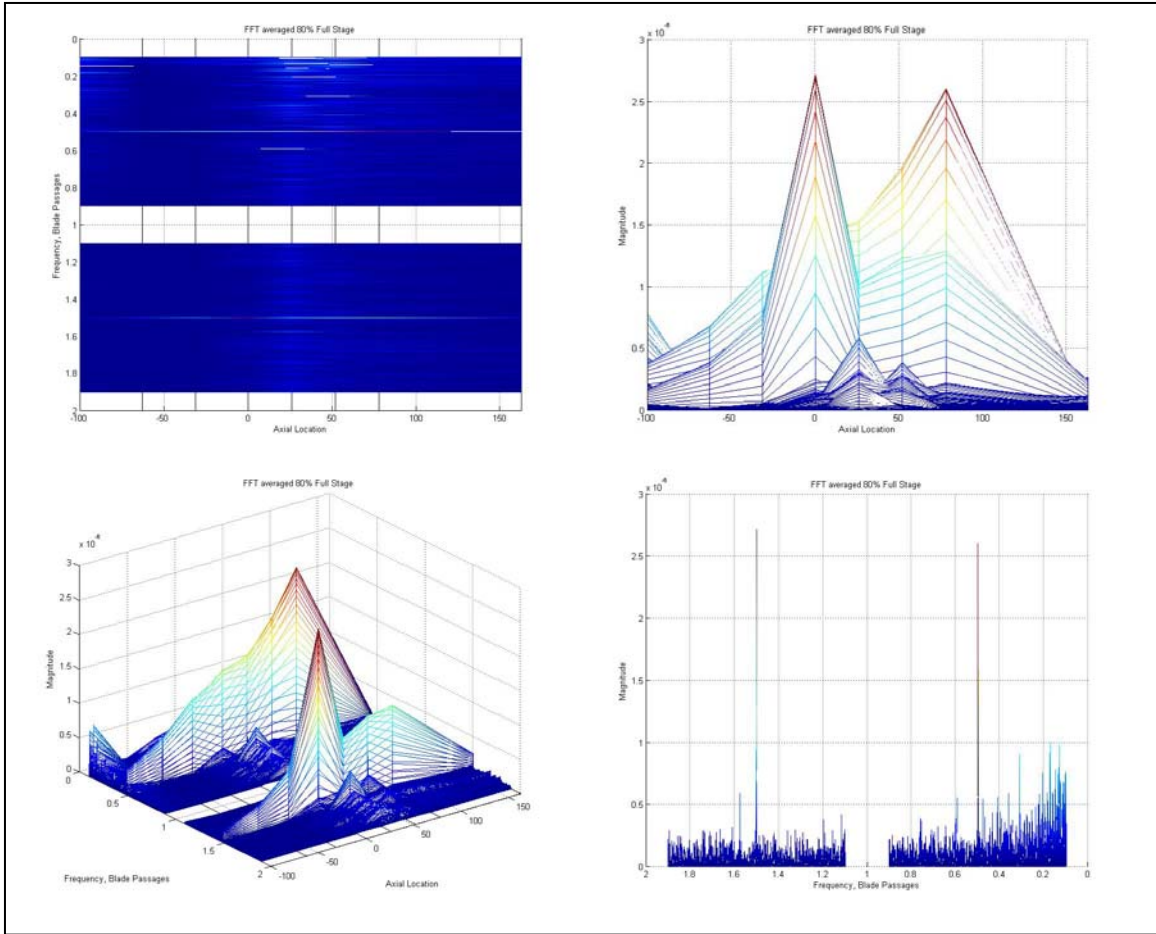


Figure 38. Full Stage Waterfall Plot of Filtered Frequency Data at 80% Speed, Near Stall

Using the waterfall plot of the filtered frequency data for all Kulite probes the frequency location, peak magnitude, and extent of blade coverage can be determined for any given speed-throttle profile. The data displayed for 80% speed in Figure 38 clearly shows two dominant peaks at 0.5 and 1.5 times the blade pass frequency with the higher frequencies dominating the blade tip and lower frequencies more prominent at the trailing edge. This hints at the presence of multiple instabilities rotating around the front of the rotor and a single instability in front of the stator.

Waterfall plots were generated for all speed-throttle settings so that the progression of instability growth as the rotor approached stall could be clearly analyzed. Figure 39 shows this progression for the TCR at 100% of rotor speed in the rotor-only

configuration. As shown in Block B, strong peaks appeared at 0.5 times the blade passage frequency as the rotor approached stall and suddenly reduced in power in the test run just preceding the onset of stall.

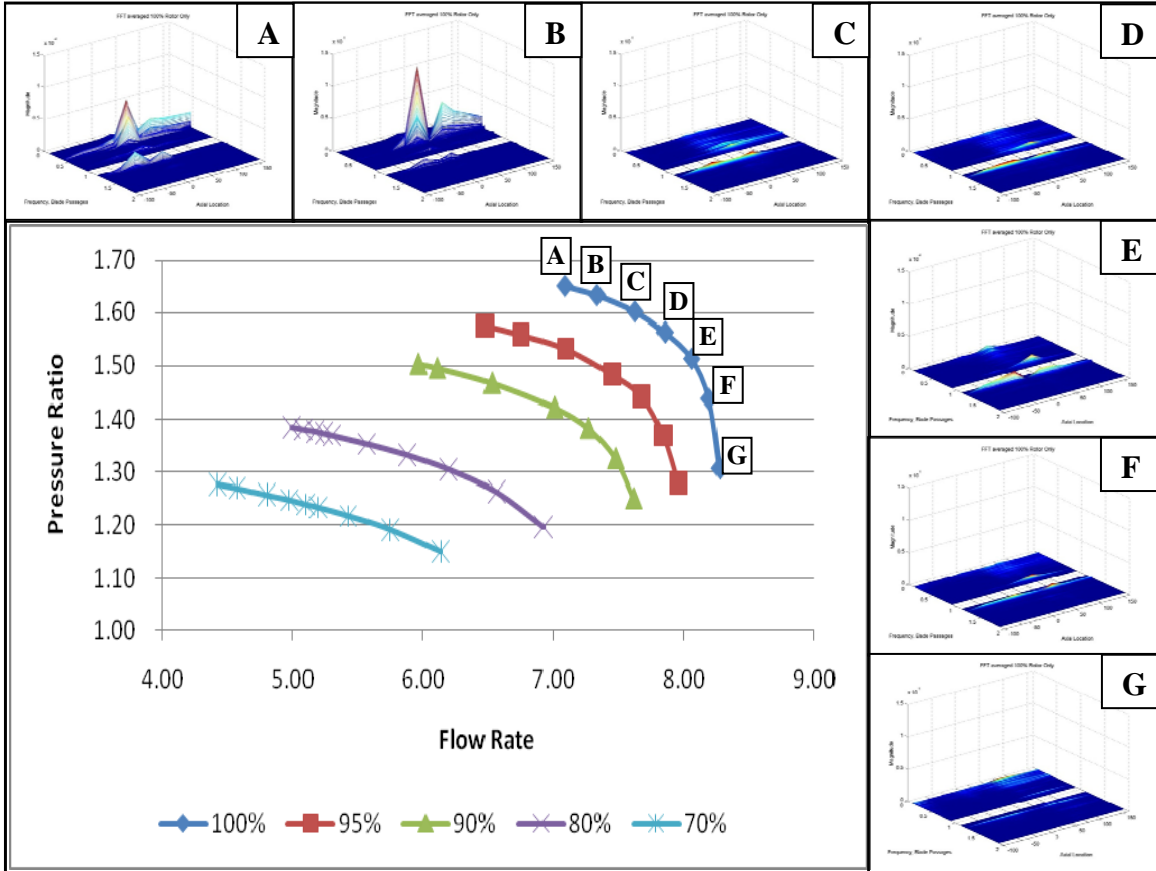


Figure 39. Rotor Only Waterfall Plots of Filtered Frequency Data at 100% Rotor Speed

Another important feature of these plots is the extent of the blade that was experiencing these high-pressure variations. In most cases there was a substantial “wake” trailing from the peaks experienced at the leading edge of the blade; however, in all the tests below 95% speed there was also a substantial transport of information forward of the blade, Figure 40.

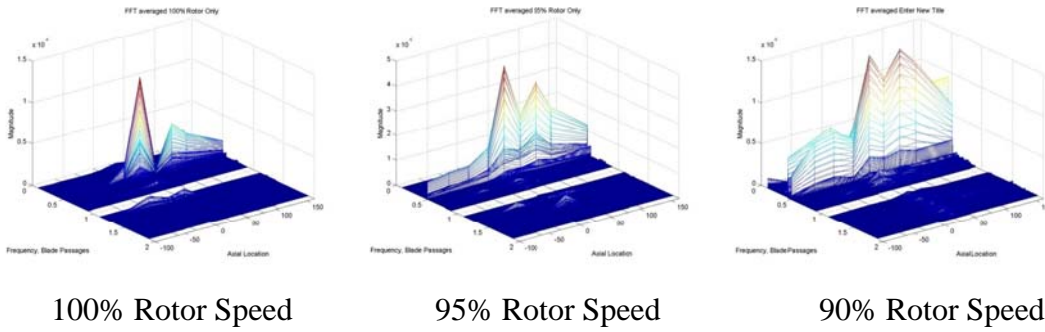


Figure 40. Waterfall Plots of Filtered Frequency Data Showed Forward Transport

Figure 41 shows the same analysis for the 95% rotor speed run in the full stage configuration. There does appear to be a series of peaks whose magnitude and location is stable in the vicinity of 0.1 and 0.9 times the blade pass frequency; however, these locations do not correspond to known pre-modal instabilities and are usually only found at the location of a single Kulite probe hinting at an unstable shock boundary interaction being registered.

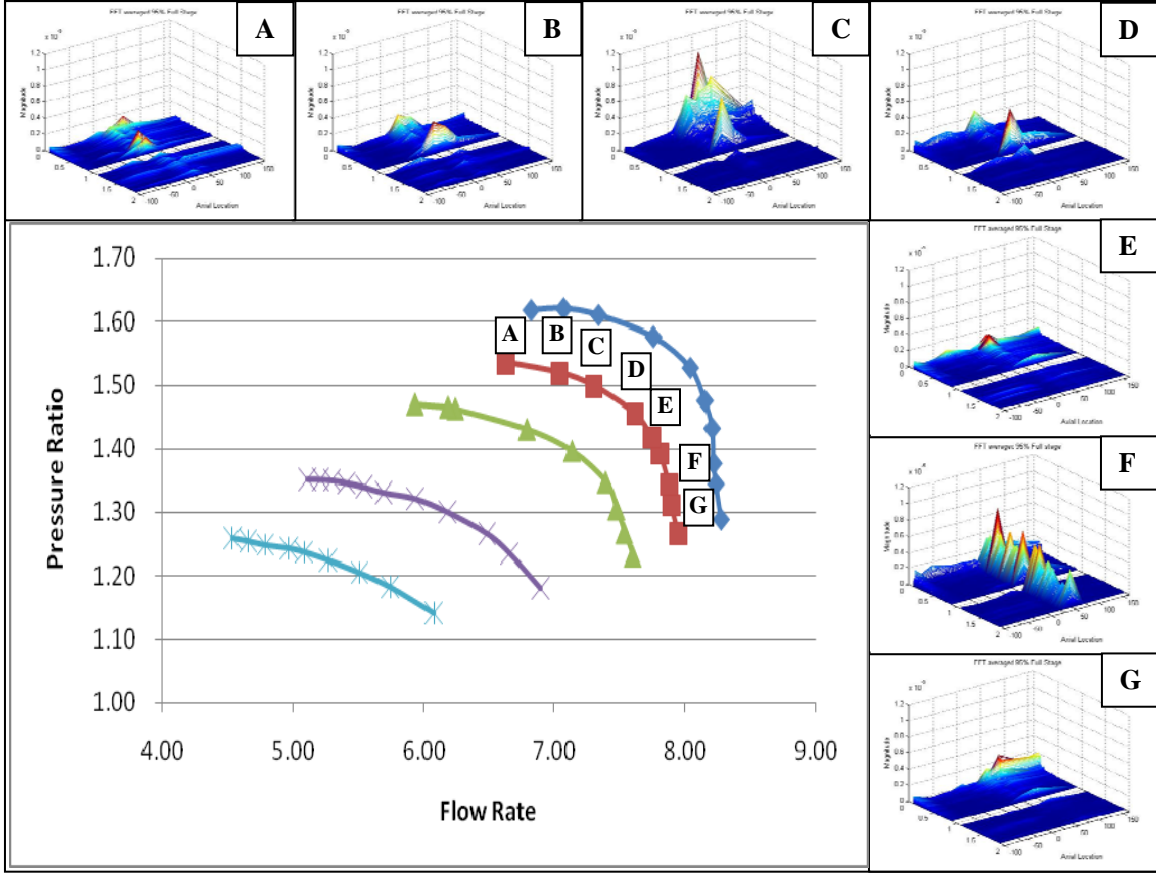


Figure 41. Full Stage Waterfall Plots of Filtered Frequency Data at 95% Rotor Speed

As a means to quantify the total power present in the rotor at a given speed-throttle profile the RMS power was calculated in the frequency range $\{0.1 \leq f \leq 0.9, 1.1 \leq f \leq 1.9\}$ by summing the peak values along a given Kulite and then averaging the power of all the Kulites.

$$RMS \ Power_{total} = \frac{\sum_{j=1}^{\#Kulites} \left(\sum_{i=0.1}^{0.9} P_i + \sum_{i=1.1}^{1.9} P_i \right)_j}{\#Kulites} \quad (1)$$

This data was then tabulated and plotted for the full stage and rotor only configuration, Figure 42. As shown the RMS power in the rotor only configuration increased as the rotor speed increased and as the throttle was closed. This behavior was not present in the stage where power levels remained constant even as the throttle began to close.

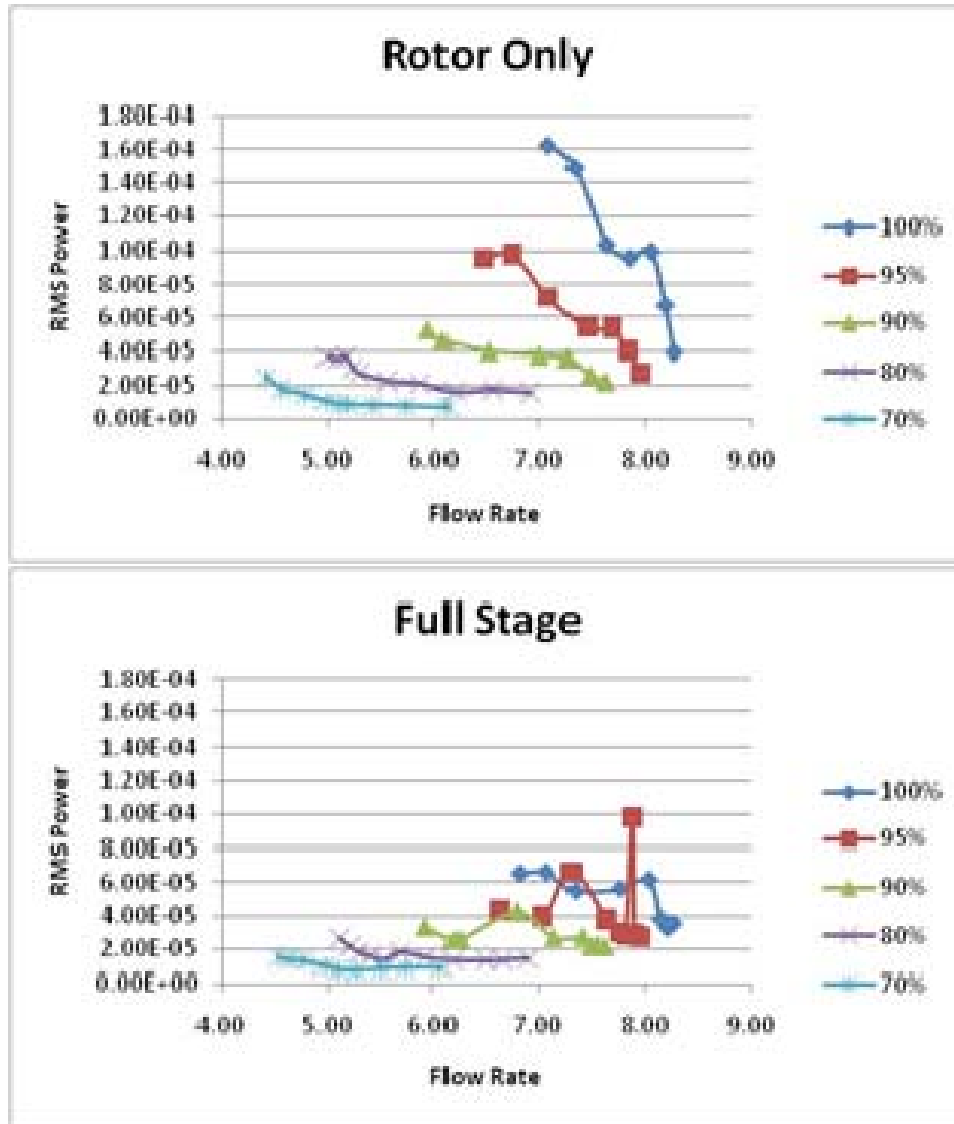


Figure 42. RMS Power of Rotor and Stage in Low Frequency Band

Further investigating the relationship between the RMS power and the onset of stall the RMS power throughout the frequency band $\{0.1 \leq f \leq 44\}$ was calculated to include the blade pass frequency peaks, Figure 43.

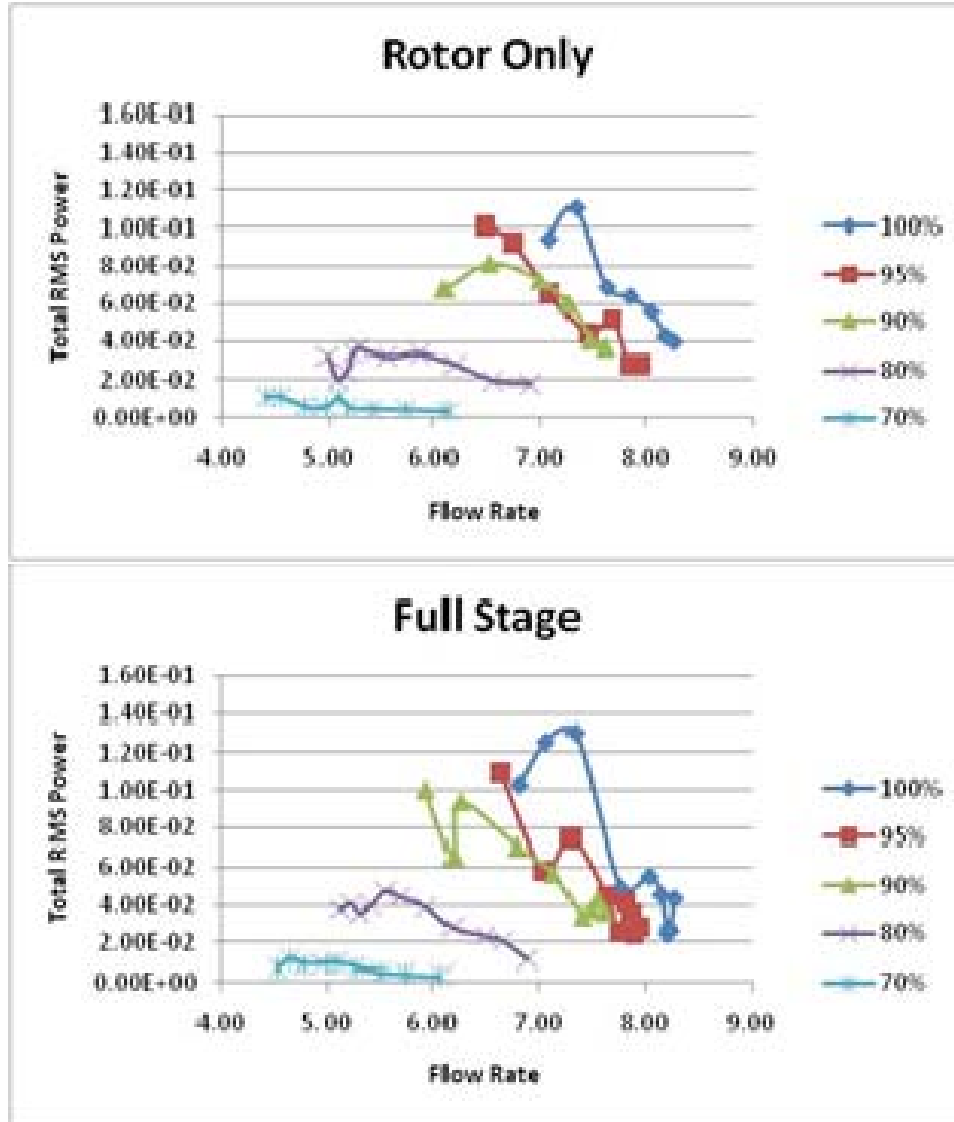


Figure 43. RMS Power of Rotor and Stage in Full Frequency Spectrum

The total frequency RMS plot in the rotor-only configuration was very similar in shape when compared to the low-frequency plots only differing in the magnitude of the power present. This is contrasted by the behavior of the full stage which now began to displayed the same shape and magnitude as the rotor only case. This prompted the development of a non-dimensional form of the RMS power so that the differences could be more easily explained, Figure 44.

$$P_{non-dim} = \frac{P_{low}}{P_{full}} \quad (2)$$

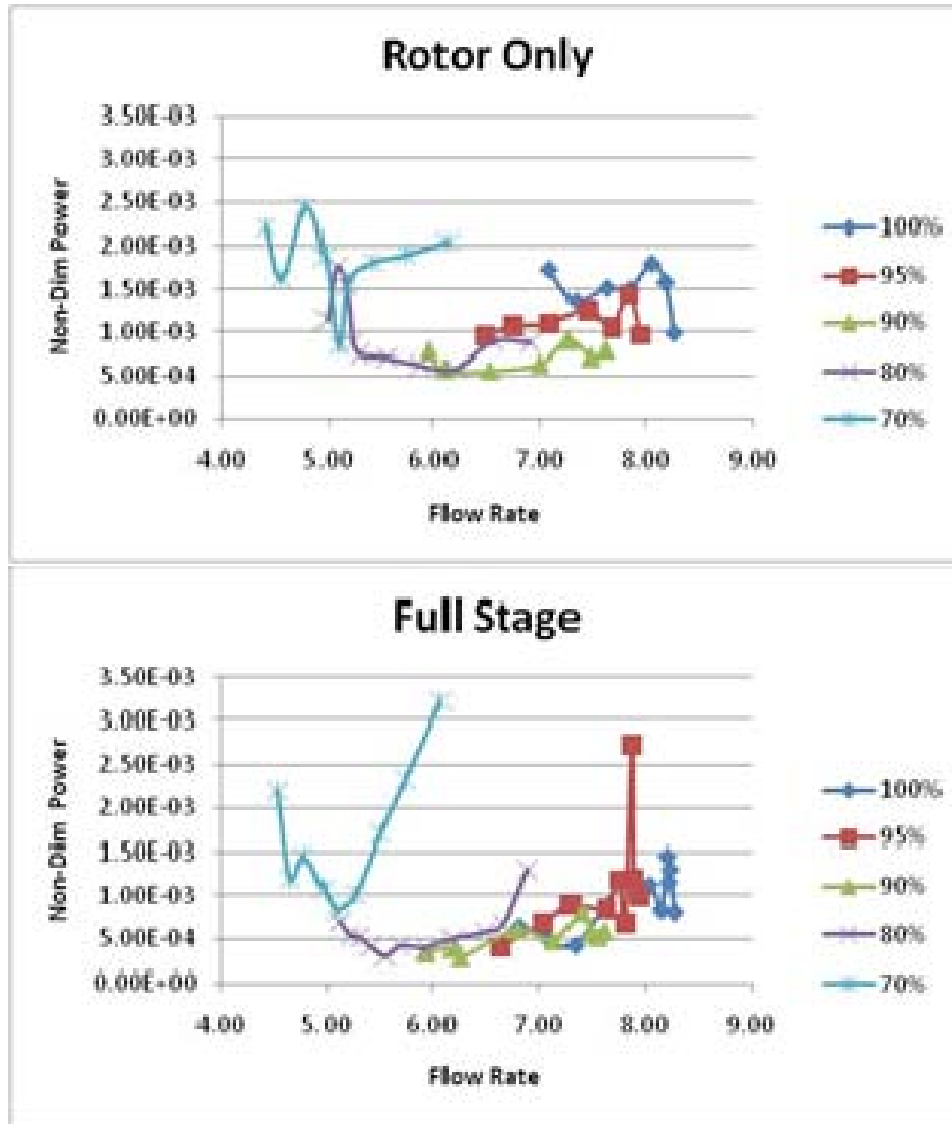


Figure 44. Non-Dimensional RMS Power for Rotor and Stage

While no clear correlation was found between the RMS power at any frequency level and the onset of compressor stall an analysis of the RMS power distribution revealed clear differences between the rotor-only and stage configurations. As shown in Figure 43 the total power of the system was generally the same at all speed-throttle profiles; however, Figure 44 revealed that the sonic and transonic rotor speeds (80% to 100%) displayed a downward trend in the stage configuration and a flat trend in the rotor only configuration.

Table 3 represents a tabulation of the RMS powers at the pre-stall throttle position for each speed. As shown the total RMS power in the rotor and stator were roughly equal while the greatest differences in behavior were present in the low frequency bands. This hints at a rotor-stator coupling that had the affect of moving the power to the higher frequency regions suggested that the inclusion of the stator had stiffened the system and raised its natural frequency. In addition, the system was being damped as indicated by the reduction in magnitude.

Rotor Speed	Rotor Only			Full Stage			% Difference		
	Total	Low Freq	Non-Dim	Total	Low Freq	Non-Dim	Total	Low Freq	Non-Dim
70%	1.13E-02	2.50E-05	2.21E-03	6.77E-03	1.49E-05	2.20E-03	25%	25%	0%
80%	3.23E-02	3.68E-05	1.14E-03	3.76E-02	2.63E-05	6.99E-04	8%	17%	24%
90%	6.81E-02	5.32E-05	7.81E-04	1.00E-01	3.32E-05	3.32E-04	19%	23%	40%
95%	1.01E-01	9.56E-05	9.47E-04	1.10E-01	4.34E-05	3.95E-04	4%	38%	41%
100%	9.42E-02	1.63E-04	1.73E-03	1.03E-01	6.57E-05	6.38E-04	4%	43%	46%

Table 3. RMS Power Comparison

B. TIME DOMAIN ANALYSIS

The filtered signal was then transferred back into the time domain through the use of MATLAB's inverse FFT algorithm so that bulk flow Mach Numbers and Inlet Angles could be calculated for the compressor inlet. This allowed a further characterization of the inlet flow and identified key differences between the rotor-only and stage configurations.

The inlet Mach number for the bulk flow was calculated using the ratio of stagnation to static pressure (P_r) and the ratio of specific heats (γ). A constant specific heat was assumed for the flow; this was reasonable because of the relatively small changes in temperature and pressure in the inlet section of the compressor.

$$M = \sqrt{\frac{2 \left(\left(\text{Pr} \right)^{\frac{1-\gamma}{\gamma}} - 1 \right)}{\gamma - 1}} \quad (3)$$

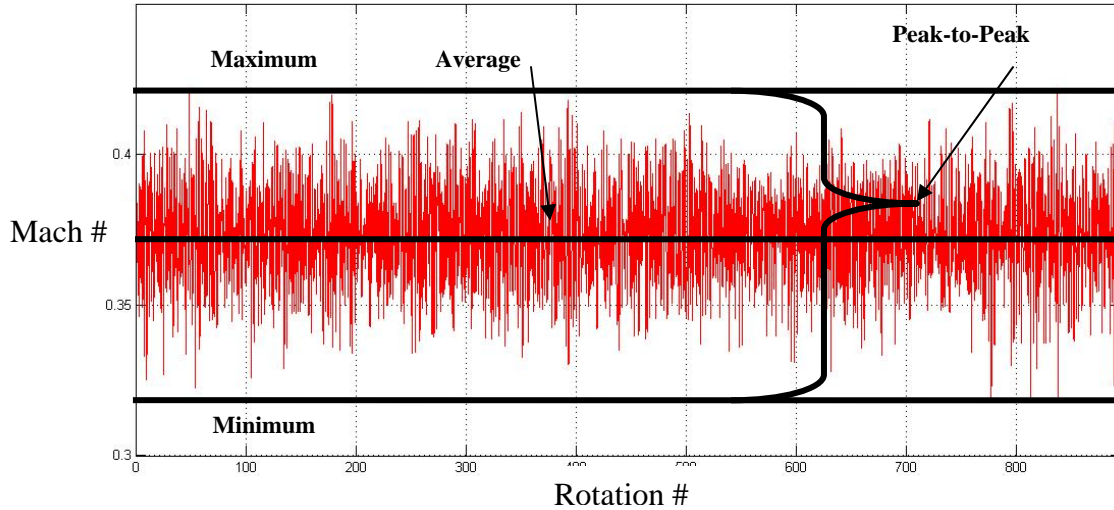


Figure 45. Raw Bulk Mach Number Data at 100% Rotor Speed

The average inlet Mach number was calculated for all speed-throttle settings and plotted versus flow rate, Figure 46. Both plots display similar behavior in the transonic ranges (90% - 100%) but show drops in Mach number in the subsonic and sonic rotor speeds (70% and 80%).

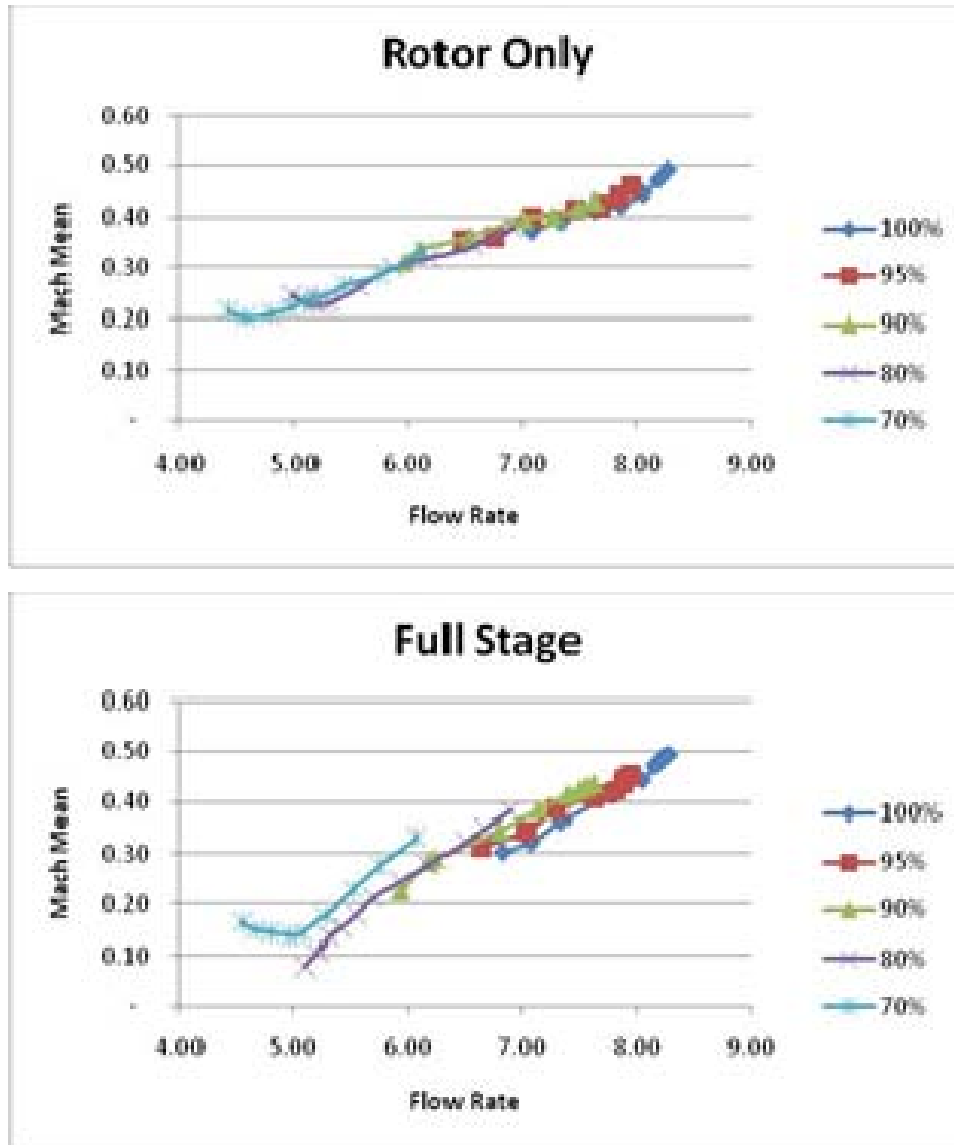


Figure 46. Inlet Mach of Bulk Flow in Rotor-only and Full Stage

The peak-to-peak variation for a given test run was calculated using the instantaneous maximum and minimum Mach number values. This data was tabulated and plotted versus mass flow, Figure 47. Both configurations displayed similar behavior for all speed-throttle settings with increased in the peak-to-peak magnitude as the rotor approached stall. In all cases, with the exception of the 80% run, this variation was as high as 50% of the mean Mach number.

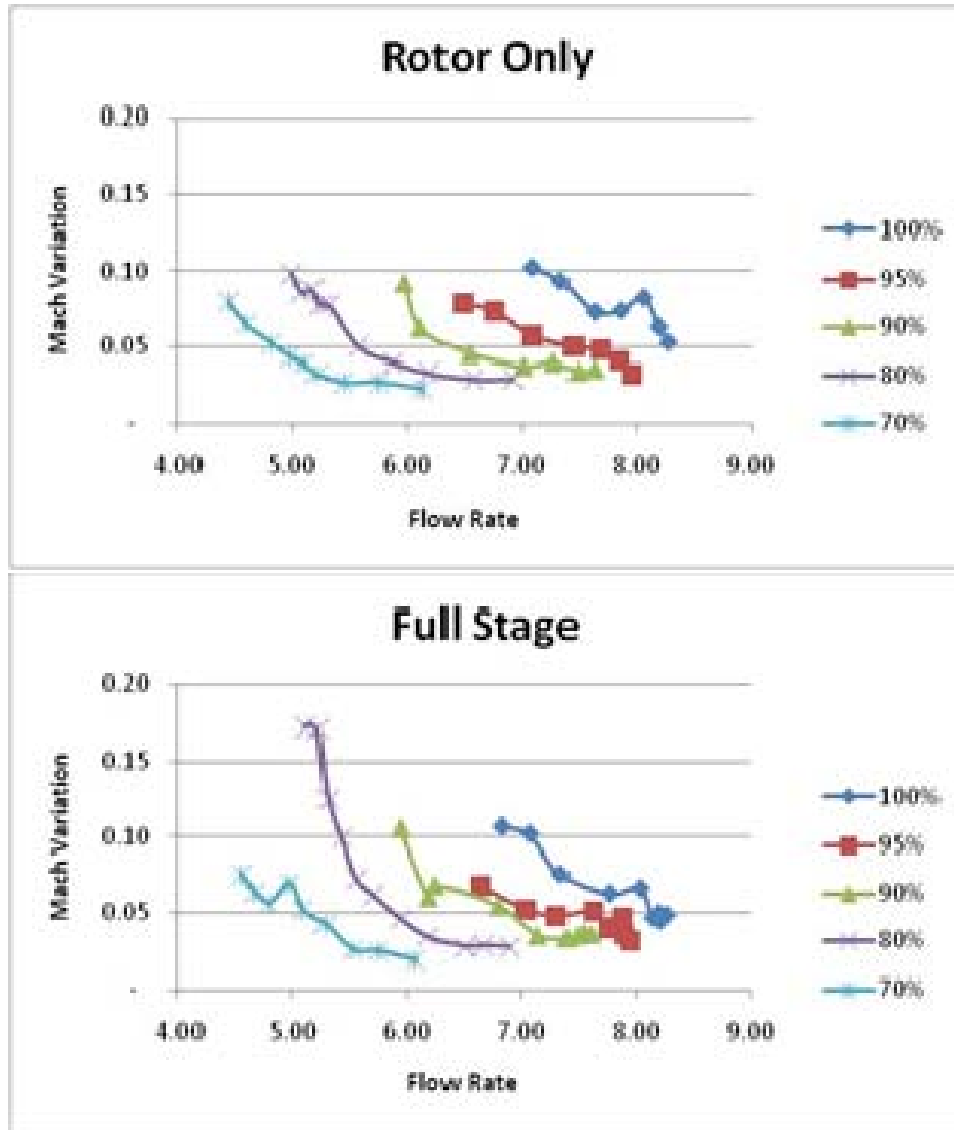


Figure 47. Peak-to-Peak Mach Variation of Bulk Flow in Rotor-only and Full Stage

As shown in Table 4, Mach numbers present in the rotor-only configuration in the pre-stall speed-throttle setting were, on average, 15% higher than those of the full stage. Also shown is a mean 10% increase in peak-to-peak variation of the bulk flow for the full stage in these same pre-stall conditions at all rotor speeds. There were inconsistencies in average Mach number data in the full-stage (revealed by the reduction in Mach from 70% to 80%). These inconsistencies could not be readily explained using this analysis.

Rotor Speed	Rotor Only		Full Stage		% Difference	
	Average	Variation	Average	Variation	Average	Variation
70%	0.22	0.08	0.16	0.08	15.8%	0%
80%	0.25	0.10	0.11	0.17	38.9%	25.9%
90%	0.31	0.09	0.25	0.11	10.7%	10.0%
95%	0.35	0.08	0.31	0.07	6.1%	6.7%
100%	0.37	0.10	0.30	0.11	10.4%	4.8%

Table 4. Inlet Bulk Mach Number Comparison

A similar analysis was also conducted by calculating the bulk flow inlet angle relative to the rotor blades so that the interaction between the changes in rotor speed and inlet Mach number could be better determined. The Axial Fluid Velocity (C_z) is calculated using the Mach number (M) from equation 3, gas constants (γ, R), and static temperature (T). The blade tip speed is calculated using the angular speed (ω) and the blade tip diameter (D). Both values are then used to determine the relative inlet angle (θ_{inlet}).

$$C_z = M \sqrt{\gamma RT} \quad U = (\pi \omega D)_{rotor}$$

$$\theta_{inlet} = \tan^{-1} \left(\frac{U}{C_z} \right) \quad (4)$$

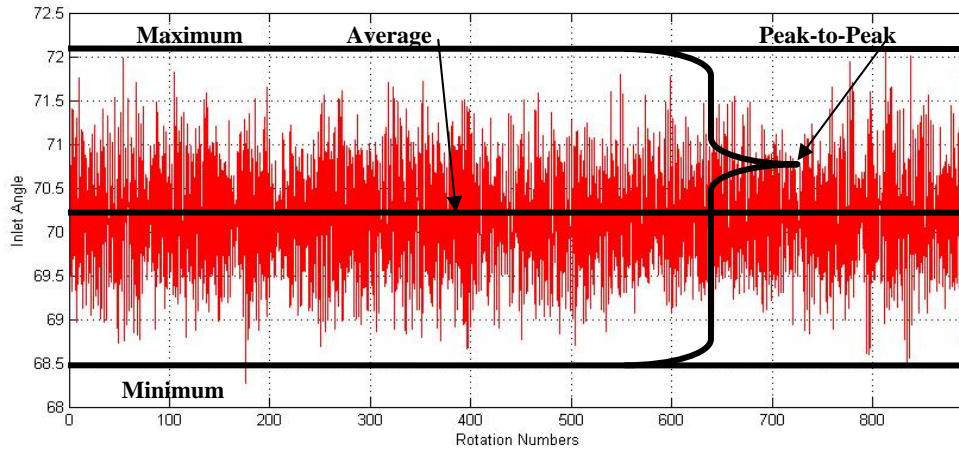


Figure 48. Raw Bulk Inlet Angle at 100% Rotor Speed

Average inlet angle and peak-to-peak variation were calculated in the same way that the average and peak-to-peak Mach was calculated. This data was then plotted versus the mass flow rate for each throttle-speed setting, Figure 49 and Figure 50.

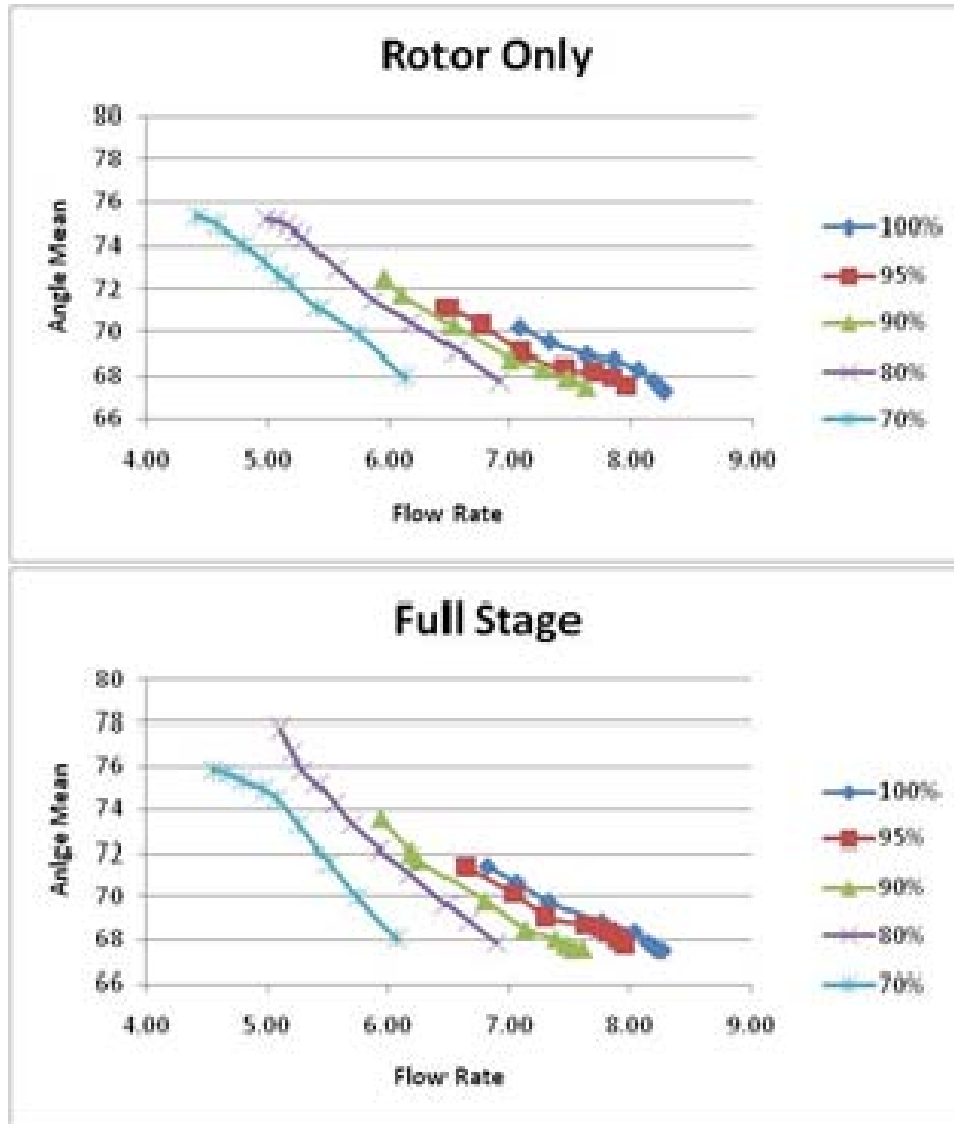


Figure 49. Mean Relative Inlet Angle of Bulk Flow in Rotor-only and Full Stage

The progression of average relative inlet angle with respect to the rotor blades was very nearly identical in both rotor-only and full stage configurations. The only difference was that the rotor only configuration was able to operate at lower flow rates prior to stall which extended the curves further to the left.

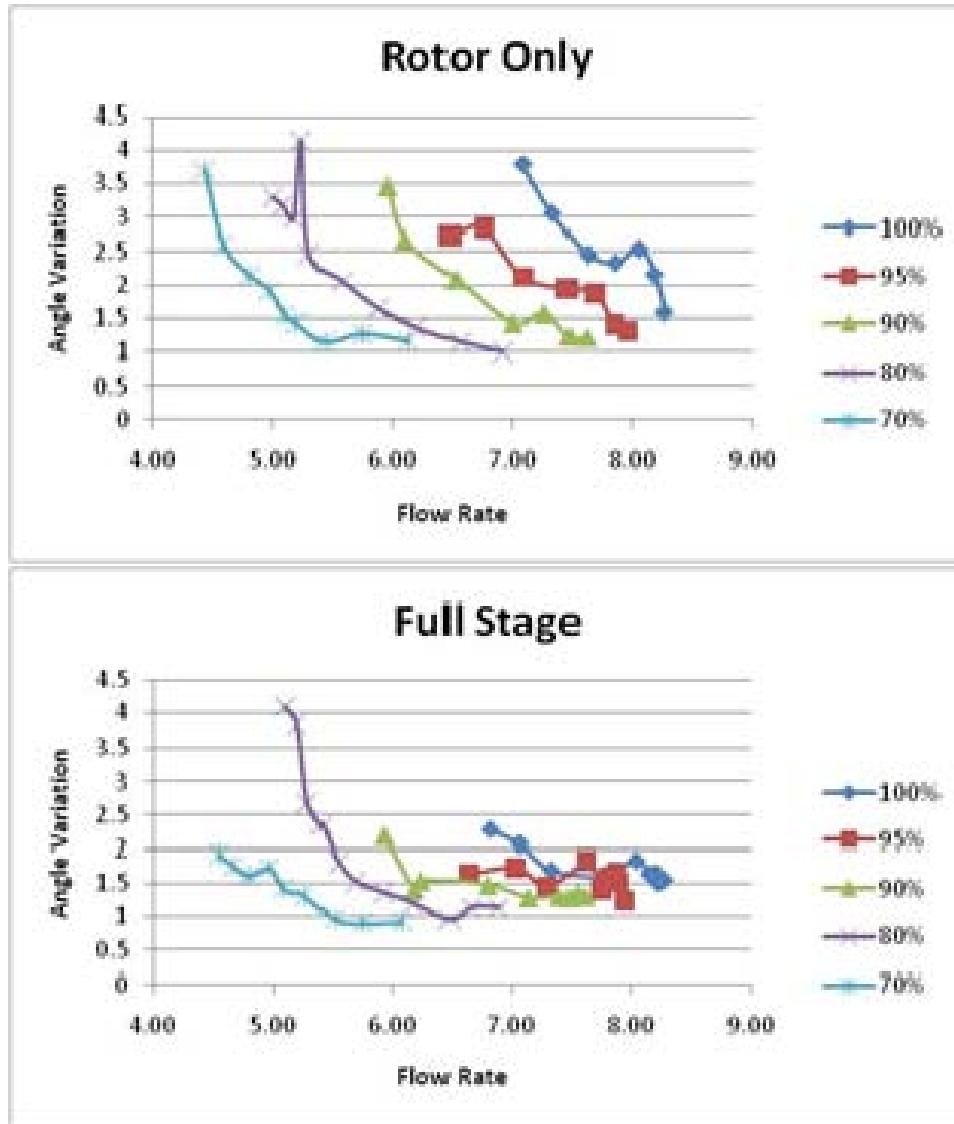


Figure 50. Peak-to-Peak Variation of Relative Inlet Angle in Rotor-only and Full Stage

As shown in Figure 50 curves for the peak-to-peak magnitude for the two operating modes were different in shape and magnitude. This was contrasted by inlet Mach number which behaved similarly in both test rig configurations. The shapes of these curves were similar to the RMS power plots, Figure 42 through Figure 44, where rotor only operations revealed a strengthening of power measurements as the flow rate was throttled and full stage operations were very nearly flat.

An analysis of the relative inlet angles was then conducted to determine the instantaneous maximum relative inlet angle because this angle was related to the loading of an individual blade, growth and separation of the boundary layer, and the inception of stall cells. This data was plotted versus mass flow for all throttle-speed settings and is displayed in Figure 51.

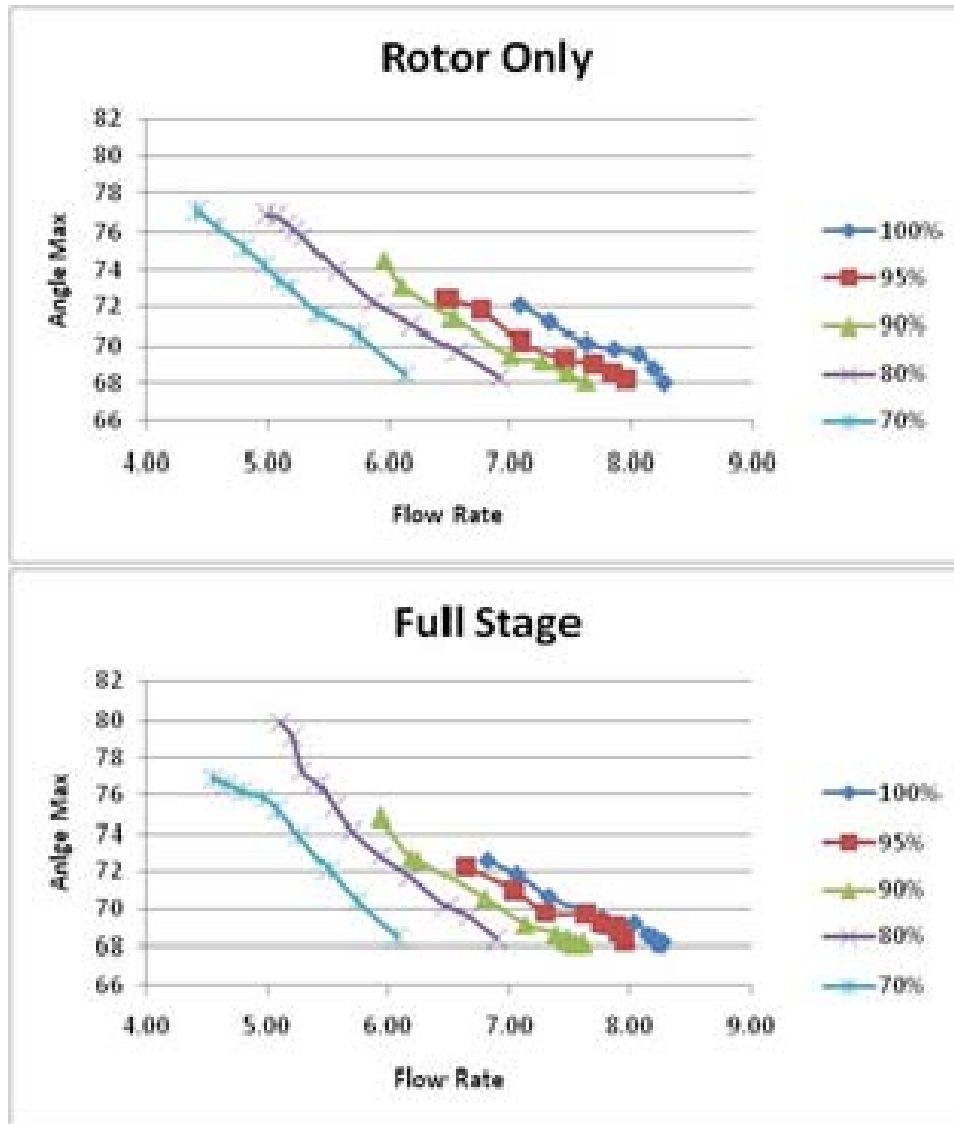


Figure 51. Instantaneous Maximum Relative Inlet Angle in Rotor-only and Full Stage

As shown in Table 5, the analysis of bulk relative inlet angle revealed that the test rig, in the rotor-only and full stage configurations, stalled at approximately the same maximum and mean angles for all speeds hinting at a stall event being initiated by the rotor vice the stator which previous research had theorized that the stator could stall first at the hub. Also shown is a generally more chaotic flow for the rotor-only configuration in a manner similar to what has been previously identified in the RMS power analysis.

Rotor Speed	Rotor Only			Full Stage			% Difference		
	Mean	Maximum	Variation	Mean	Maximum	Variation	Mean	Maximum	Variation
70%	75.3	77.1	3.68	75.7	76.9	1.91	0.26%	0.13%	31.7%
80%	75.1	76.9	3.17	77.8	79.9	3.84	1.77%	1.9%	9.56%
90%	72.5	74.6	3.47	73.5	74.9	2.19	0.68%	0.20%	22.6%
95%	71.1	72.4	2.70	71.4	72.2	1.65	0.21%	0.14%	24.1%
100%	70.2	72.1	3.79	71.4	72.6	2.28	0.85%	0.35%	24.9%

Table 5. Relative Inlet Angle Comparison

C. PRESSURE CONTOUR ANALYSIS

Pressure contour plots of the blade passage were generated using the methodology previously described in Chapter IV. This enabled the visualization of the flow field around the blades at steady-state operations by averaging the pressure data at each blade pitch into a single frame.

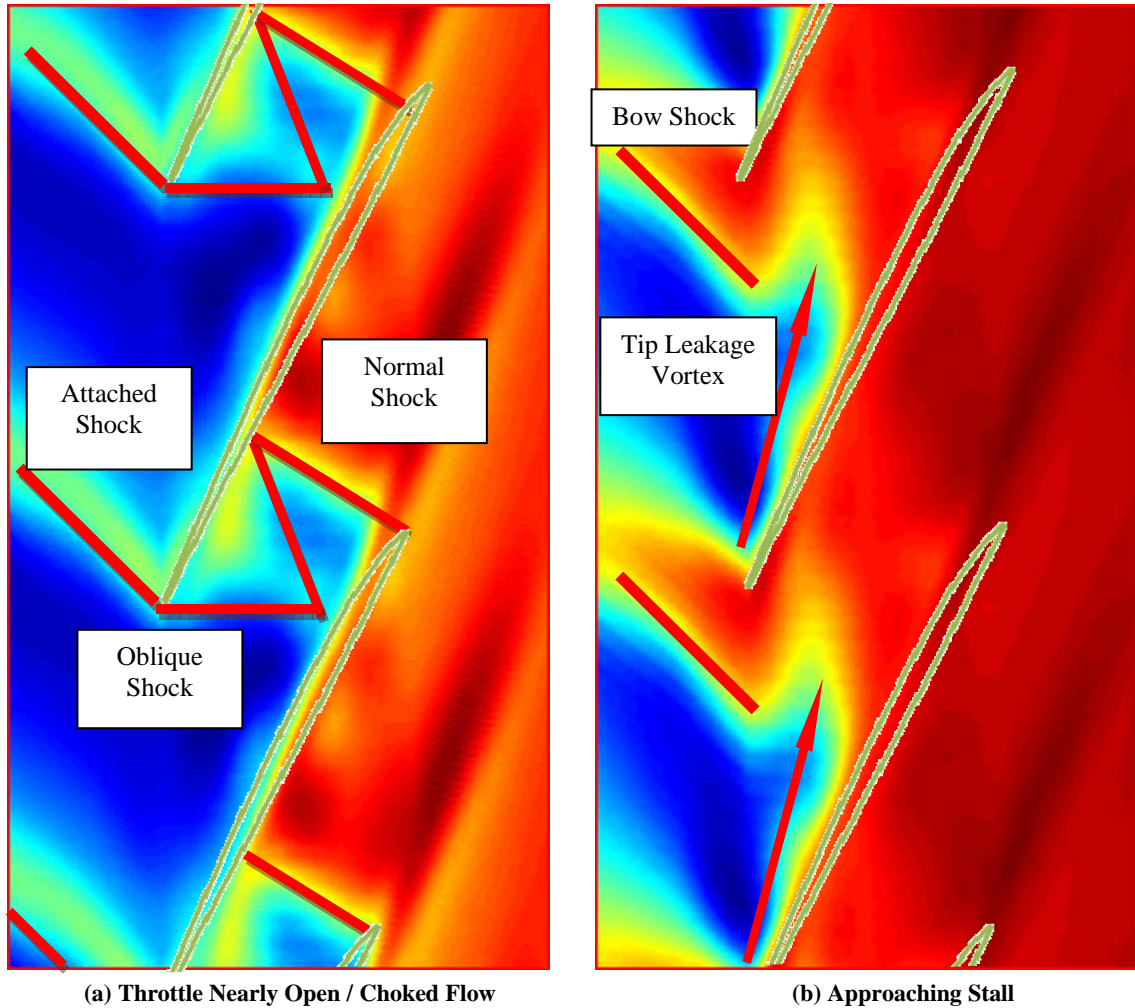


Figure 52. Rotor Only Pressure Contour Plot at 100% Rotor Speed

An Analysis of these pressure contour plots revealed several structures that could be indentified and used to explain the frequency analysis results previously shown. Figure 52a and Figure 52b represent flow fields on opposite ends of the progression from fully open throttle to the pre-stall throttle setting. These two were selected for this sample analysis because they best represented the types of structures found at all speed-throttle profiles.

As shown in Figure 52a, the open throttle mode of operation displayed attached and oblique shocks. The oblique shock reflected off the suction side of the adjacent blade. At open throttle setting a strong normal shock was present at the trailing edge of the blade. This was contrasted by the near-stall throttle, Figure 52b, where the shock had

detached from the blade, which created an unpinned bow shock. The oblique and normal shocks that had moved forward of the passage now experienced a strong tip leakage vortex were it interacted with the detached bow shock and impinged on the pressure side of the adjacent blade.

Figure 53 shows the progression of the casing pressure field in the rotor at 100% speed in the rotor-only configuration as it approached stall, Block A, from an initial full open throttle, Block G.

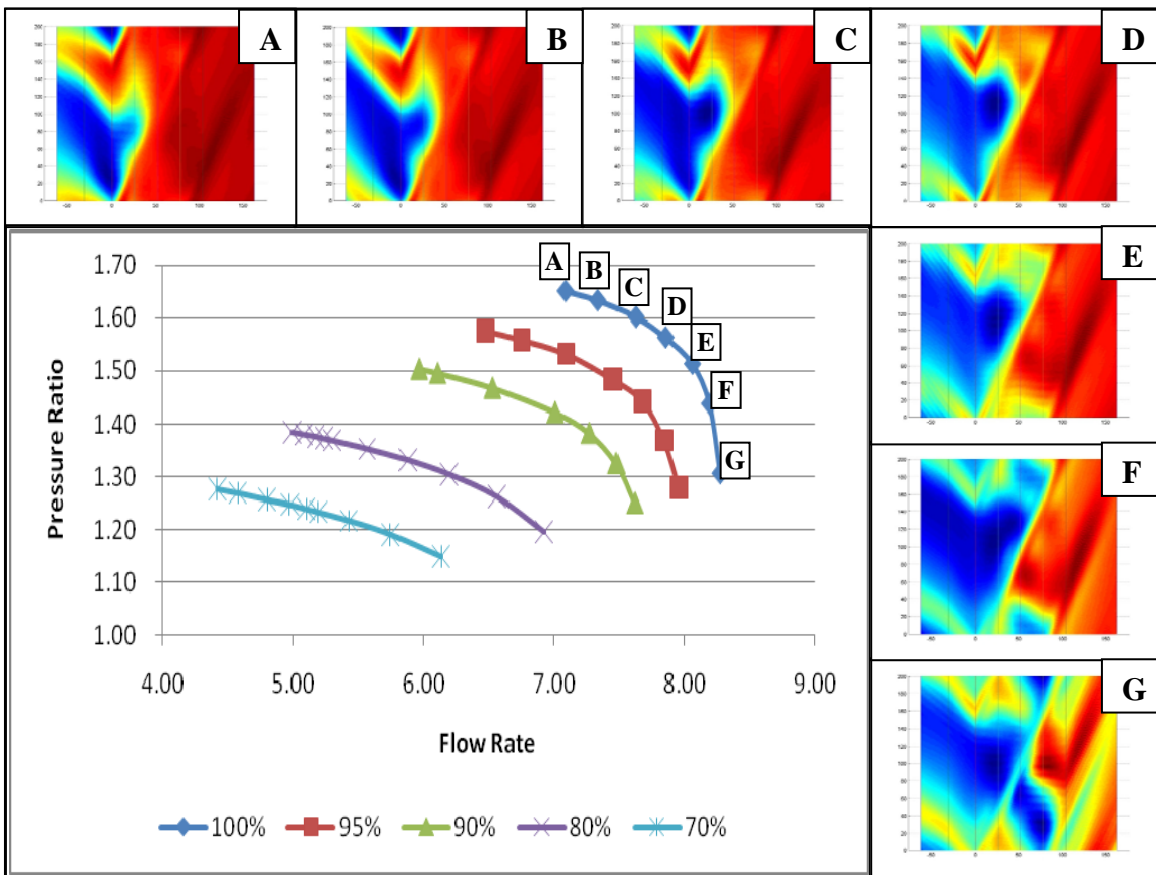


Figure 53. Rotor Only Steady State Pressure Contour Plots at 100% Rotor Speed

Using Figure 52 as a key the following observations of Figure 53 can be noted:

- With the throttle fully open, Block G, presented a oblique and attached shocks with relatively weak pressure gradients. At this throttle setting nearly all the compression was accomplished by the flow turning through

blades and the strong normal shock at the trailing edge; this corresponded to the low efficiency of the rotor in this operation.

- Block E, displays a weak attached, a stronger oblique shocks, and a weak normal shock at the trailing edge. With the compression being shared most effectively between the obliques, normal shock, and blade this corresponded to the peak efficiency achieved in this test series.
- Block D, shows a sudden disappearance of the oblique and normal shocks. This marked the point where the compressor efficiency has begun to fall. This was also the point where the tip-leakage vortex first appeared high velocity air was injected deep into the blade passage which deformed the shock.
- Block A, the pre-stall condition of this rotor displayed no oblique and only a normal bow shocks. Also present was a strengthened tip leakage vortex that impinged on the pressure side of the blade.

Figure 54 shows the progression of the rotor in the full stage configuration at 95% rotor speed as it approached pre-stall conditions, Block A, from an initial full open throttle, Block I. The Block lettering is irregular in this figure so that labelling would mirror the additional figures found in the appendices. It is also important to note that these plots differ from those shown above with the elimination of the Kulite Probes positioned at the trailing edge of the blade. This has the net affect of creating a “bleeding” of the pressure contours after the last probe.

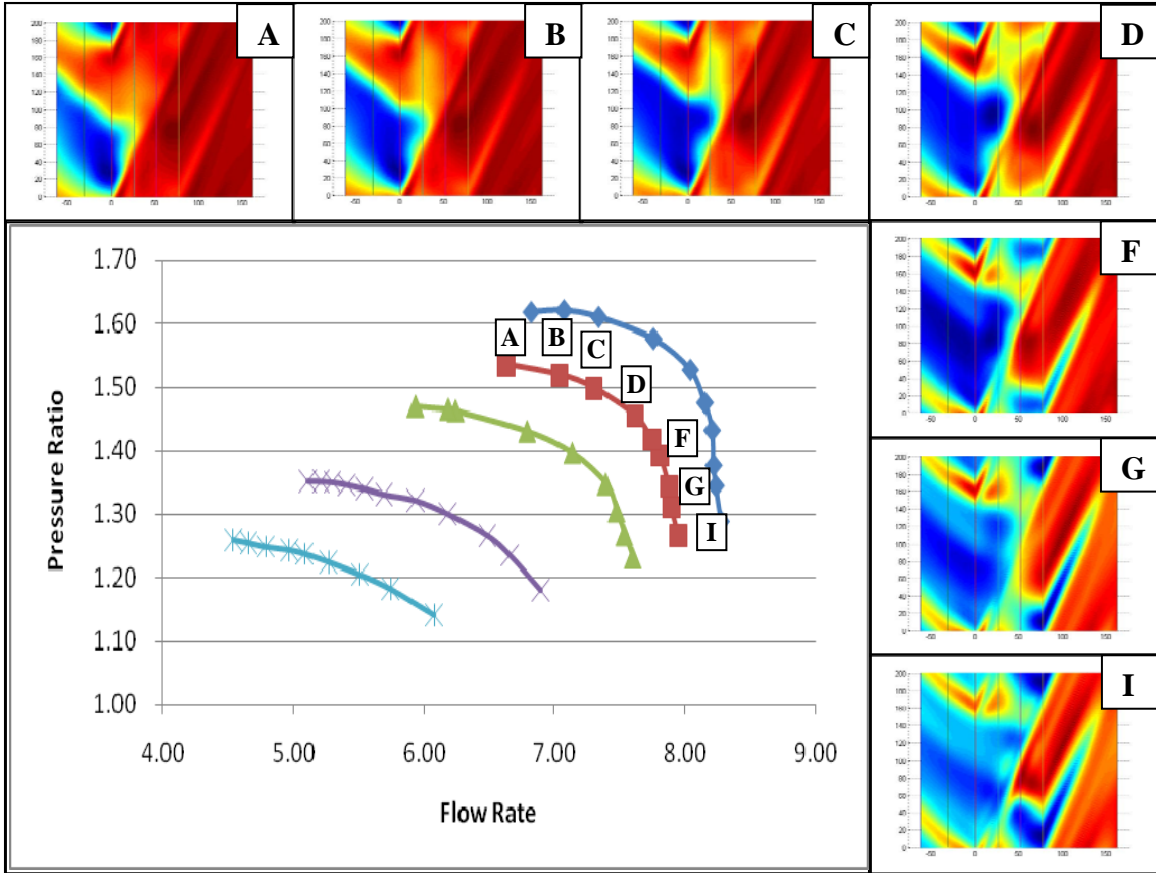


Figure 54. Full Stage Steady State Pressure Contour Plots at 95% Rotor Speed

While Figure 54 maintains a similar progression from the attached shock and oblique, Blocks D thru I, to the bow shocks seen in Blocks A thru C there are differences in the last two pre-stall datasets:

- In Blocks A and B the characteristic tip vortex had diminished vice strengthened like the rotor-only configuration. In its place was a more evident shock-boundary layer interaction.

This difference was most likely due to the flow restriction caused by the stator that had the effect of moving higher pressure air forward into the rotor blade passages. It is important to note that a similar progression from open throttle to pre-stall occurred at all rotor speeds in both the rotor-only and stage configuration.

D. CORRELATION OF FREQUENCY AND TIME DOMAIN ANALYSIS

Drawing together the products of the time and frequency analysis, in the steady state, an attempt to correlate the findings was critical in providing some justification for the large abrupt changes in flow that were recorded.

Figure 55 shows blade passage plots for the TCR at 100% Speed in the Rotor-Only configuration.

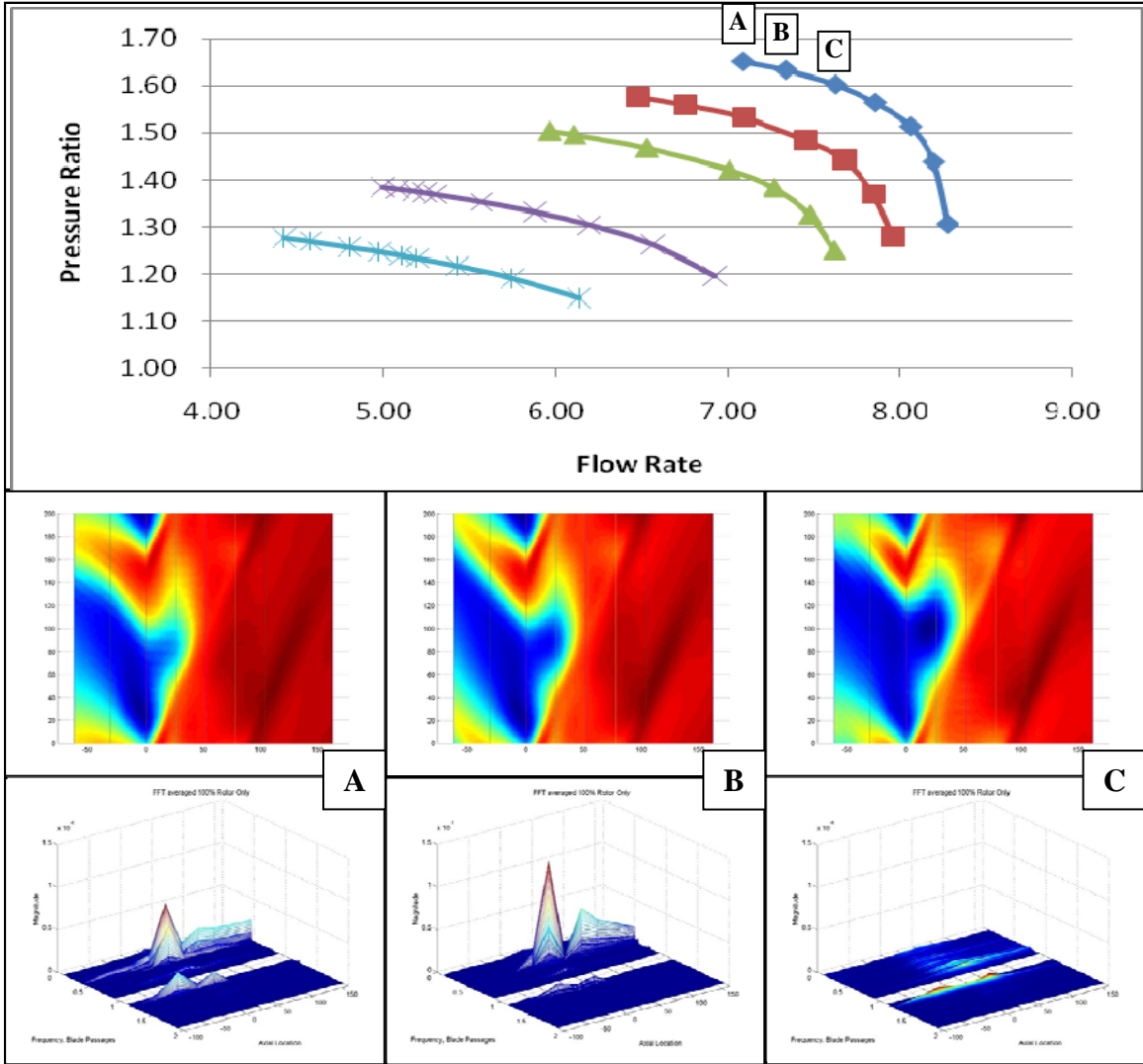


Figure 55. Rotor Only Pressure Contour and Frequency Data Comparison at 100% Rotor Speed

Using components from the previously discussed analysis, the following observations can now be made:

- An increase in RMS power from Condition C to Condition B was experienced by the rotor. This corresponded to the speed-throttle profile where the bow shock preceding the blades suddenly detached from the leading edge.
- A decreased in RMS power from Condition B to Condition A was also shown. As shown in Figure 55, there was a corresponding forward shift of the bow shock and a reduction in the pressure gradients associated with the tip leakage vortex.

These observations are reinforced by Figure 56 where the standard deviation of the pressure was plotted within the blade passages for the same throttle settings. As shown there was a characteristic shift of the high deviation oscillations from the blade tip to mid-passage. This indicated movement in the bow shock, which was not unusual, as it was detached from the leading edge.

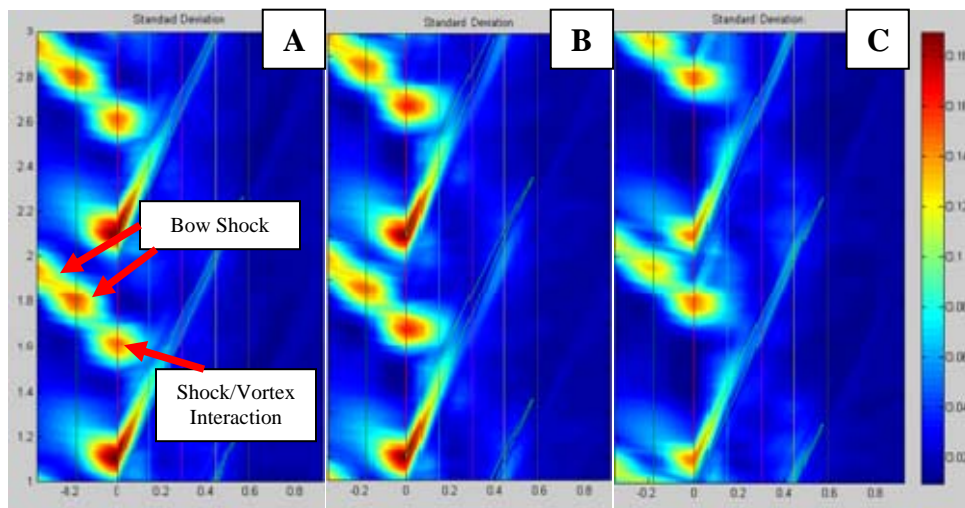


Figure 56. Rotor-Only Standard Deviation Pressure Contours at 100% Rotor Speed

Similarly, Figure 57 shows the progression of conditions within the blade passage at 95% Speed in the Full Stage Condition.

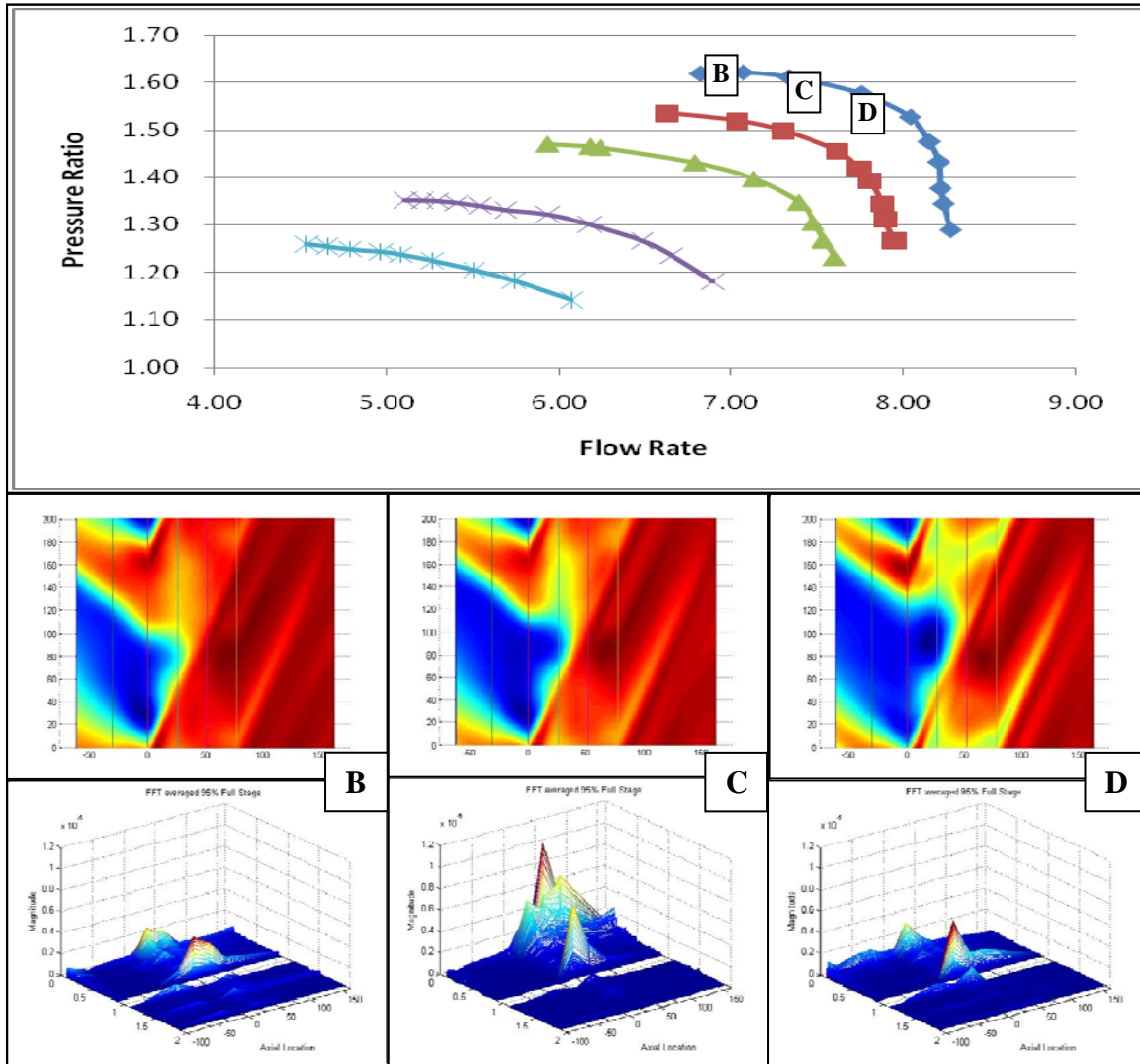


Figure 57. Full Stage Pressure Contour and Frequency Data Comparison at 95% Rotor Speed

The following observations are made:

- An increase in low frequency oscillations immediately after the attached shock detached from the blade (Condition D to C).
- An attenuation of the oscillation after the higher pressure fluid pushed the shock forward ahead of the blade (Condition C to D).

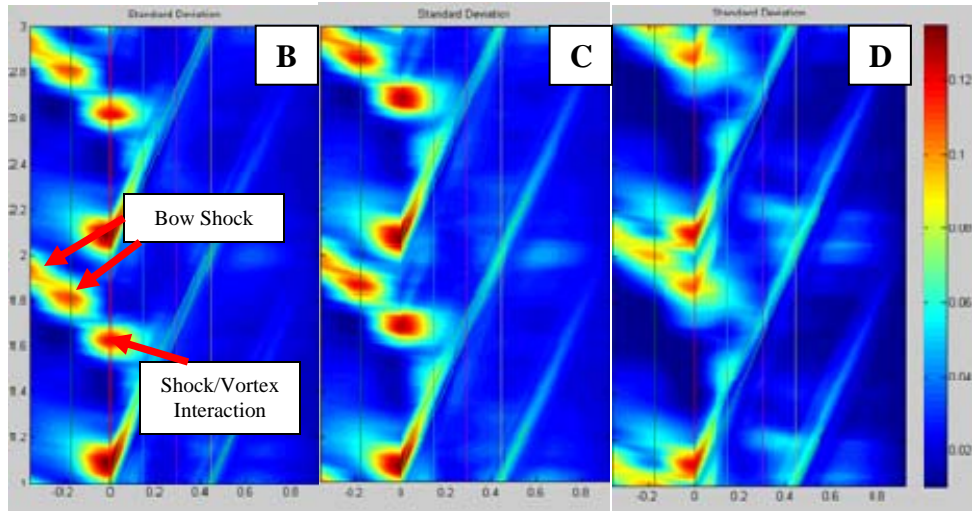


Figure 58. Full Stage Standard Deviation Pressure Contours at 95% Rotor Speed

The standard deviation plot for these runs, Figure 58 shows the same characteristic forward shift of the shock and reduction in tip vortex.

E. STALL INVESTIGATION

As discussed previously, stall events are investigated in a single test run at a given speed and usually requires a longer time run out than the standard 2-second sample required for steady state operations. Because of the extreme file sizes associated with these stall tests a targeted approach was required so that only those rotations of interest were analyzed.

1. Rotor Only Configuration

Since stall was always accompanied by large changes in rotor speed this data was plotted so that the rotation where stall first occurred could be easily identified.

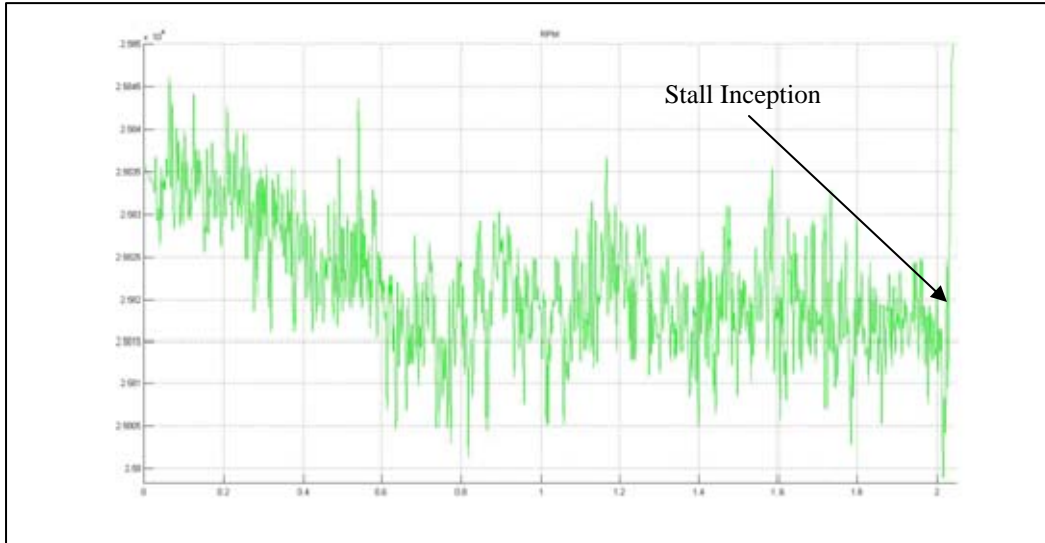


Figure 59. Full stage RPM Entering Stall Event at 95% Rotor Speed

Figure 59 shows the rotor in full stage configuration as it approached stall at 95% rotor speed. As shown, there was a characteristic surge in rotor speed at the instant of stall. Since the initiation of a stall cell was associated with great deviation in flow as it was forced around the blockage into adjacent blade passages the bulk inlet angle was then plotted to assist in the identification of the precise rotation where stall first occurred, Figure 60.

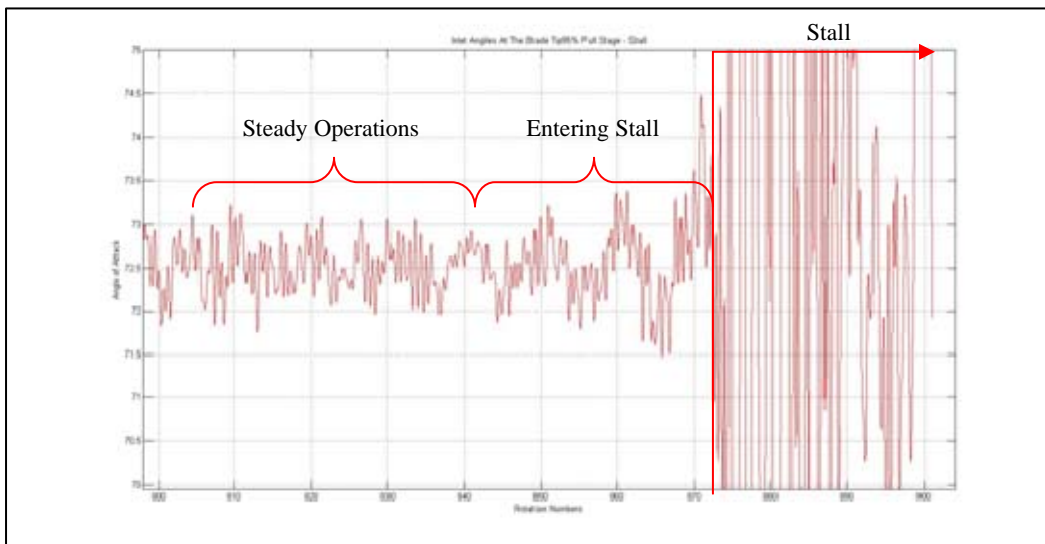


Figure 60. Full Stage Bulk Inlet Angle Entering Stall Event at 95% Rotor Speed

Pressure contour plots of the entire rotor were then assembled over the identified rotations in the Stead, Pre-Stall, and Stall regions identified so that the onset conditions of stall could be more clearly visualized, Figure 61. The features that characterize these regions within a full stage are:

- Blade Passage Instabilities existed in all operating conditions; including steady operating conditions.
- As the rotor enters stall it went through several cycles of stall cell formation and recovery. While the stall cell grew across more blade passages it moved around the annulus backward in the relative frame.
- Once the entire rotor was stalled, it began to surge where it partially recovered and stalled as discussed in the introductory chapter.

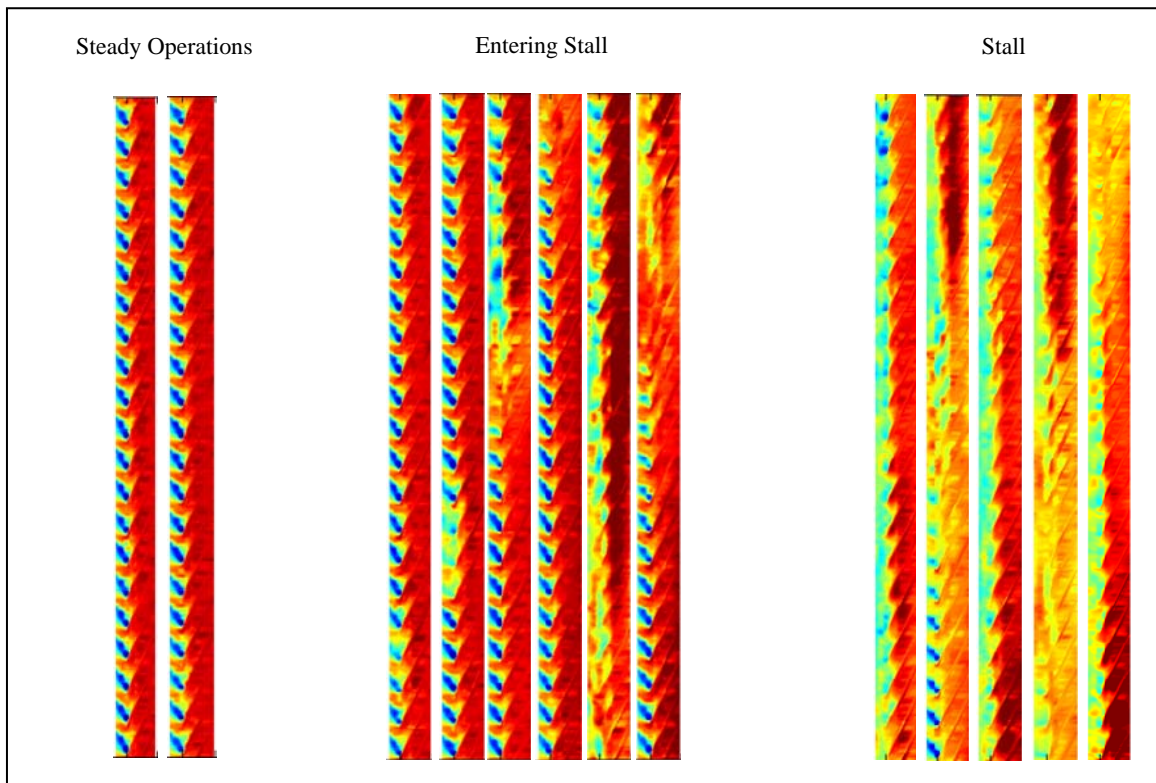


Figure 61. Full Stage Entering Stall at 95% Rotor Speed

An analysis of the blade passages in steady state operations focused on the region of instability and adjacent effected zones, Figure 62. As shown regions adjacent to the instabilities, that decreased incident angles, tended to “grow” larger tip leakage vortices. This was expected since this change in incident worked to further decrease pressure on the suction side of the blade and increases the gradient across the blade tip driving more flow toward the blade edge.

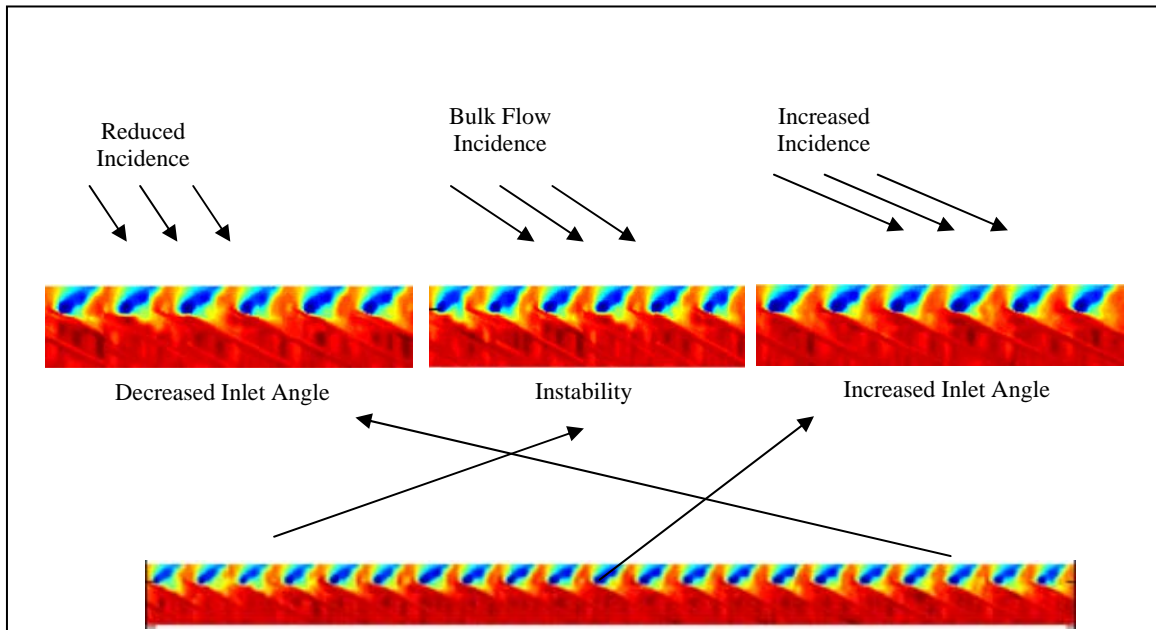


Figure 62. Full Stage Steady State Blade Passage Instabilities at 95% Rotor Speed

2. Full Stage Configuration

The above was analysis conducted at 100% of rotor speed in the rotor only configuration. Plotting the rotor speed versus time revealed the approximate location of the initiation of stall at the instant of rotor over-speed, Figure 63.

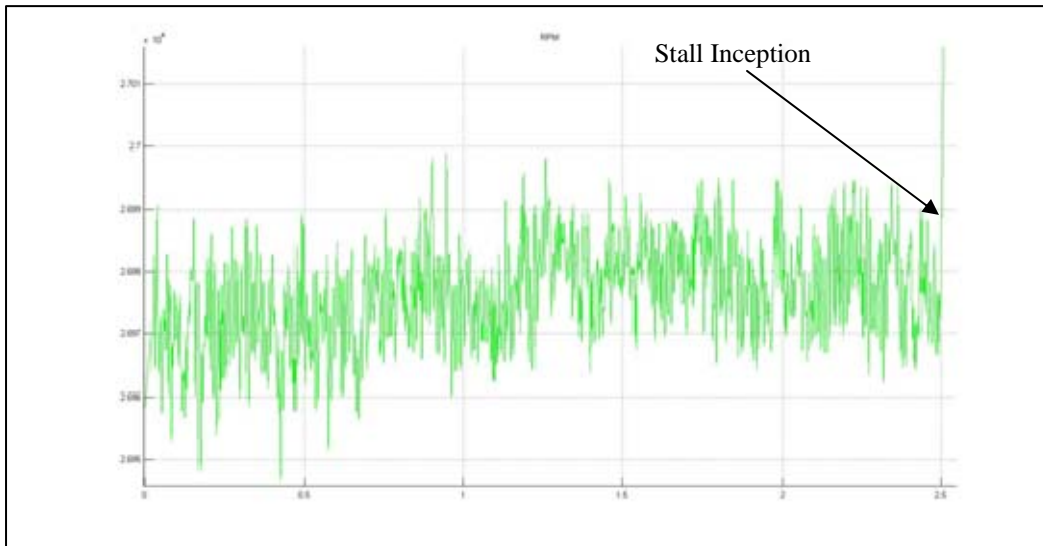


Figure 63. Rotor Only RPM Entering Stall Event at 100% Rotor Speed

This approximate location was then used to identify the exact moment of stall using the bulk flow inlet angle.

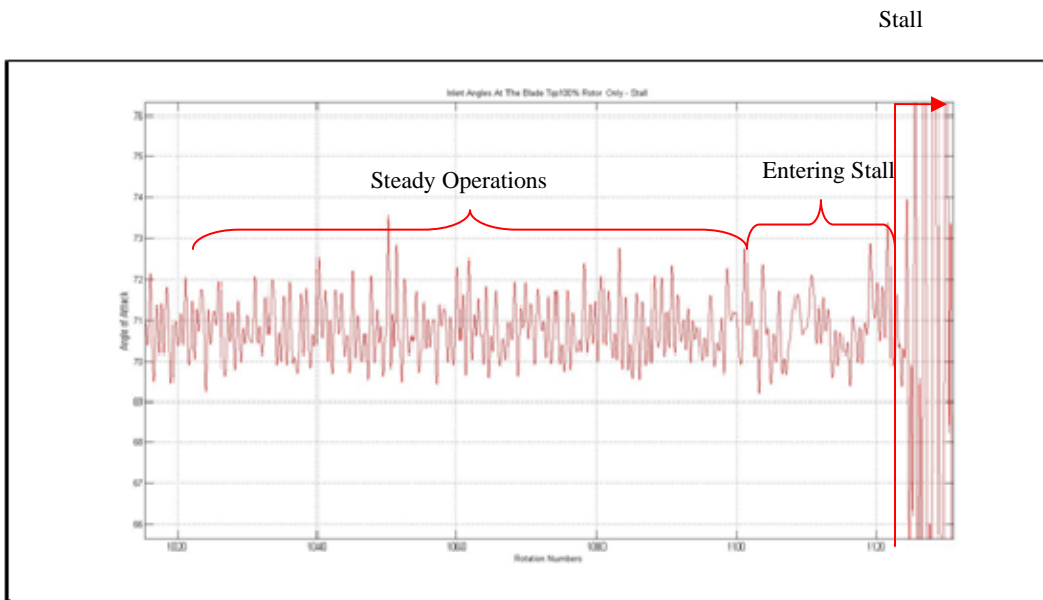


Figure 64. Rotor Only Bulk Inlet Angle Entering Stall Event at 100% Rotor Speed

As shown in Figure 64, the same three regions of steady, pre-stall, and stall were still present however the region of pre-stall was greatly diminished in length and did not display the same prominent oscillations that the full stage did.

Generating contour plots of rotations within three regions yielded the following characteristic blade passages over time, Figure 65.

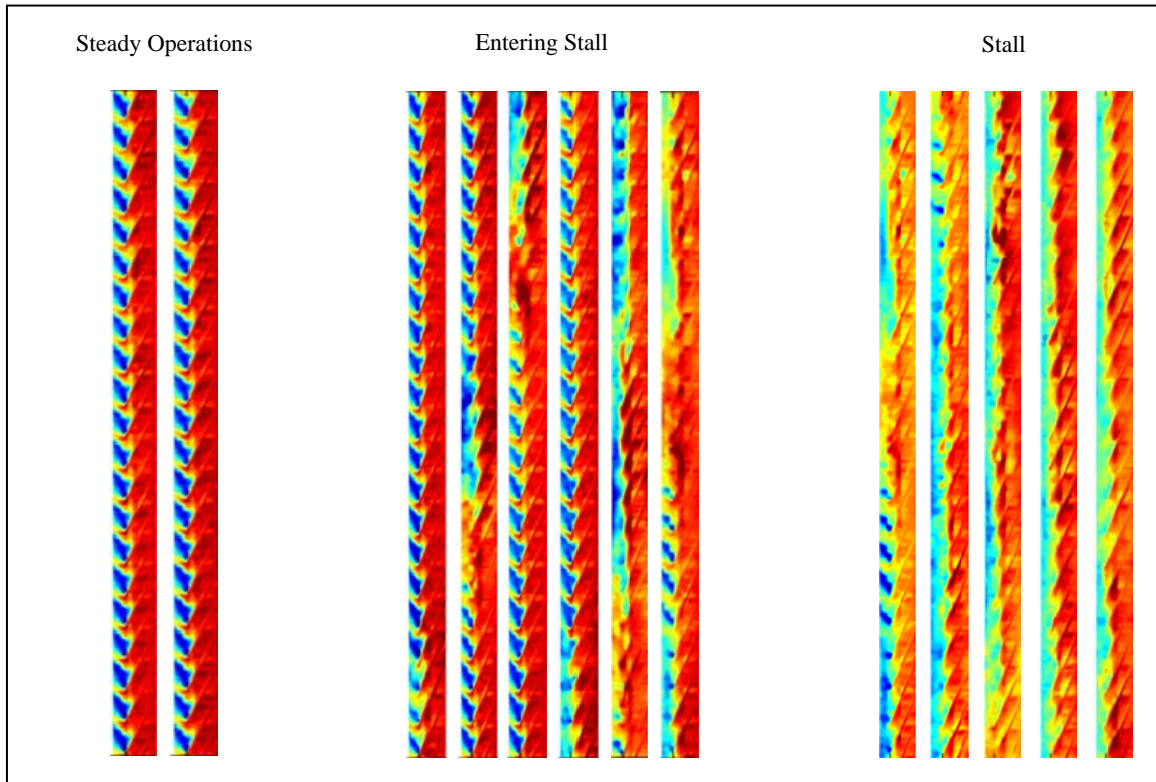


Figure 65. Rotor Only Entering Stall at 100% Rotor Speed

An analysis of the rotations within these operating regions yielded the following observations when compared to the full stage analysis:

- The rotor still exhibited blade passage instabilities even when operating in steady state conditions.
- Inception of stall was initially focused around a few blades but quickly began to expand to adjacent blades as flow was redirected around the stall cell. The relative motion of the stall cell was retrograde to rotor motion.
- Once the stall cell expanded to cover the entire blade, it did not go through a cycle of recovery and stall like the full stage.

An analysis of stall cell formation and growth in the steady operations region was also conducted, Figure 66.

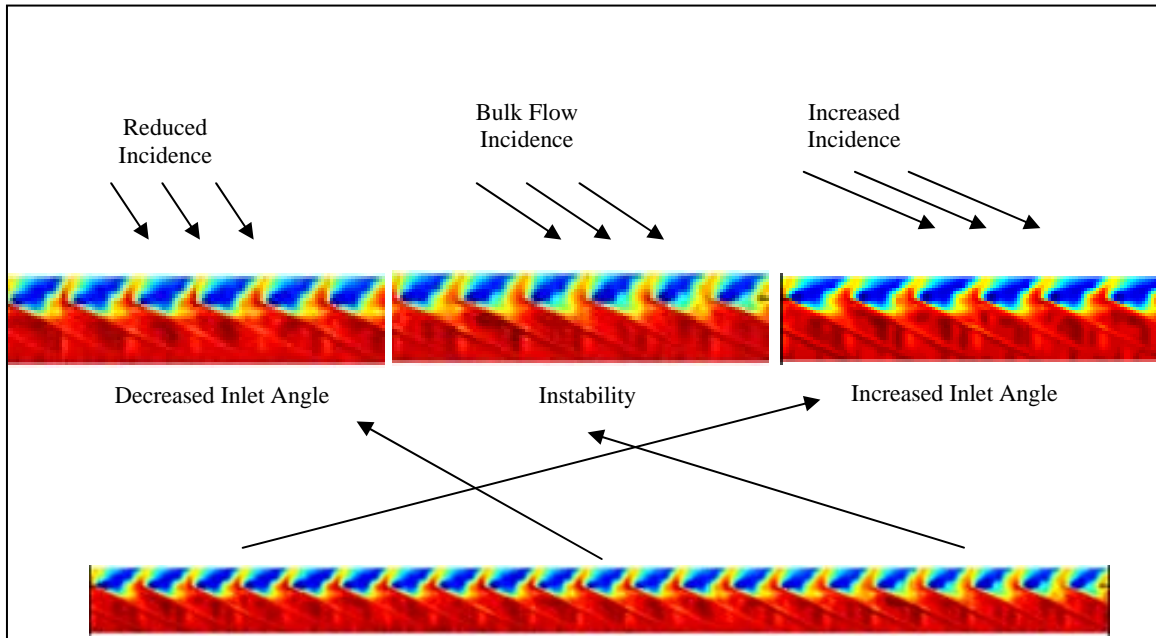


Figure 66. Rotor Only Steady State Blade Passage Instabilities at 100% Rotor Speed

Figure 66 shows the location of steady state instability and the adjacent blade passages that are affected by the flow moving around the blockage. As noted in the full stage instability analysis, areas of decreased incident tended to display larger tip leakage vortices because of the low-pressure regions that were created on the suction side of the blade. This was contrasted by the areas of increased incident where lower-pressure regions were formed on the pressure side of the blade, consequently reducing the size of the tip leakage vortices.

VIII. CONCLUSIONS

The purpose of this research was to develop an integrated easy to use data analysis tool to enable rapid and consistent data analysis regardless of configuration or rotor geometry. This tool then enabled a detailed investigation of the Transonic Compressor Rig (TCR) to characterize differences in the behavior of the rotor-only and full-stage configurations, to identify candidate pre-stall indicators that could be used to predict stall prior to its inception, and to develop a more complete understanding of how a rotor departs from the idealize axi-symmetric assumption when operating at steady-state.

A. INTEGRATED DATA ANALYSIS TOOL

The TCR Data Analysis tool developed for this research enabled a comprehensive analysis of all the data captured during the experimental phase. The capability to rapidly access the relevant information within a given test within hours of its completion will allow future experimentation to be more responsive to failures in equipment or enable deeper investigation of unexpected behavior on the fly. This code base was developed in such a way that data from any rotor can be quickly imported and analyzed with small adjustments to geometric constants available in the GUI. This provides a consistency to future analysis that up to this point was not possible.

B. STEADY-STATE OPERATION

The analysis of the stage in steady-state operation revealed a configuration that was much stiffer than the rotor only configuration since the RMS power was less concentrated in the low frequency bands. This stiffening is largely explained by the stator acting to effectively reduce the air mass behind the rotor since it was this mass that is inversely proportional to frequency which is raised and then attenuated.

A strong correlation between bulk flow maximum relative inlet angle and stall inception was also found with both configurations achieving a 71-degree inlet flow angle in the sonic speeds (90% to 100%) and 75-degrees inlet flow angle in the subsonic and

transonic speeds (70% and 80%). Further analysis comparing the frequency domain data with the time-average pressure contour plots identified a connection between RMS power and the presence of an unpinned bow shock.

Investigation of the standard deviation measured at each data point within the passage over an entire test run also showed that regions of large deviation traveled forward of the blade and into a mid pitch location just prior to stall. In all cases, this instability travelled from the blade tip toward 0.6 times the blade pitch. These two factors, bulk inlet angle and instabilities moving toward pitch center, stood out as indications that a stall event was imminent.

C. STALL INCEPTION ANALYSIS

Analysis of the rotations just preceding and following a stall event focused on the steady nature of any pre-stall instability, stall cell development and growth, and the behavior of the cells once the cell has formed across the entire rotor. In both configurations, the stall cells formed in localized region, across 3-4 blade passages, which rotated at part speed. Once the throttle position was adjusted, the stall cell grew to cover the whole annulus within 5-10 rotations.

Primary differences in behavior between the rotor-only and full stage configuration was in the transition period from steady operation toward stall and the stall event itself. The stage exhibited strong oscillations in the inlet angle going into stall and displayed a greater ability to recover. Once having stalled it then began to partially recover and stall in a cyclical way. The rotor by contrast showed no oscillation in inlet angle during the transition phase and displayed no ability to recover from stall once the annulus was completely stalled.

IX. RECOMMENDATIONS

As discussed in previous theses the incorporation of a more realistic engine installation would lend more validity to the results discussed in this research. This would require a shorter or serpentine intake to the TCR so that it would operate similarly to any future military aircraft.

Future tests using the full stage will also require an increase in the number of pressure transducers over the stator so the interaction between the rotor and stator can be better evaluated and understood. As currently outfitted, it is not possible to sense any flow disturbance downstream of the rotor or the presence of instabilities on the stator. Since it is these rotating instabilities on the stator that are the root cause of compressor surge identifying their location and strength in relation to stall cells on the rotor is critical to developing a better understanding of the TCR in this configuration. This system should also sample up to the Kulites theoretical limits of 300 kHz providing a greater amount of resolution to the data already being processed.

THIS PAGE INTENTIONALLY LEFT BLANK

LIST OF REFERENCES

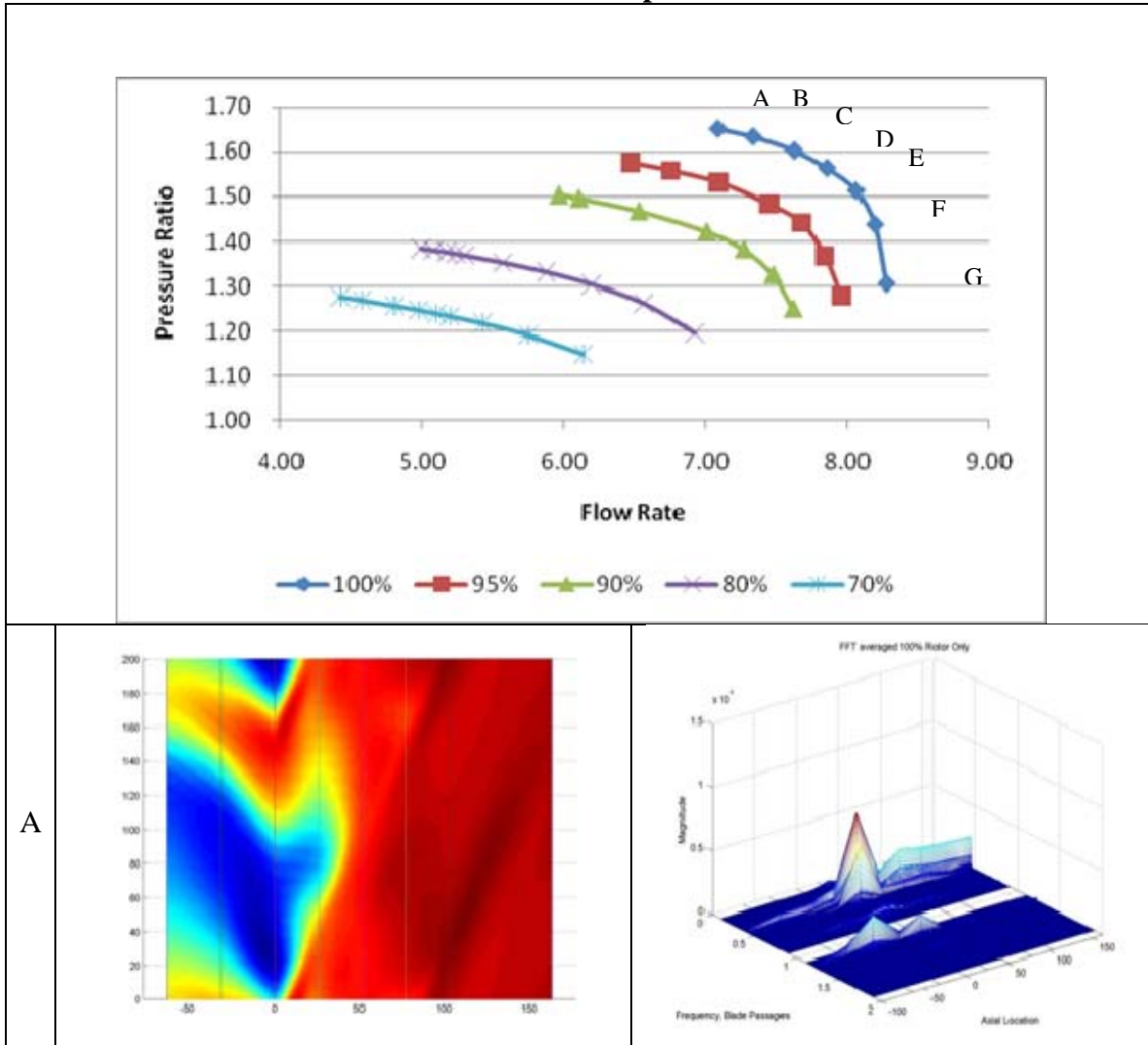
- [1] N.I. Sanger, "Design of a Low Aspect Ratio Transonic Compressor Stage Using CFD Techniques." ASME Journal of Turbomachinery. Vol. 118. July 1996, pp. 479-491
- [2] M.W. Rodgers, Unsteady Pressure Measurements on the Case Wall of a Transonic Compressor. Master's Thesis. Naval Postgraduate School, Monterey, CA, June 2003.
- [3] I. Villegas, Flow Filed Surveys In a Transonic Compressor Prior to Inlet Steam Ingestion Tests. Master's Thesis. Naval Postgraduate School, Monterey, CA, September 2005.
- [4] M.D. Brunner, Experimental and Computational Investigation of Flow in a Transonic Compressor Inlet. Master's Thesis. Naval Postgraduate School, Monterey, CA, September 2005.
- [5] T. Payne, Inlet Flow-Field Measurements of a Transonic Compressor Rotor Prior to and Suring Steam-Induced Rotating Stall. Master's Thesis. Naval Postgraduate School, Monterey, CA, December 2005.
- [6] S.E. Zarro, Stead-State and Transient Measurements Within Compressor Rotor During Steam-Induced Stall at Transonic Operational Speeds. Master's Thesis. Naval Postgraduate School, Monterey, CA, Septemeber 2006.
- [7] A.J. Gannon, G.V. Hobson, T.A. Payne and S.E. Zarro, "The Effect of Steam Ingestion on Transonic Rotor Stall Margin." ASME GT2007-28068. Gas Turbine Congress and Exhibition. Montreal, Canada, May 2007.
- [8] J.J. Koessler, Experimental Investigation of High-Pressure Steam Induced Stall of a Transonic Rotor. Master's Thesis. Naval Postgraduate School. Monterey, CA, June 2007.
- [9] A.J. Gannon and G.V. Hobson, "Pre-Stall Modal Instabilities in a Transonic Compressor Rotor". ISABE-2007-1348. International Symposium of Air Breathing Engines. Beijing, China, September 2007.
- [10] A.J. Gannon and G.V. Hobson, "Pre-Stall Instability Distribution Over a Transonic Compressor Rotor." ASME GT2008-51512. Turbo Expo 2008: Power for Land, Sea, and Air, Berlin, Germany, June 2008.

- [11] A.M. Hurley, Experimental Investigation of High-Pressure Steam-Induced Surge in a Transonic Compressor Stage. Master's Thesis. Naval Postgraduate School. Monterey, CA, June 2008.
- [12] P. Hill and C. Peterson. Mechanics and Thermodynamics of Propulsion. Massachusetts: Addison-West Publishing Company, Inc., 1992.

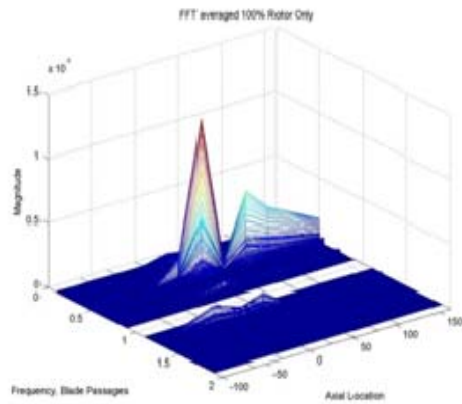
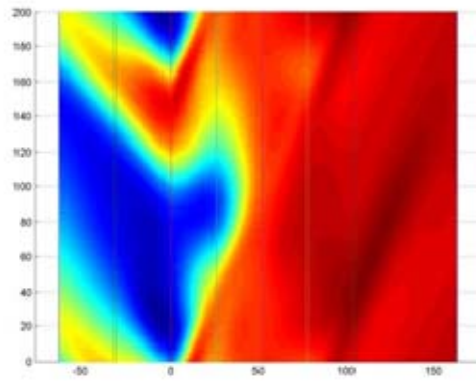
APPENDIX A: ROTOR-ONLY KULITE DATA

Rotor Only Data

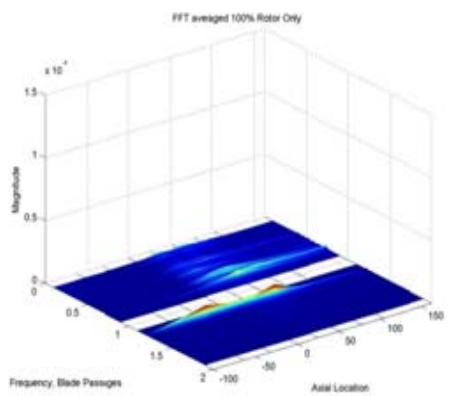
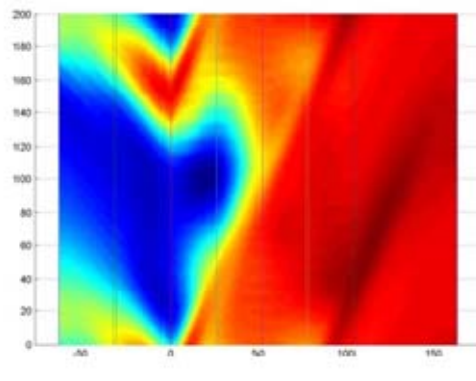
Steady State Analysis Plots 100% Rated Speed



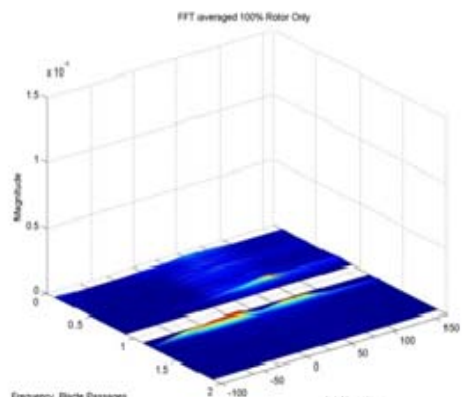
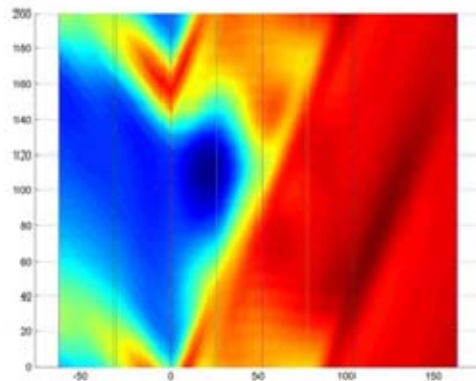
B



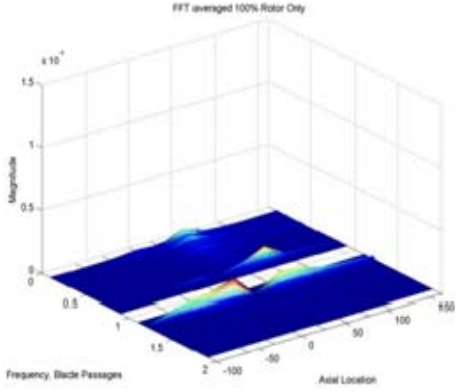
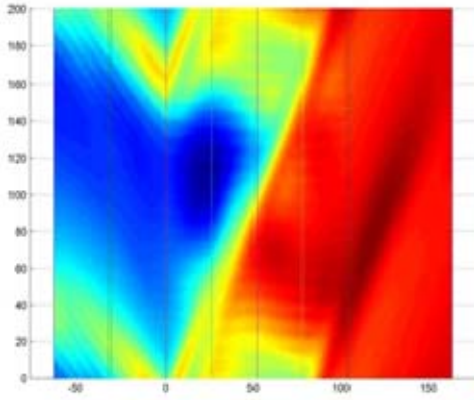
C



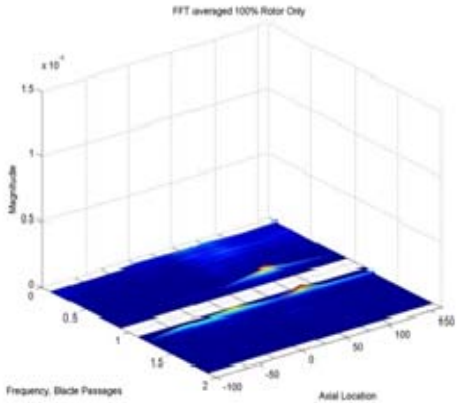
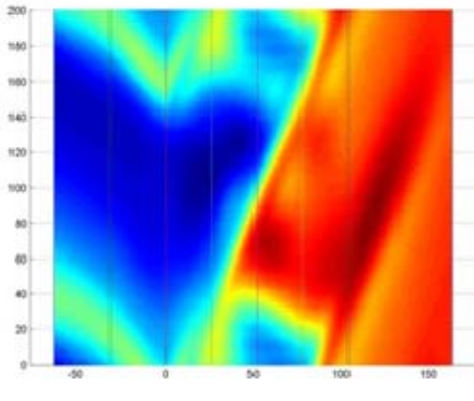
D



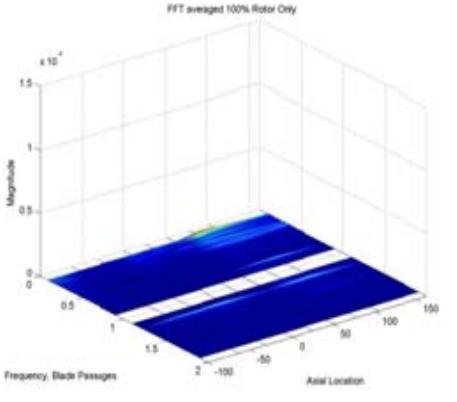
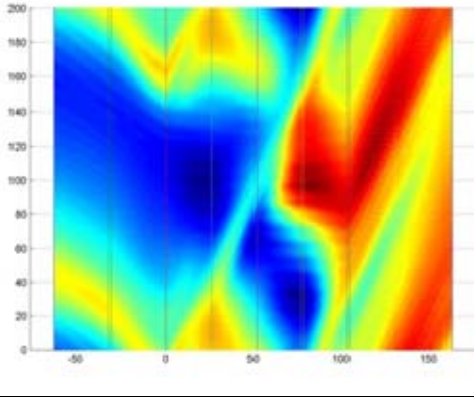
E



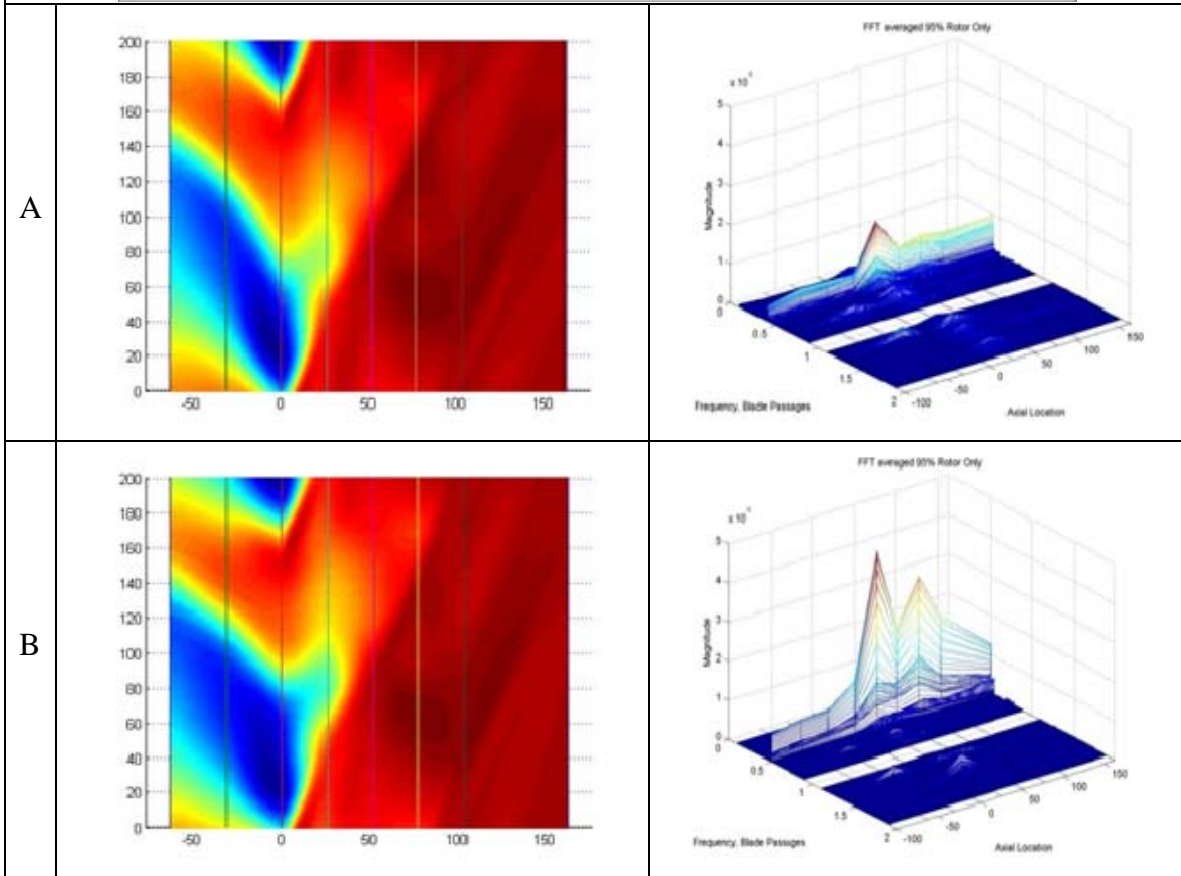
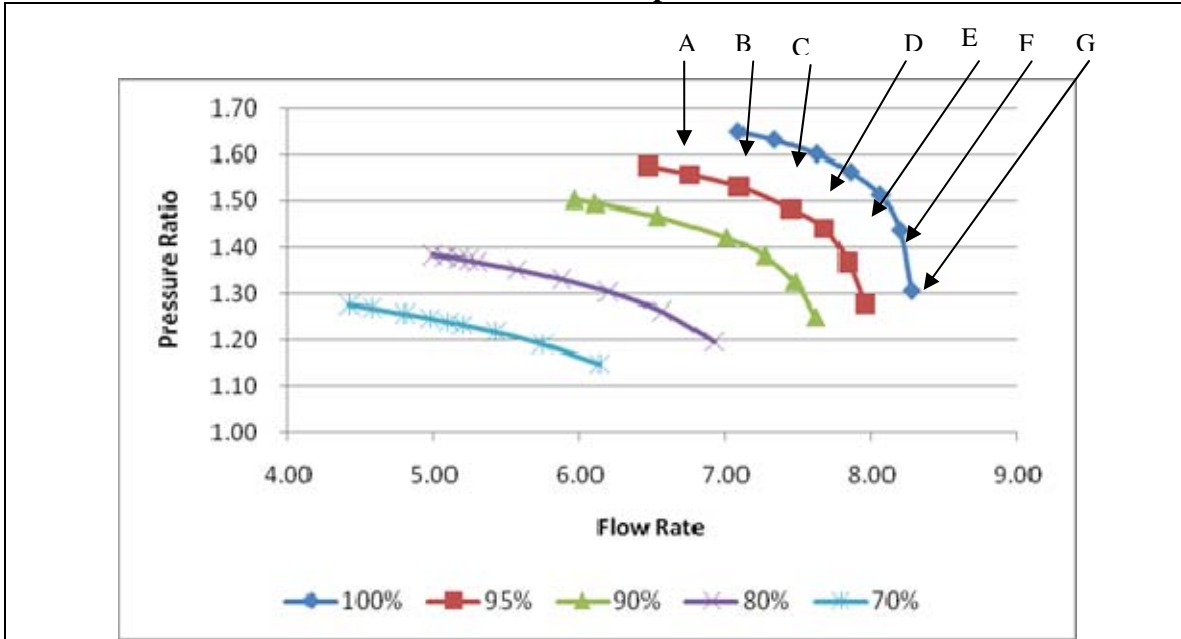
F

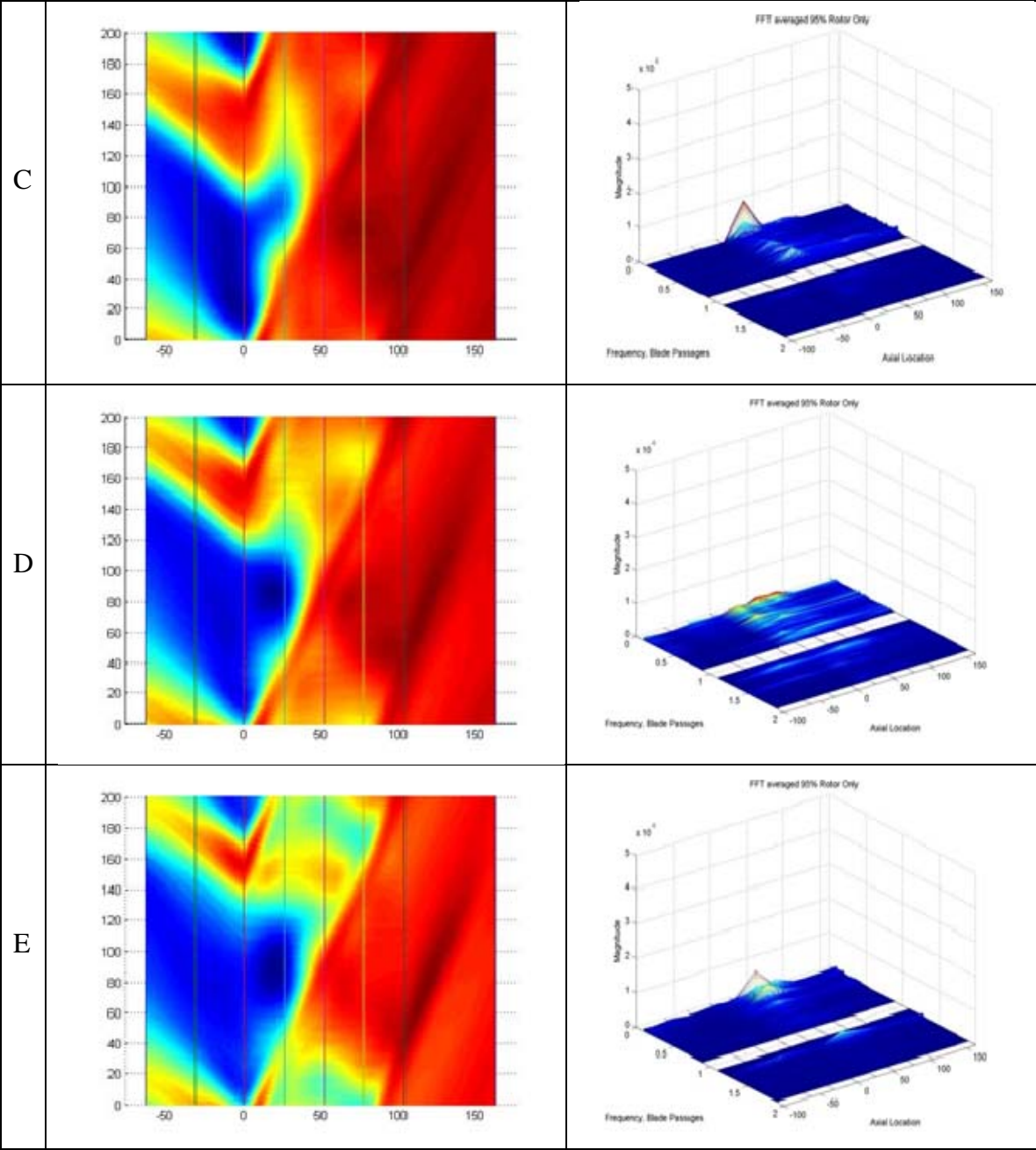


G

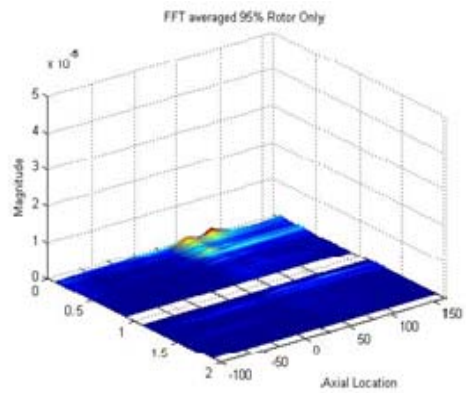
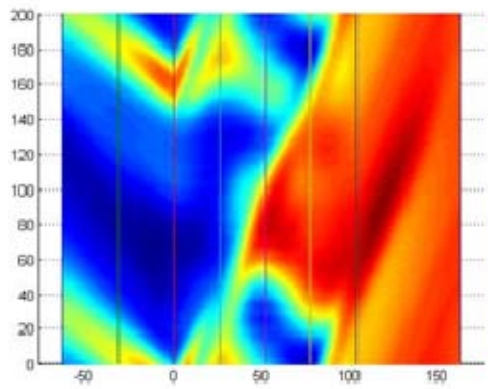


95% Rated Speed

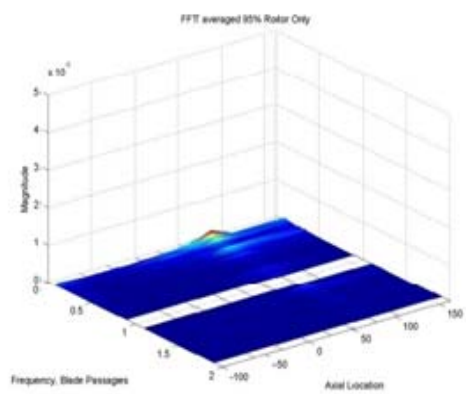
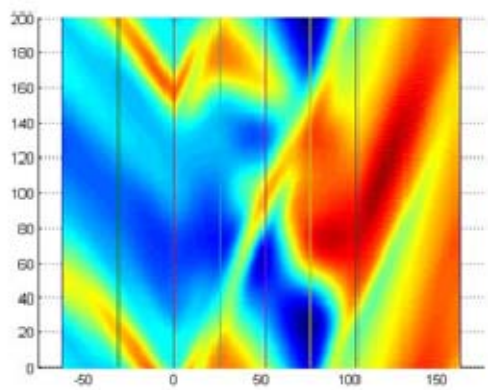




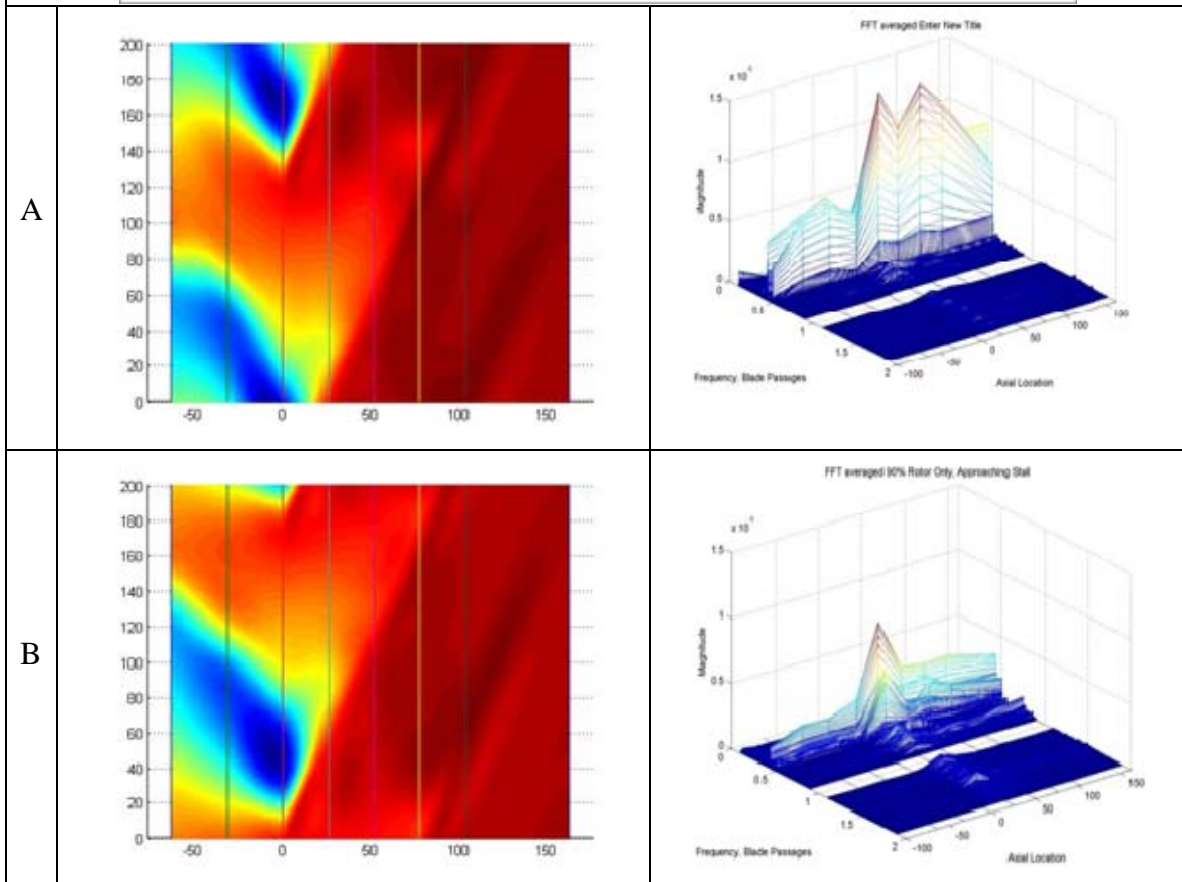
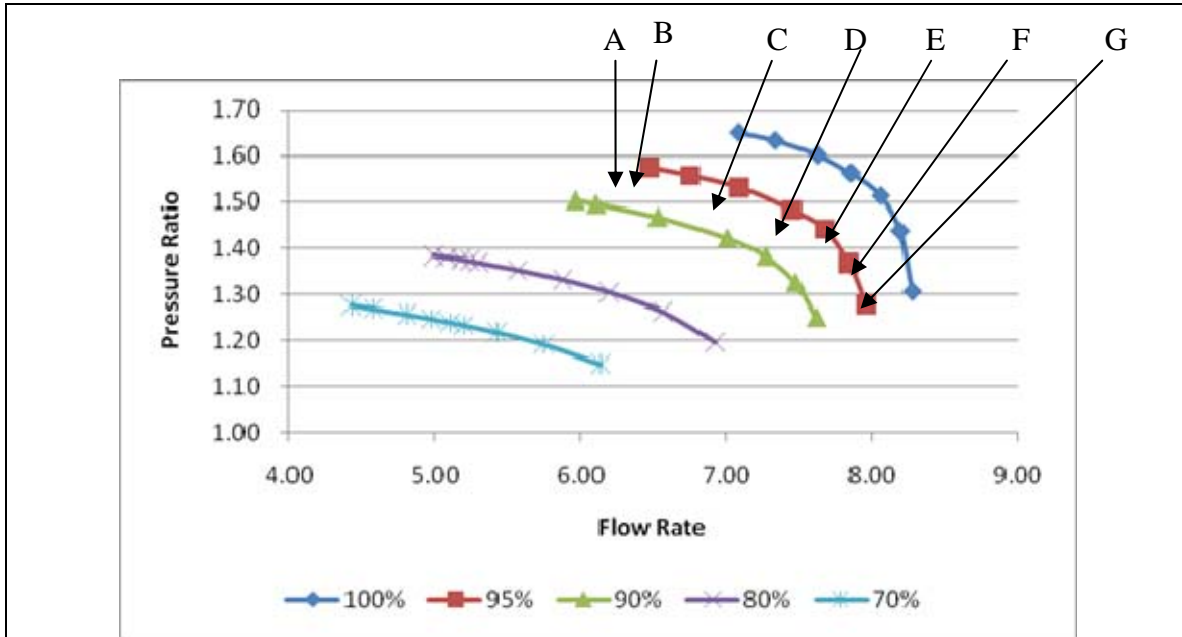
F

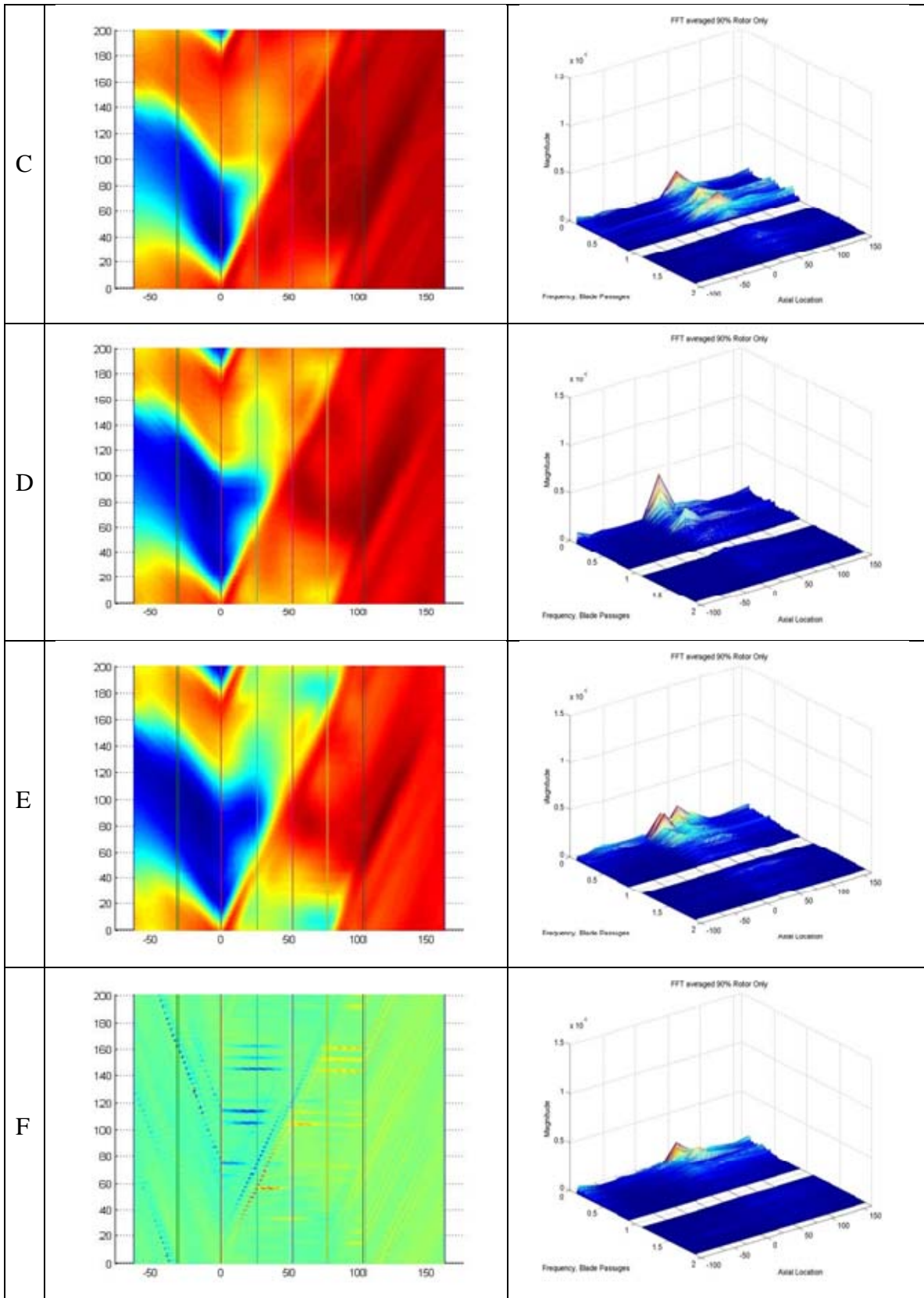


G

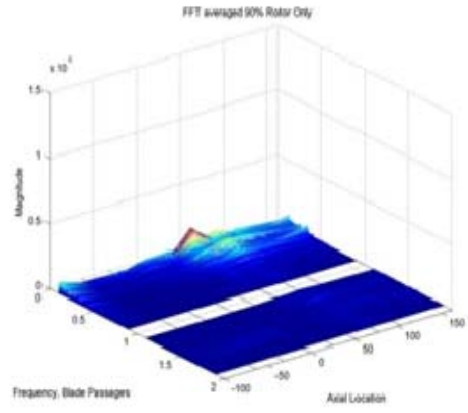
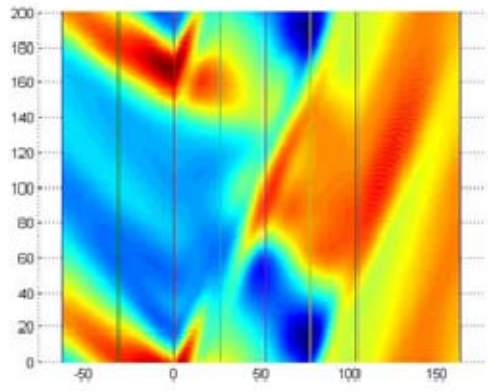


90% Rated Speed

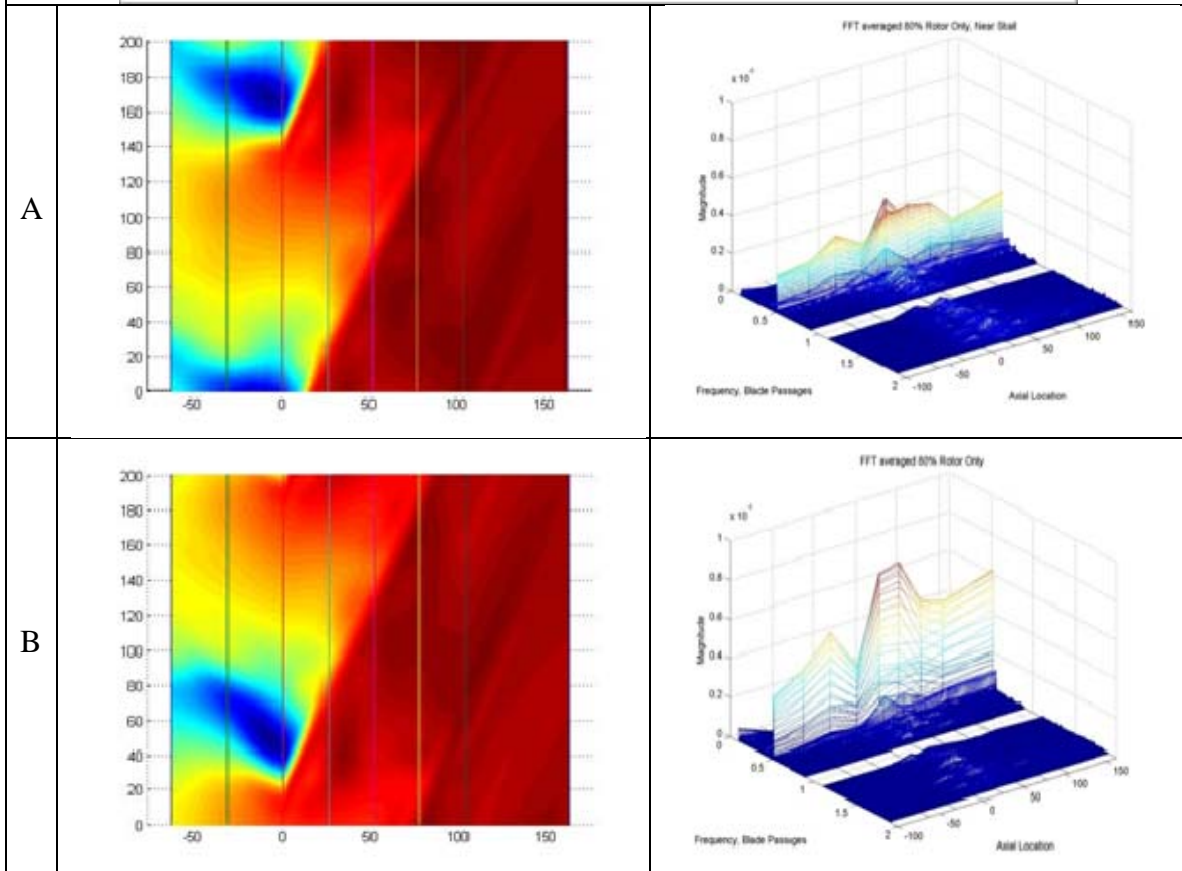
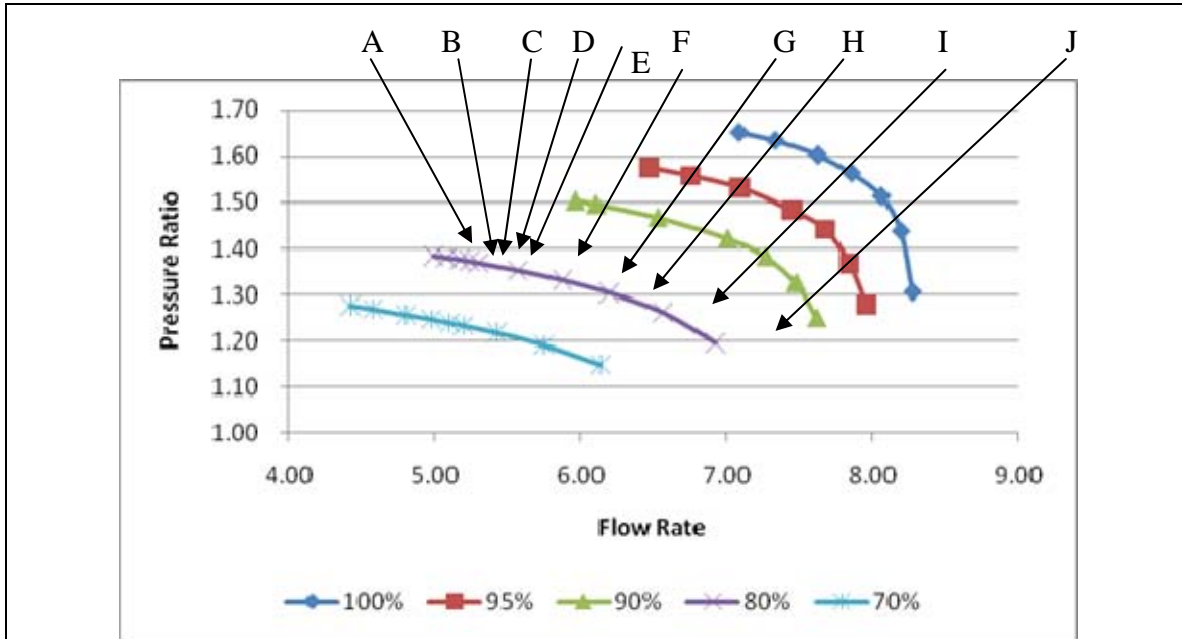


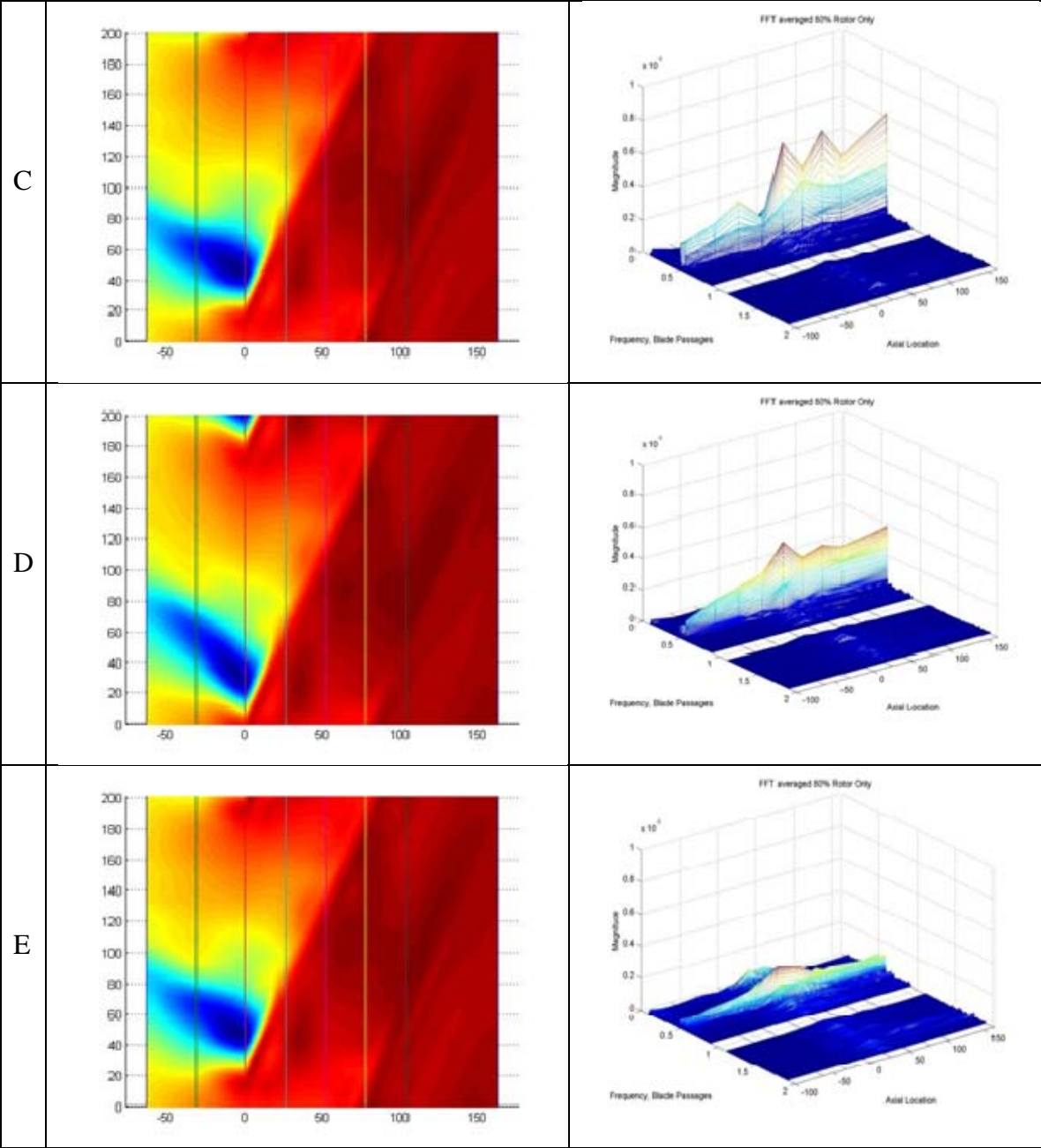


G

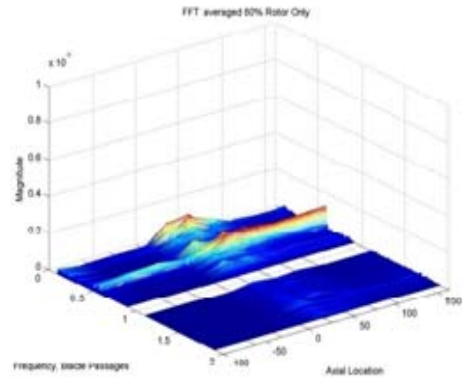
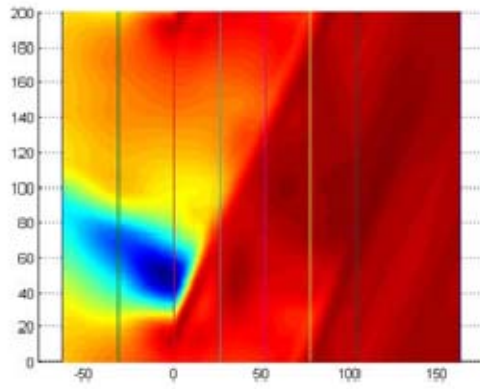


80% Rated Speed

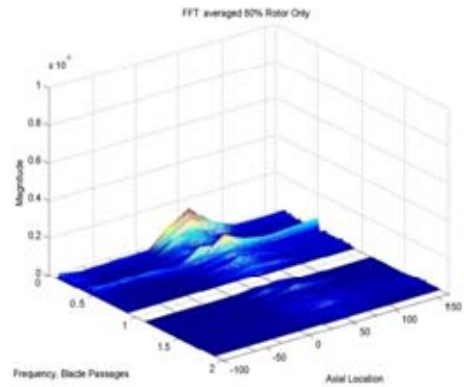
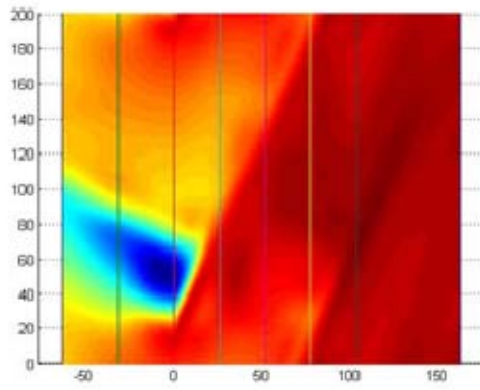




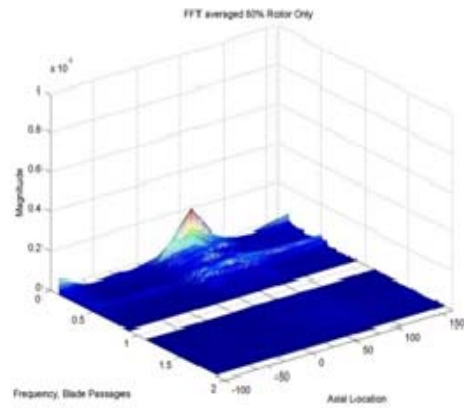
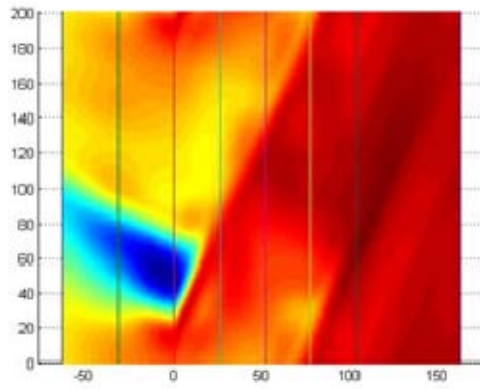
F



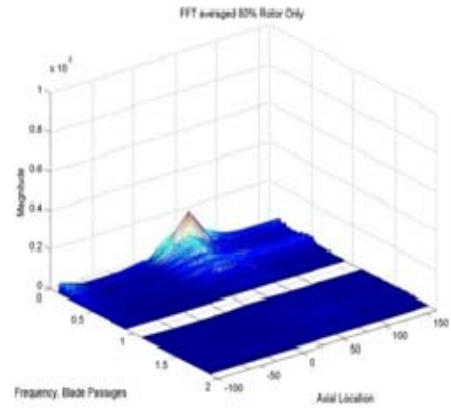
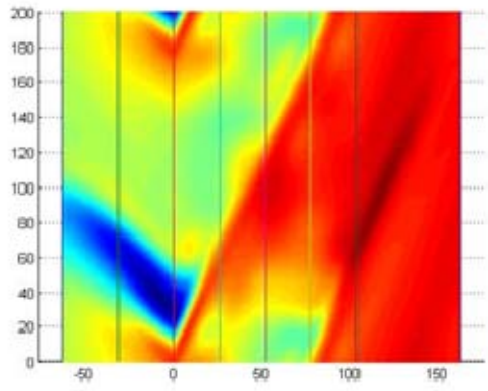
G



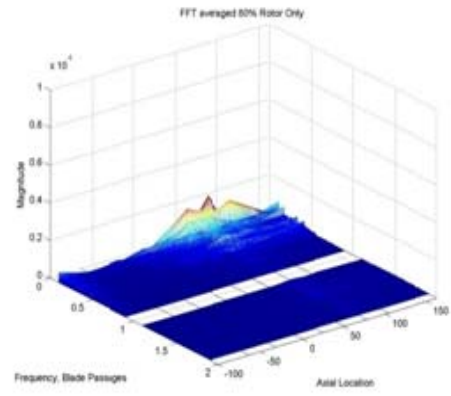
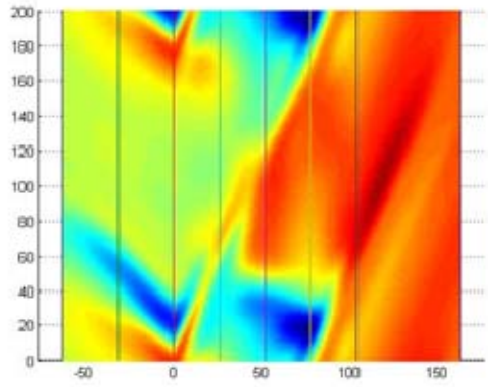
H



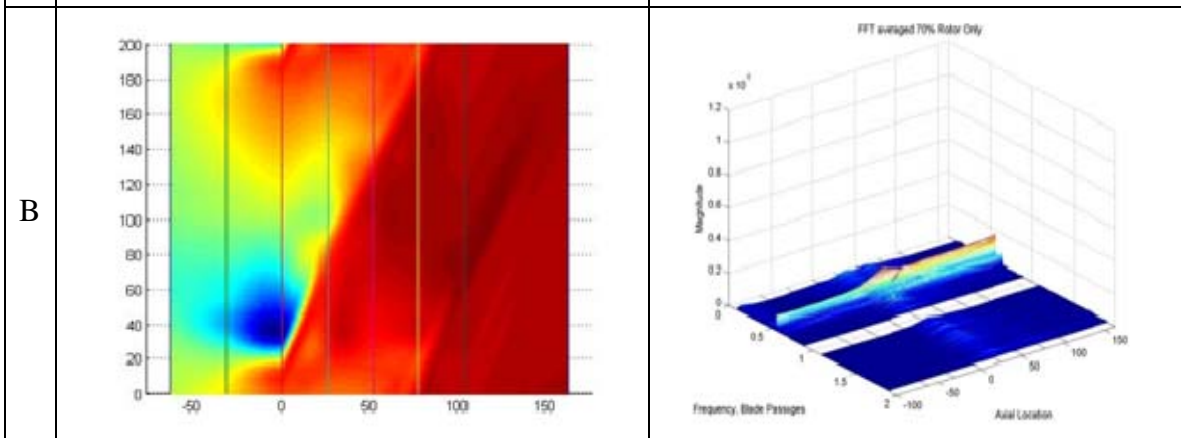
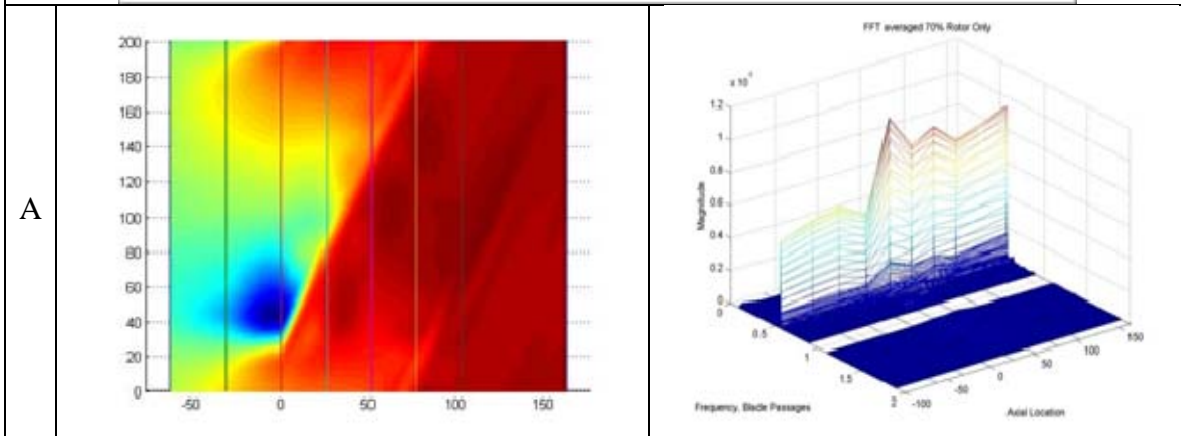
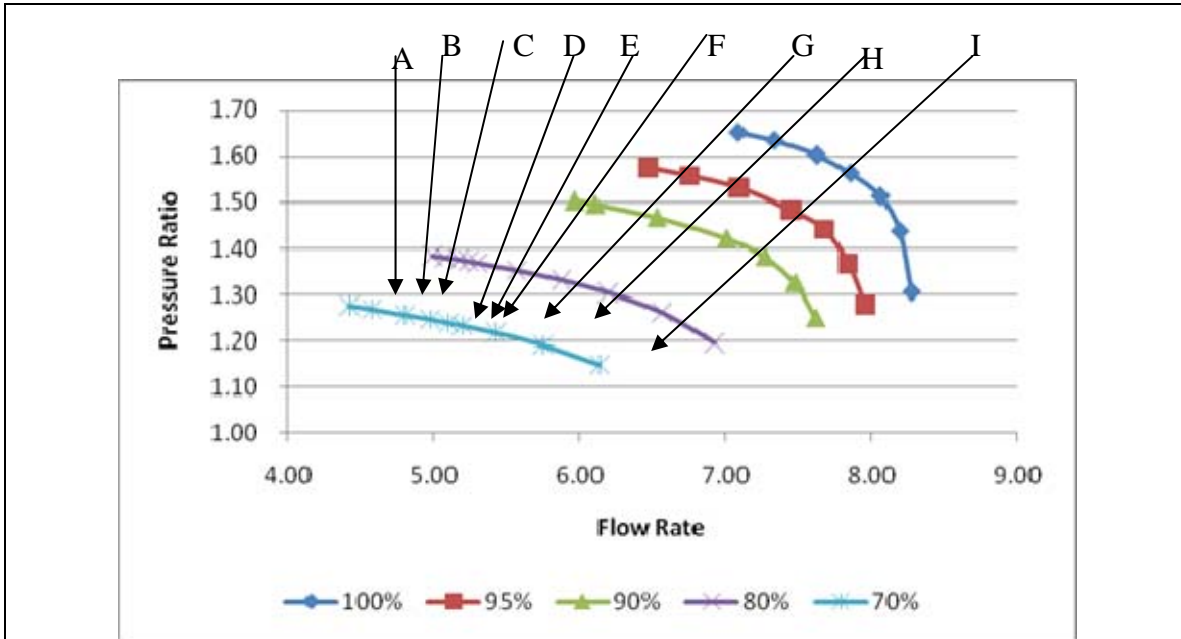
I

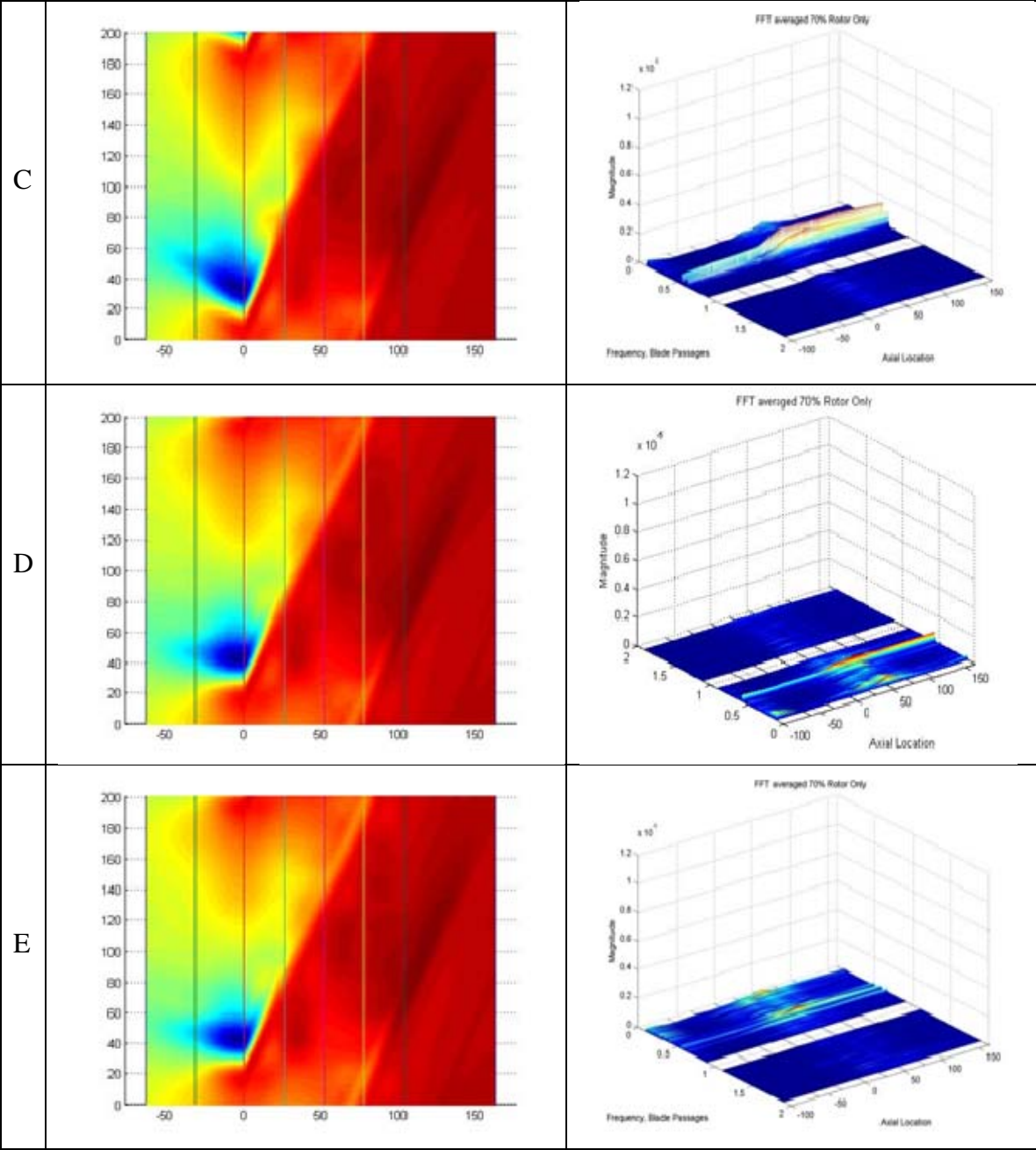


J

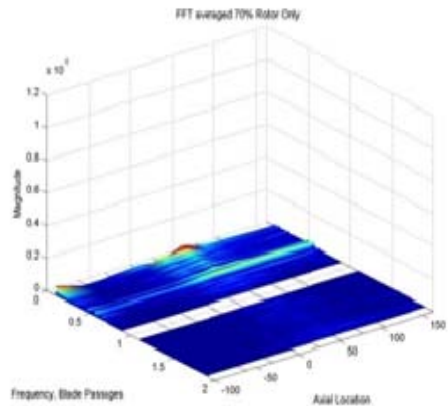
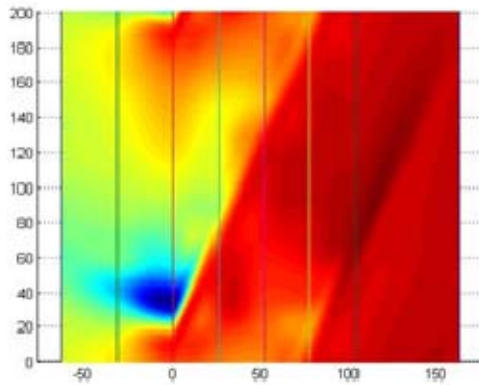


70% Rated Speed

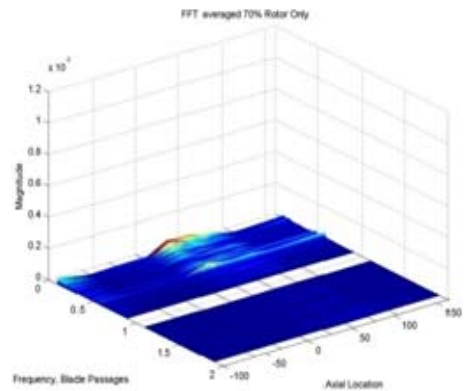
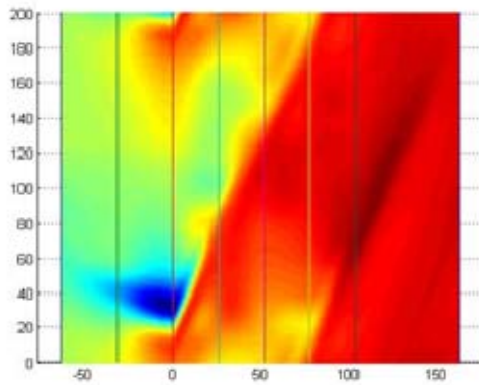




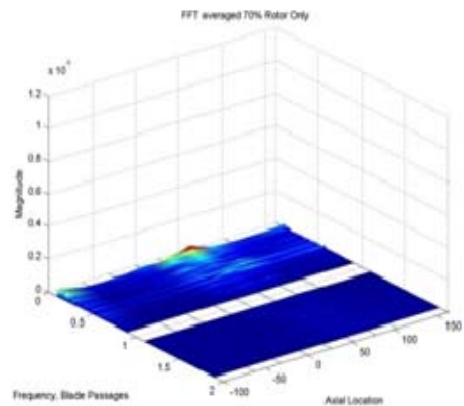
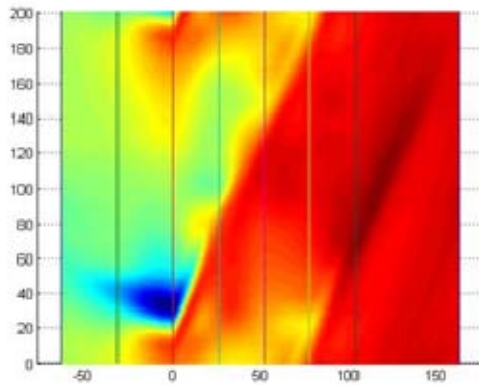
F



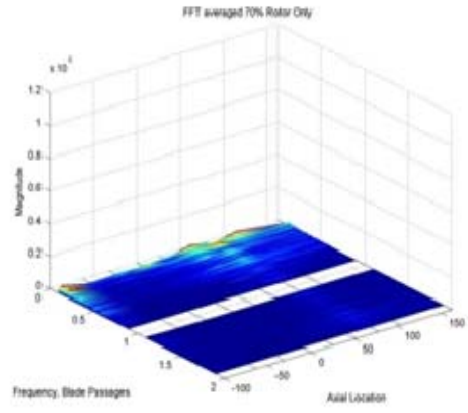
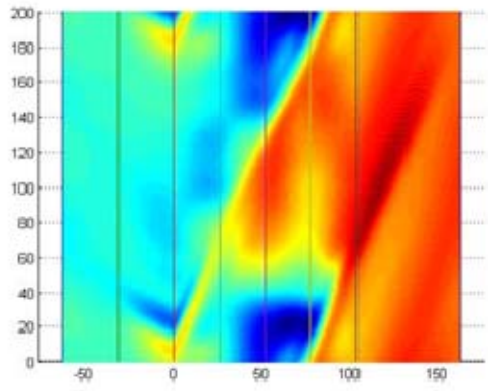
G



H

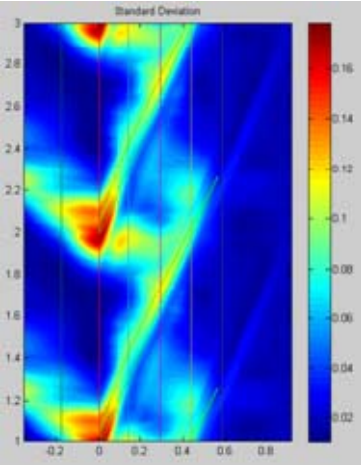
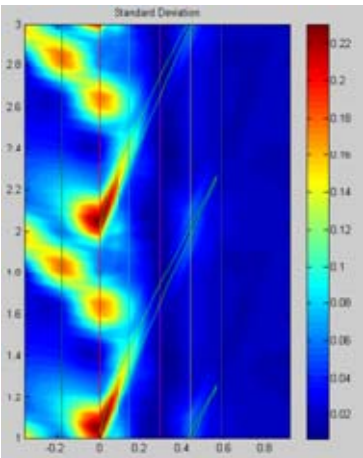


I

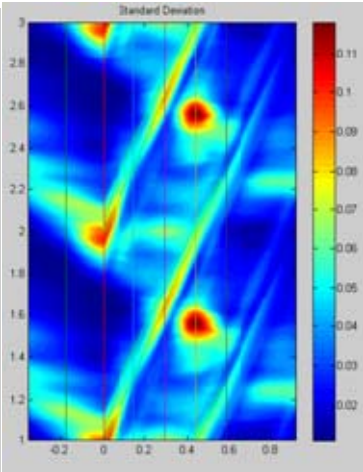


**Standard Deviation Plots
100% Rated Speed
Peak Efficiency**

Near Stall

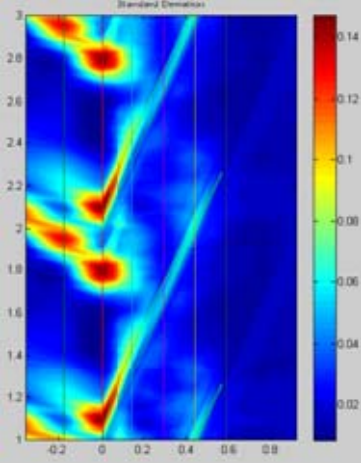
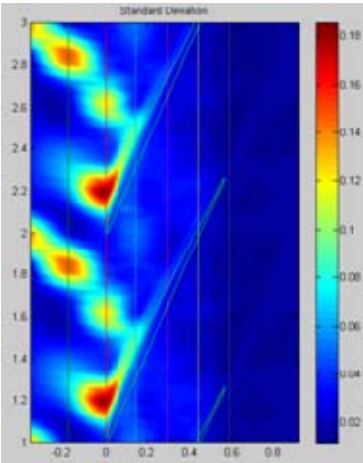


Choked

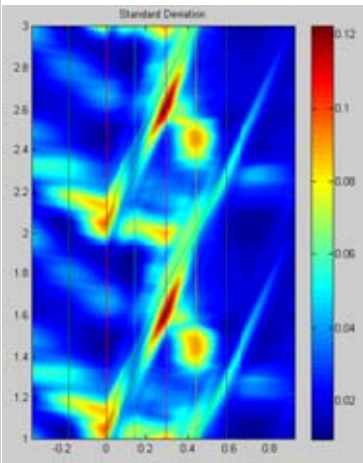


**95% Rated Speed
Peak Efficiency**

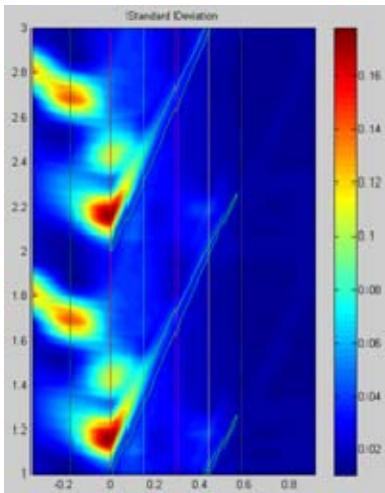
Near Stall



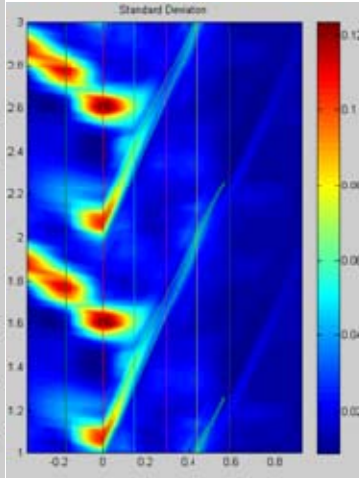
Choked



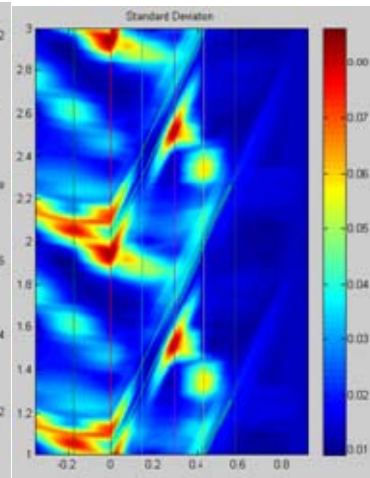
Near Stall



**90% Rated Speed
Peak Efficiency**

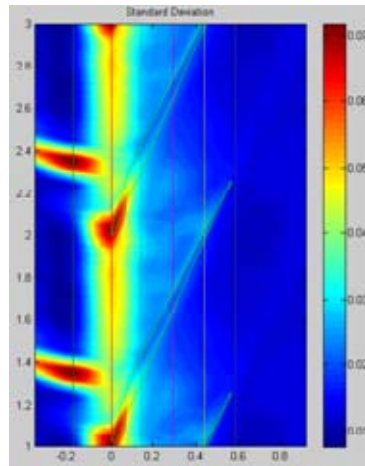


Choked

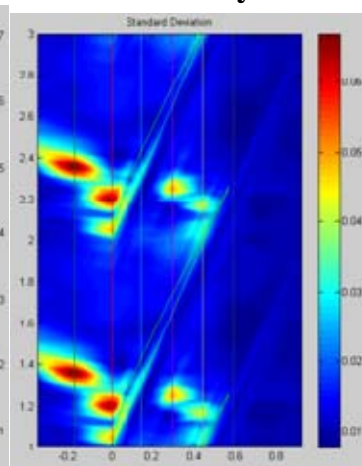


80% Rated Speed

Near Stall



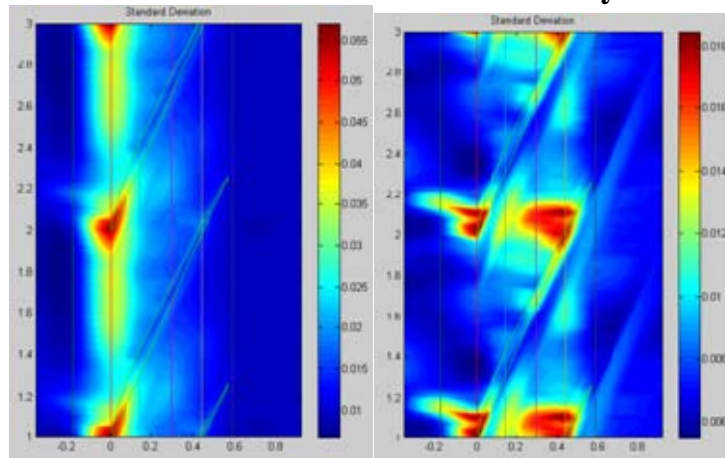
Peak Efficiency/Choked



70% Rated Speed

Near Stall

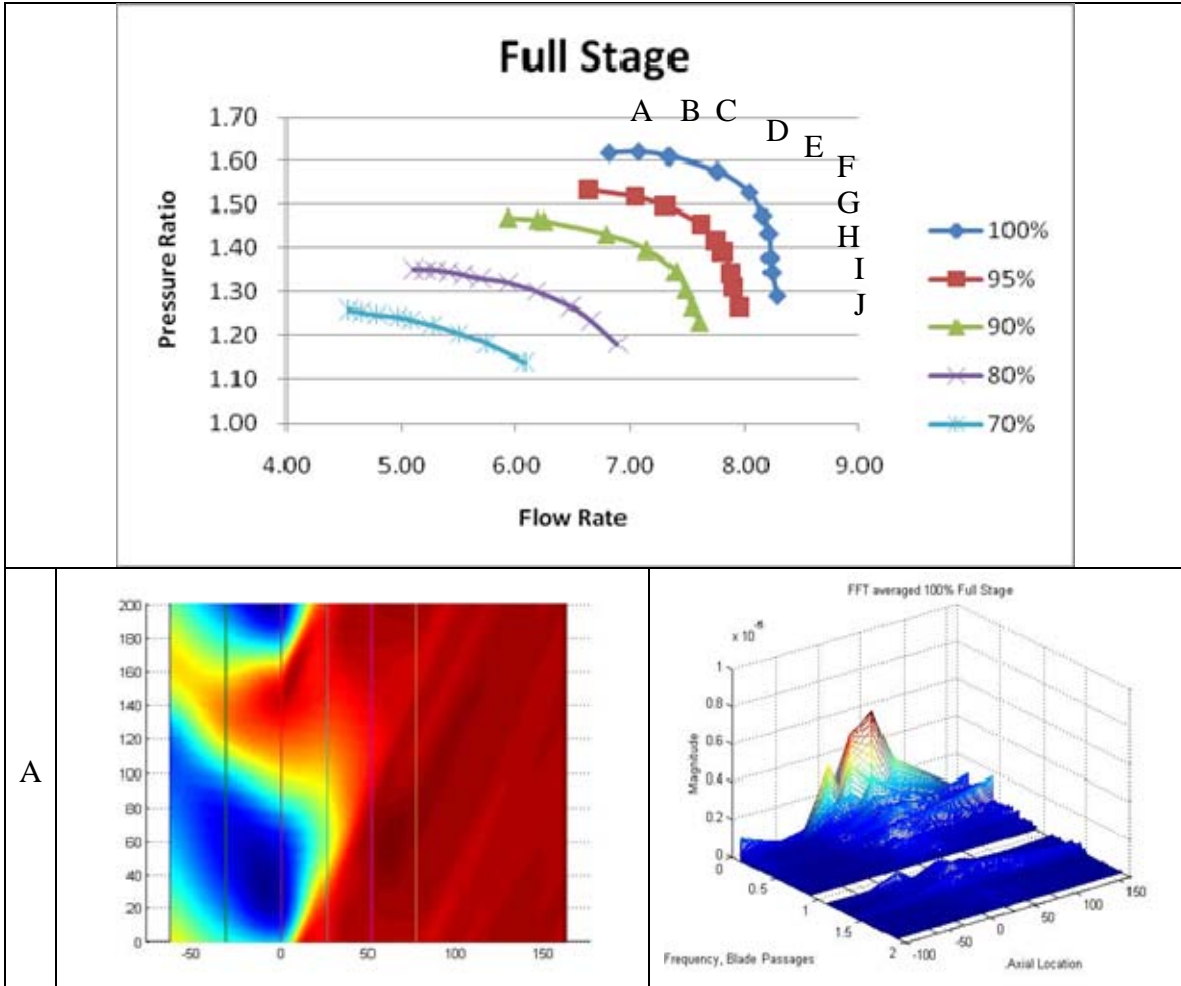
Peak Efficiency/Choked

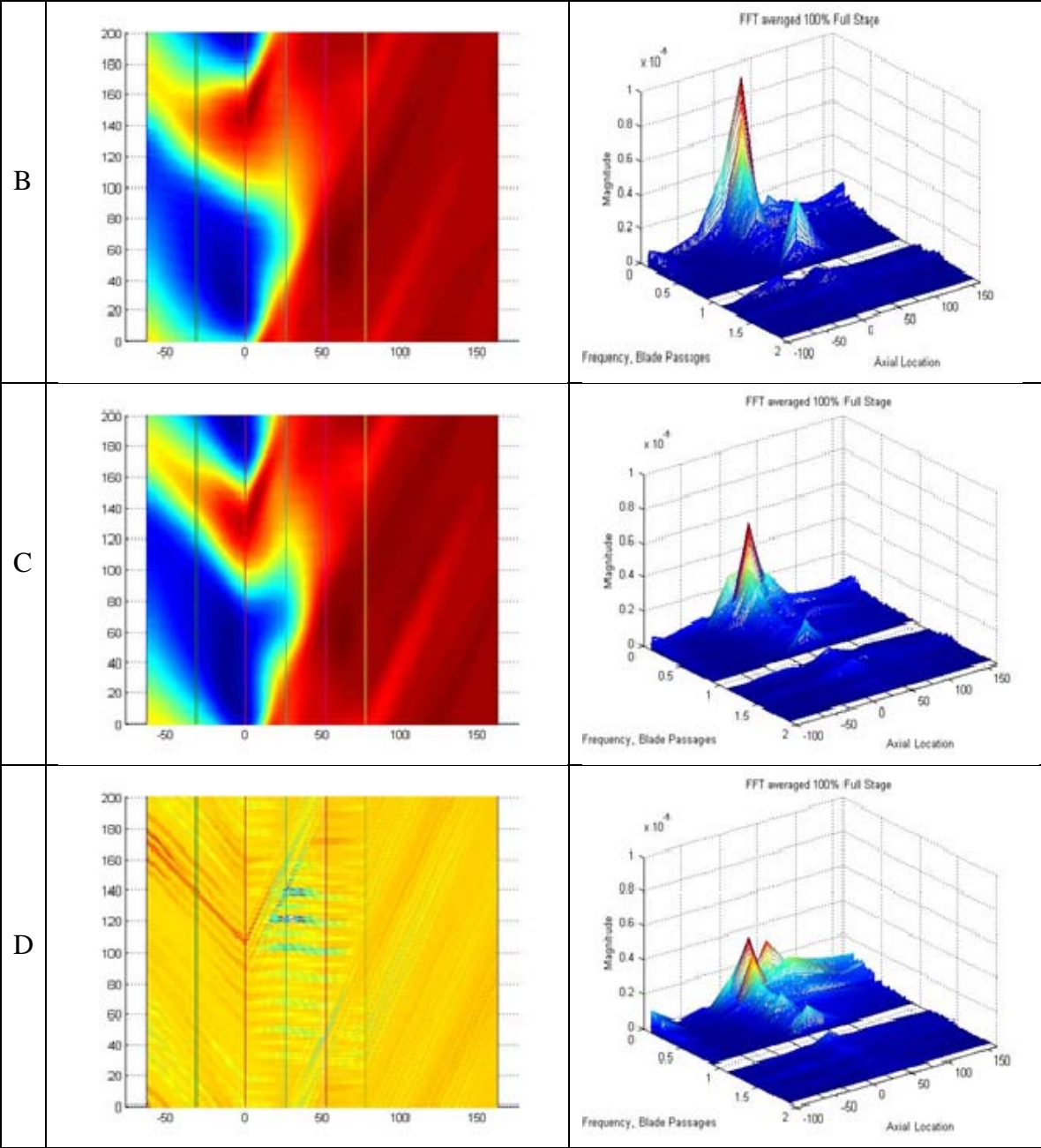


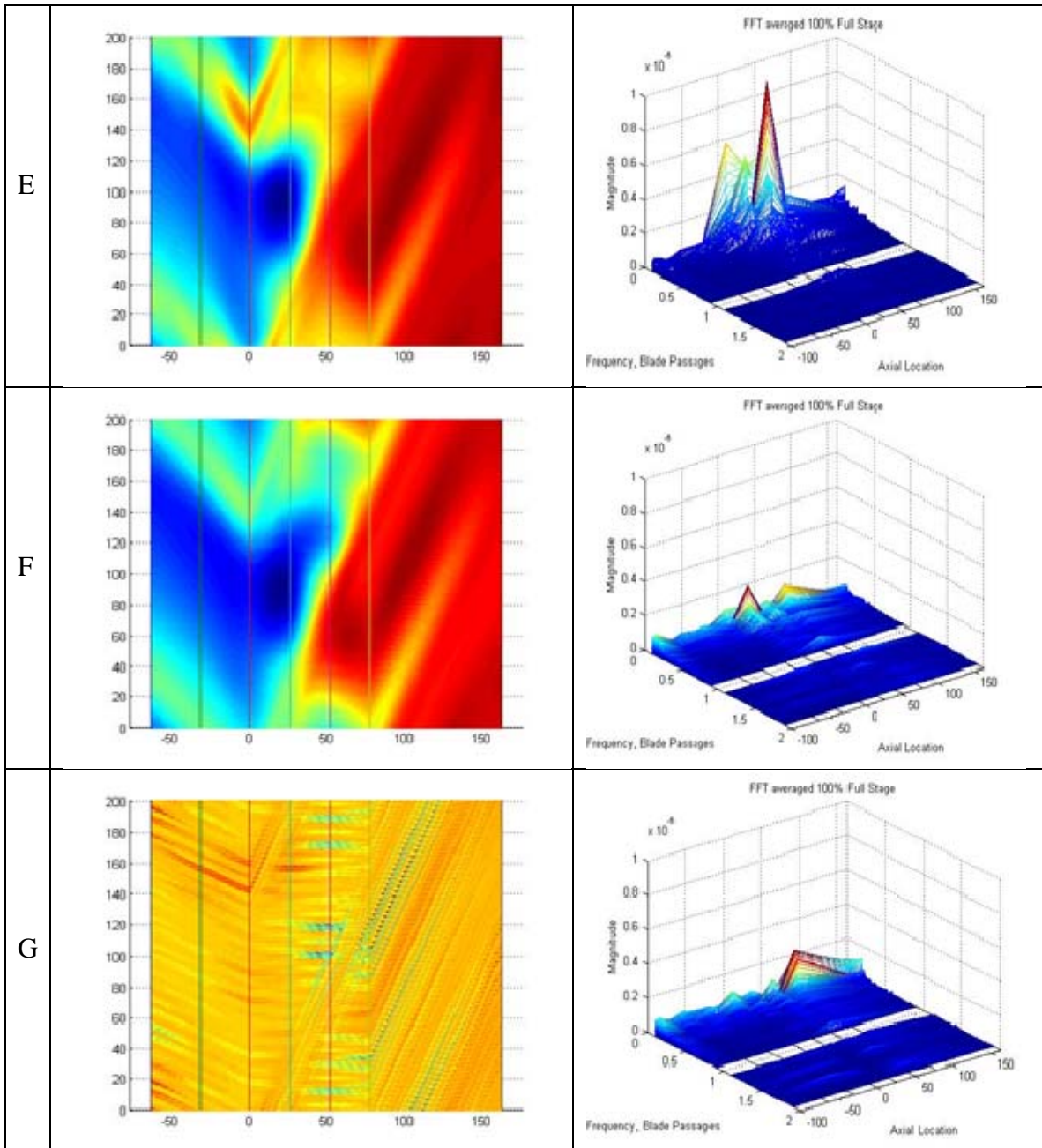
APPENDIX B: FULL STAGE KULITE DATA

Full Stage Data

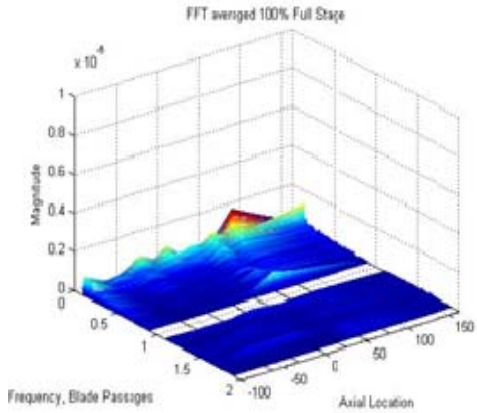
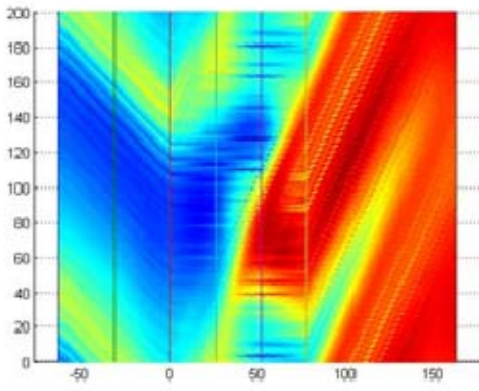
Steady State Analysis Plots 100% Rated Speed



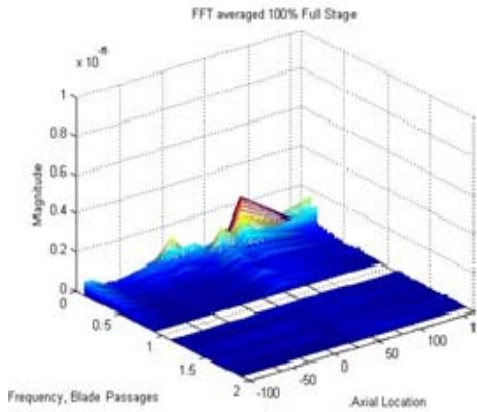
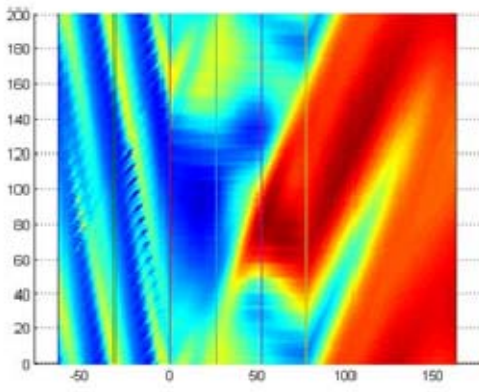




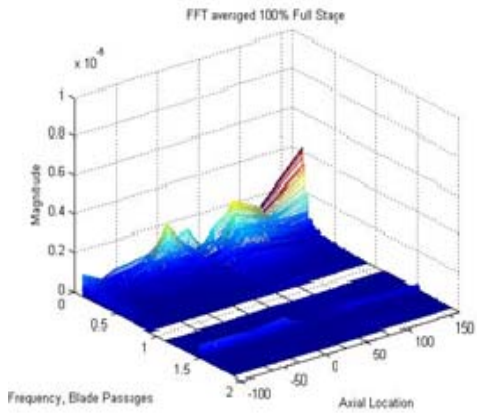
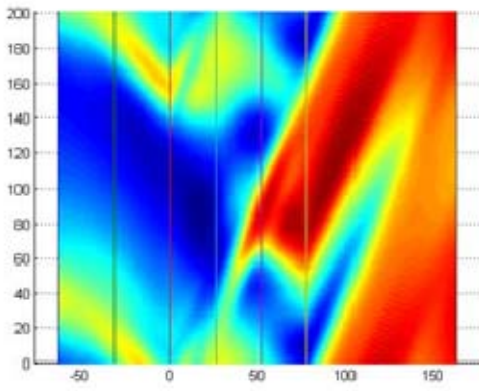
H



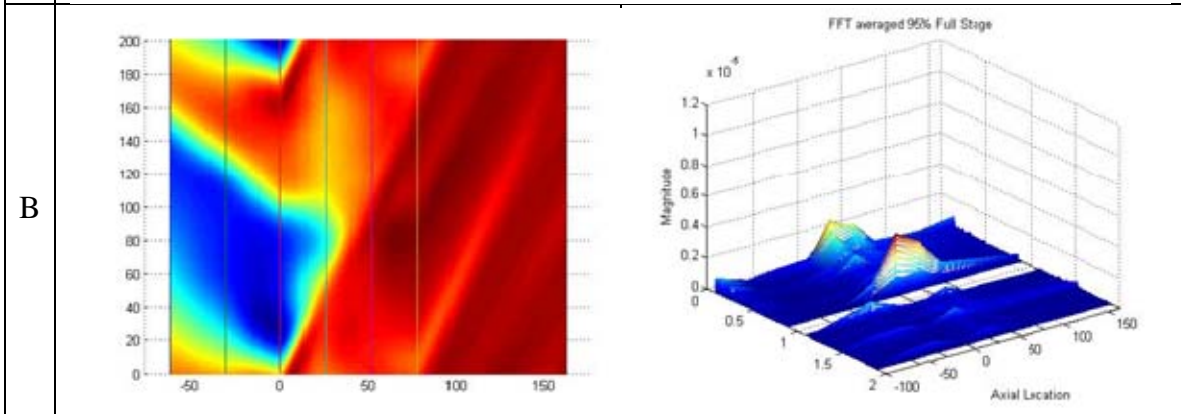
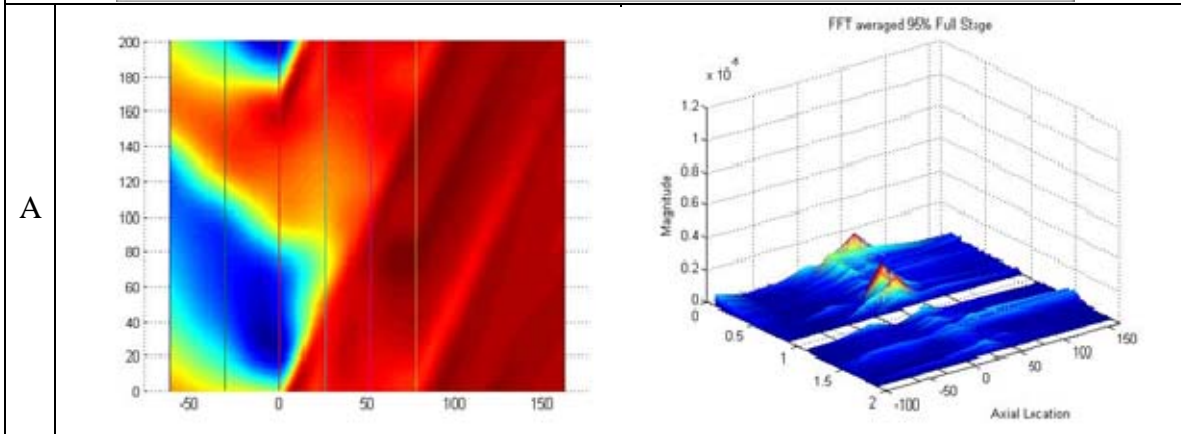
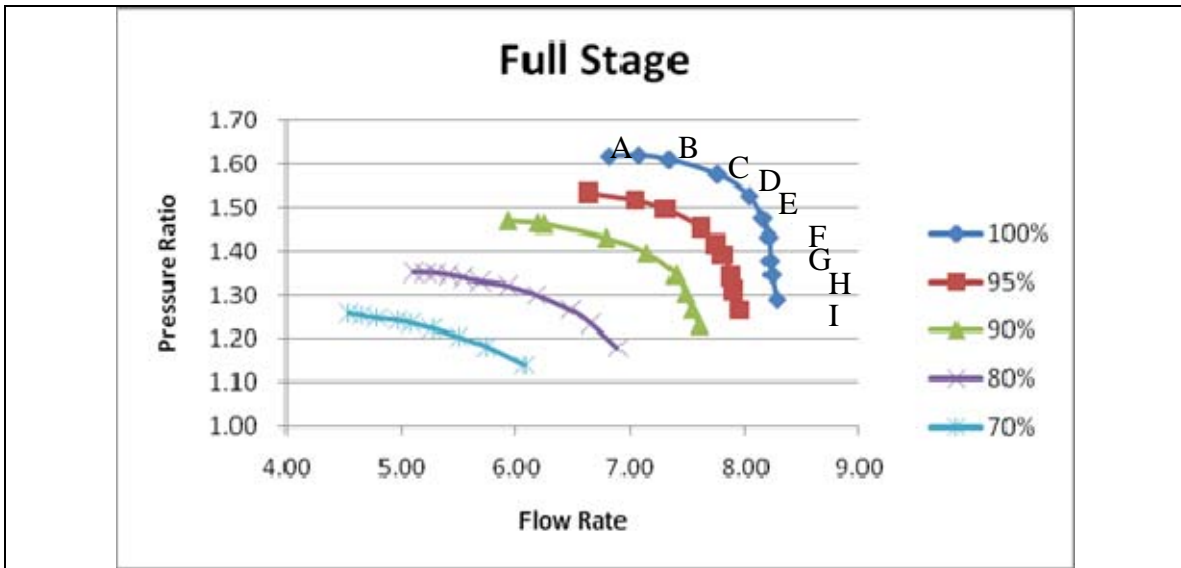
I

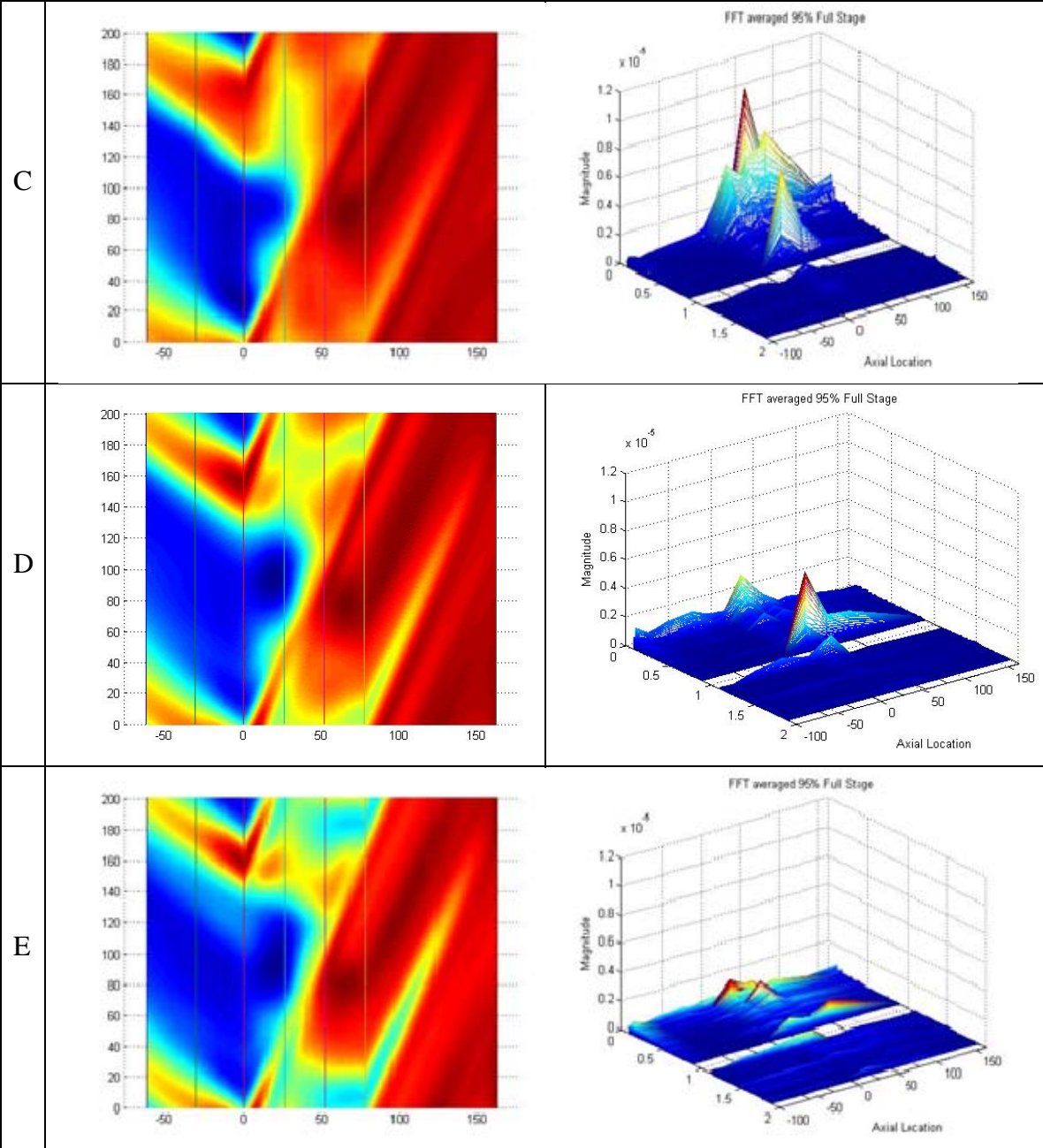


J

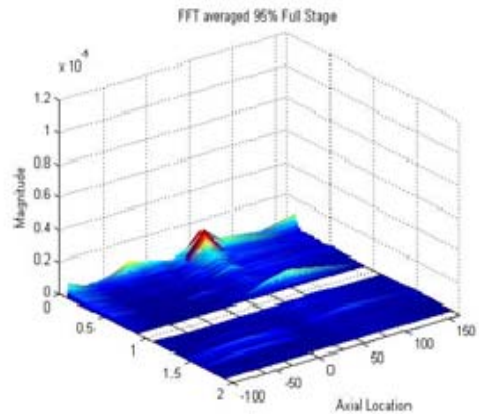
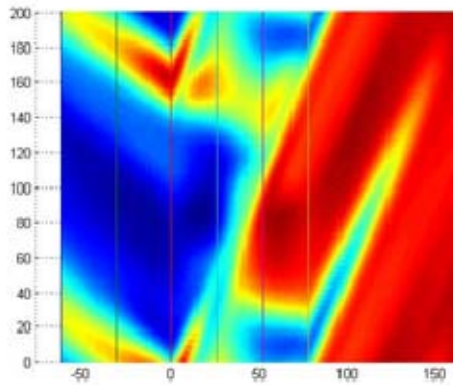


95% Rated Speed

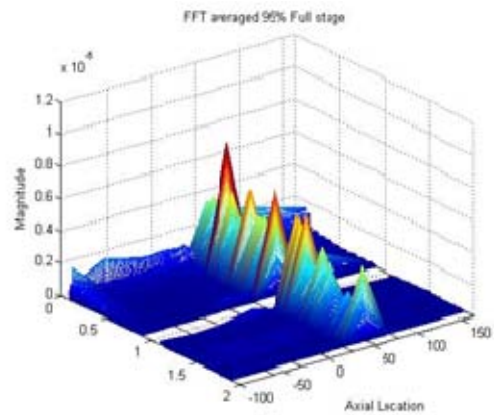
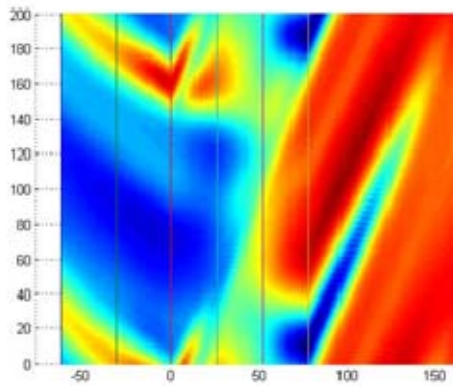




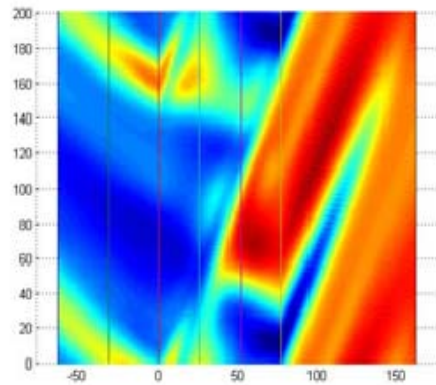
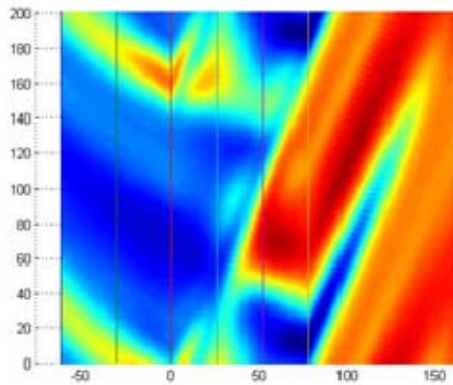
F

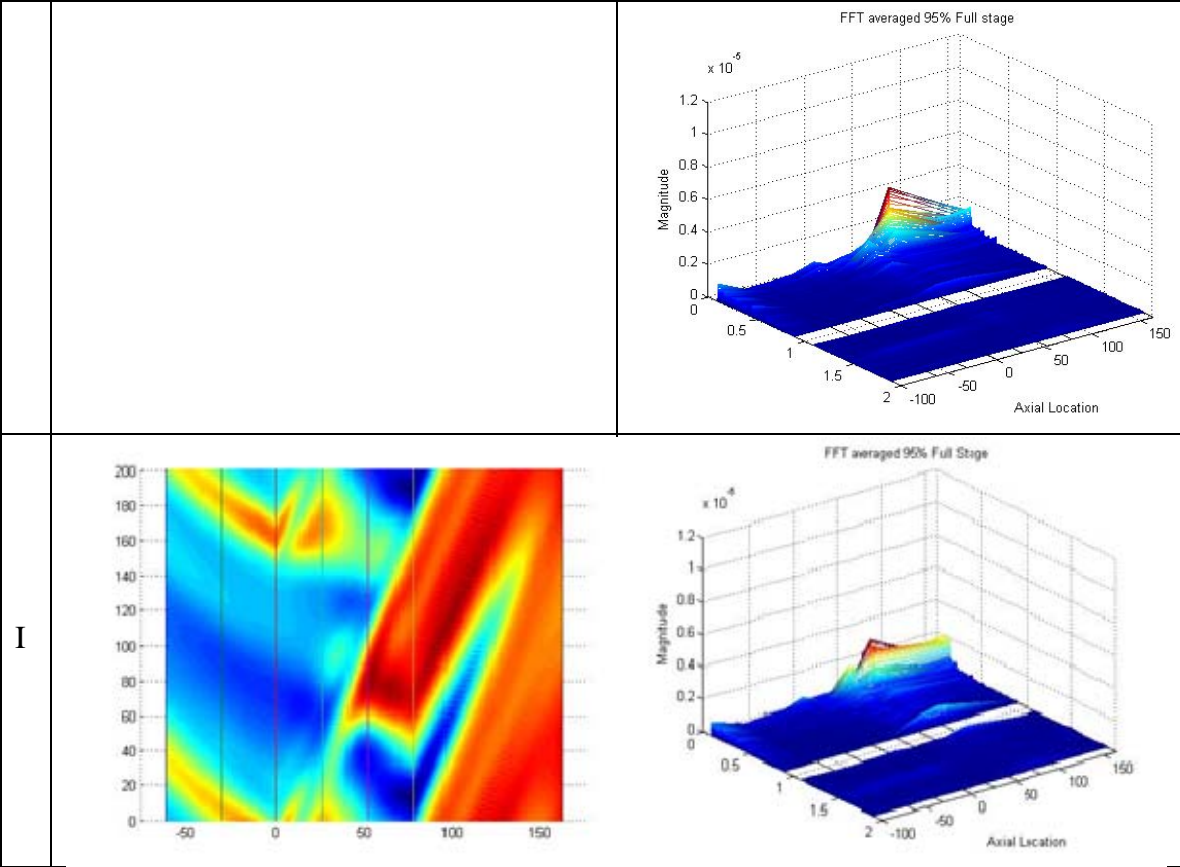


G

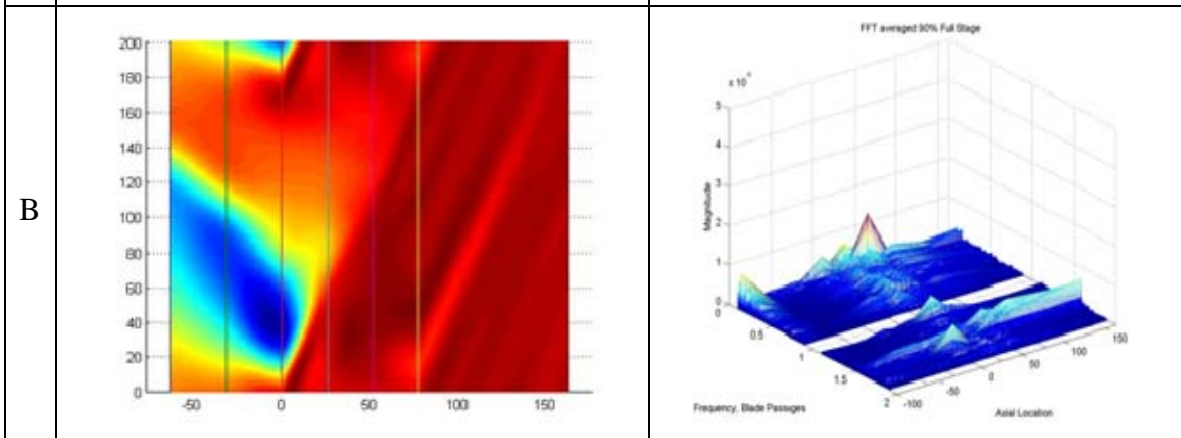
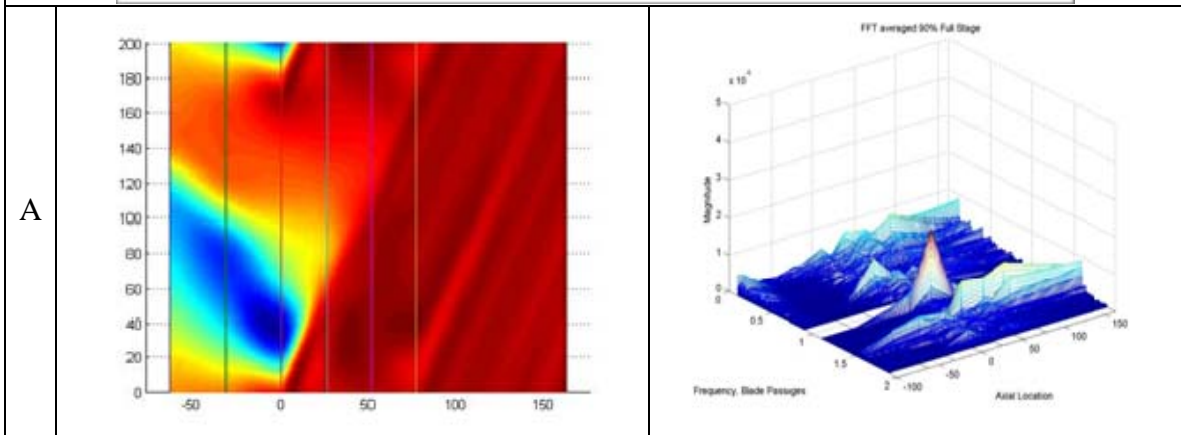
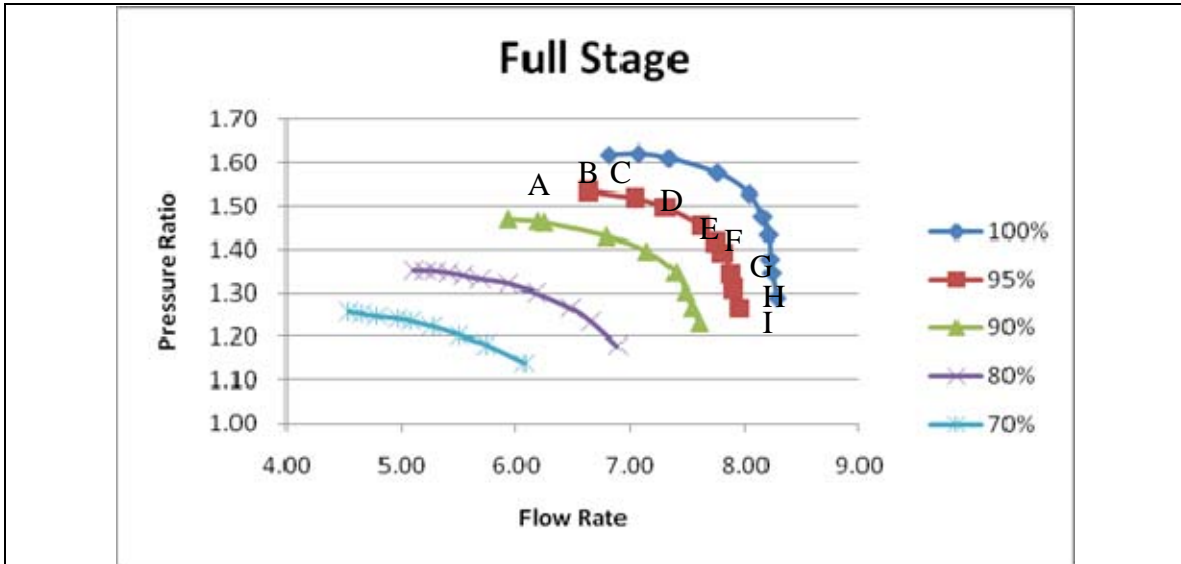


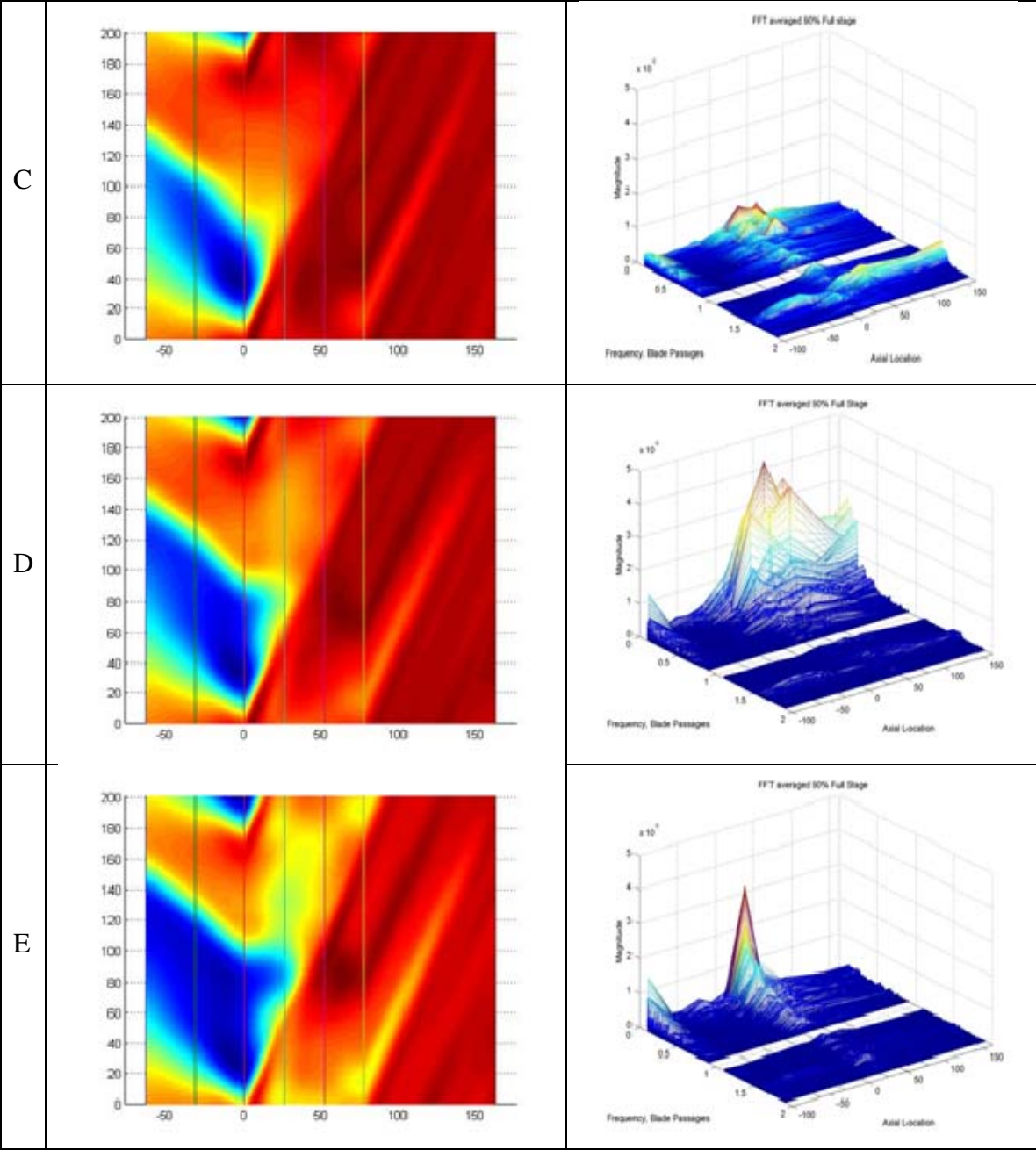
H



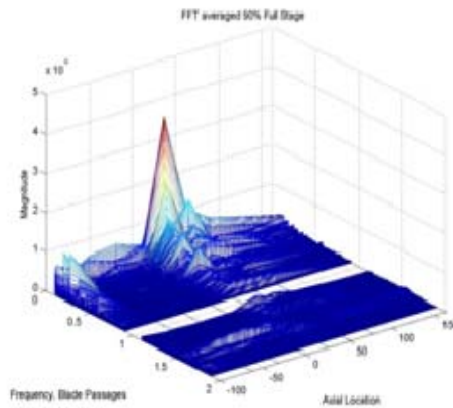
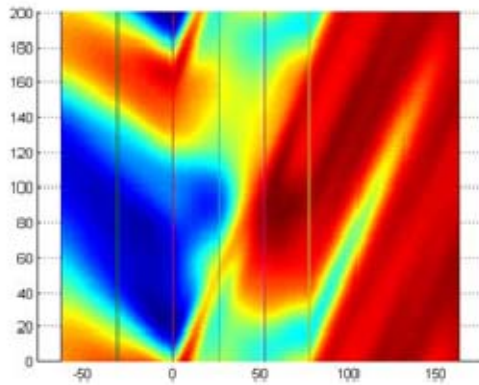


90% Rated Speed

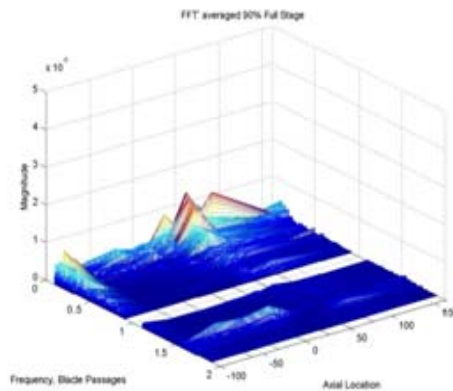
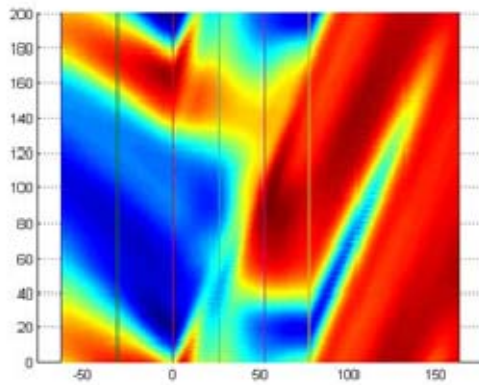




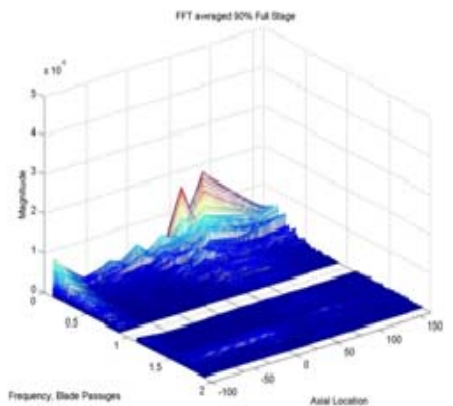
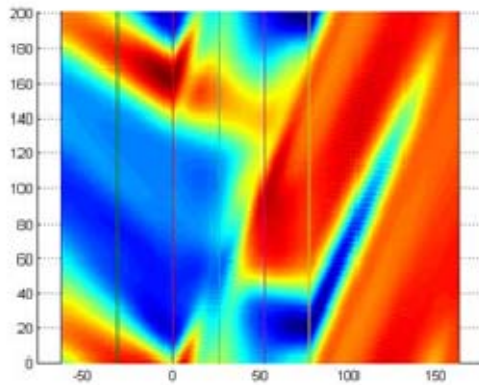
F



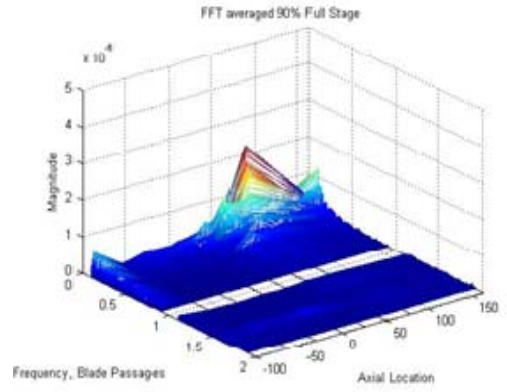
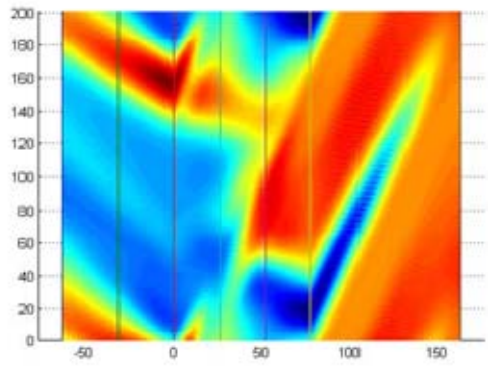
G



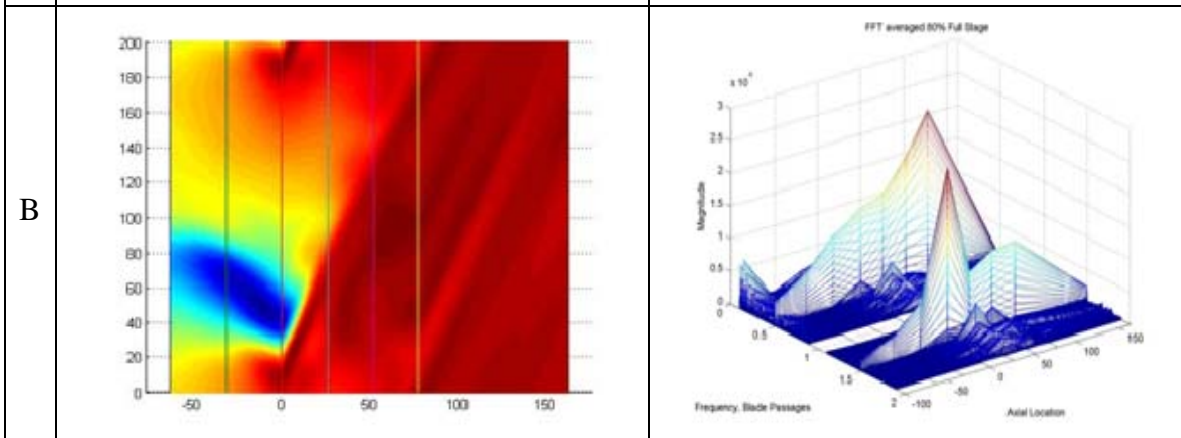
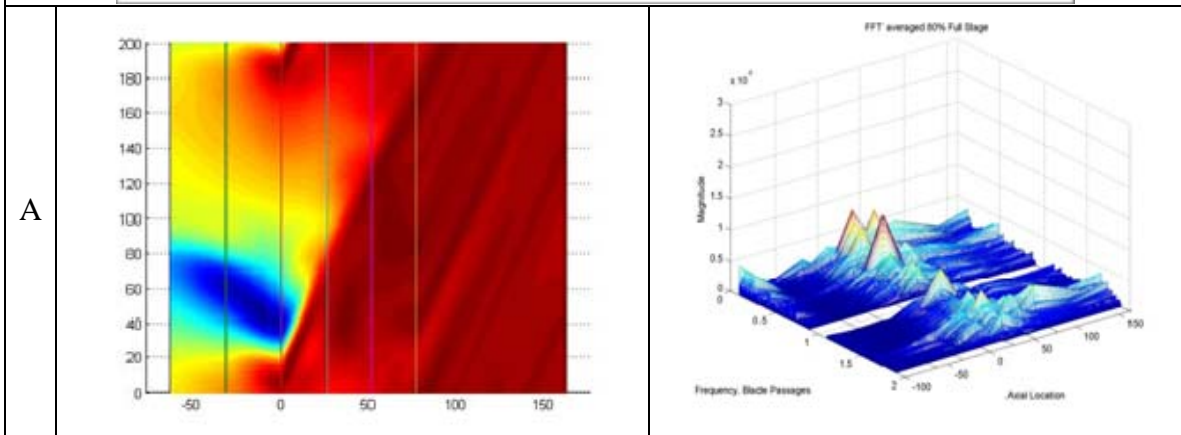
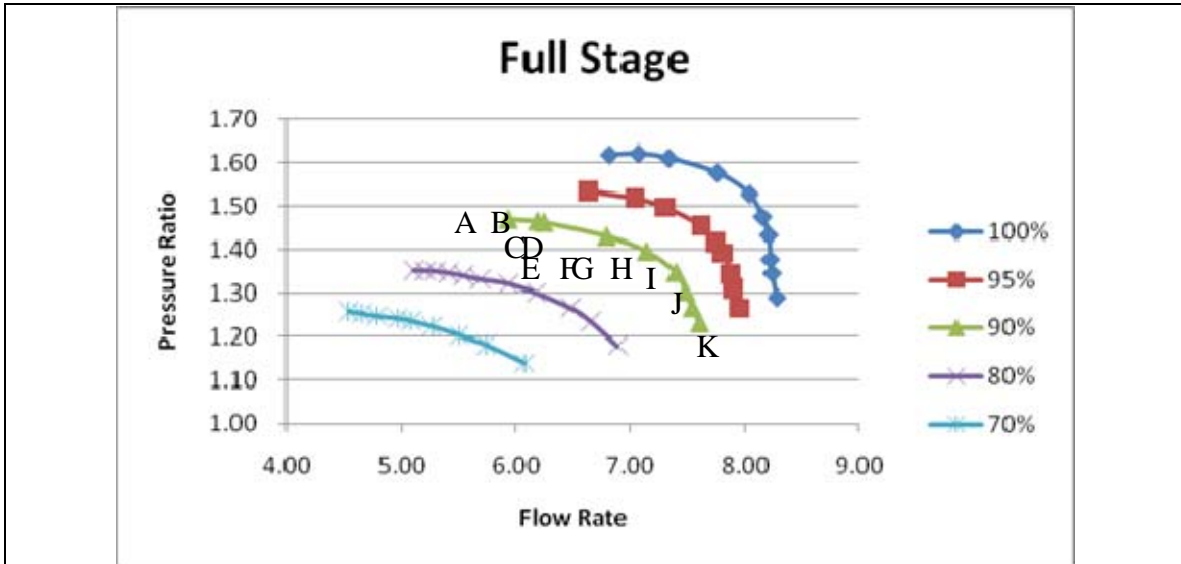
H

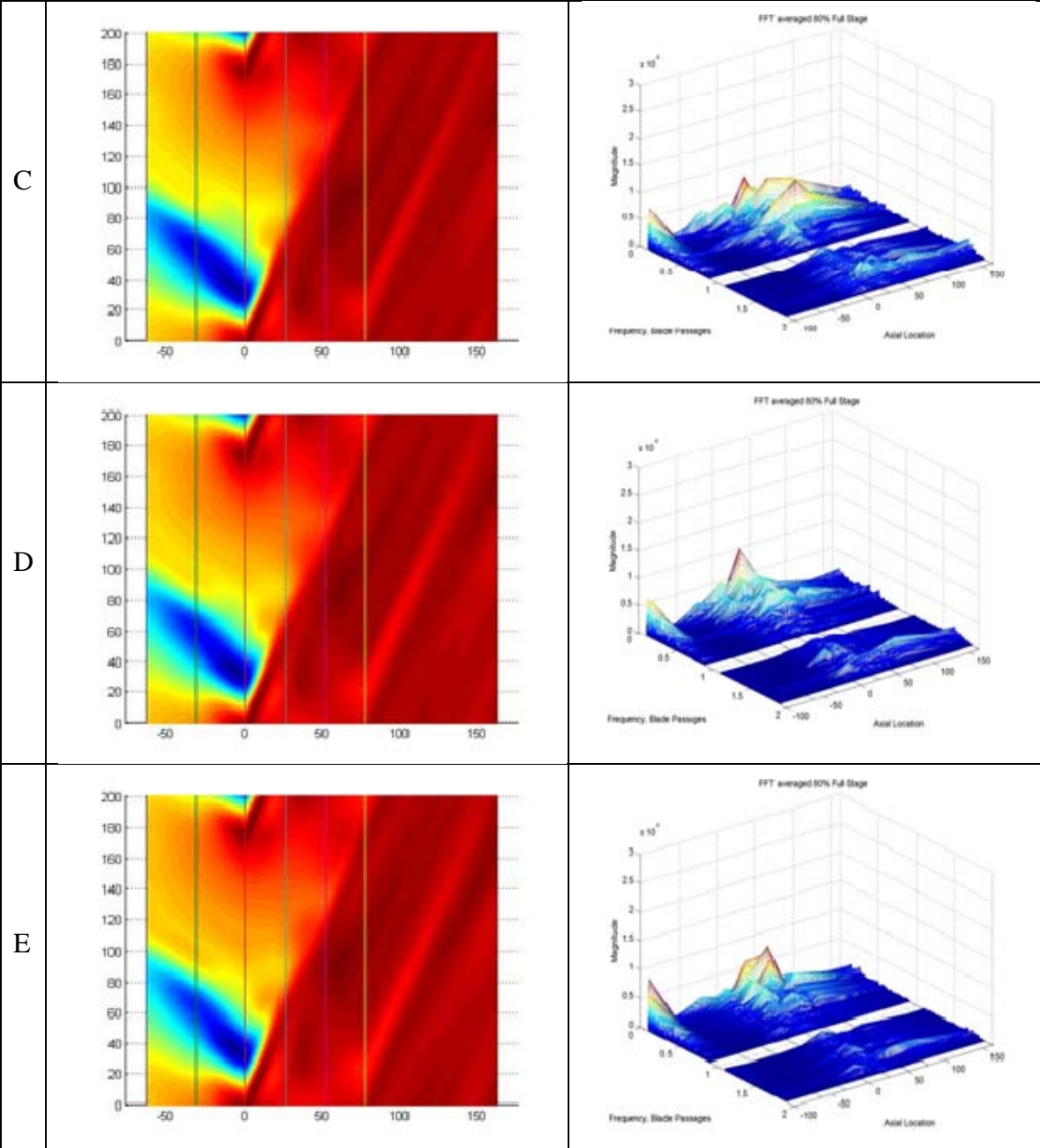


I

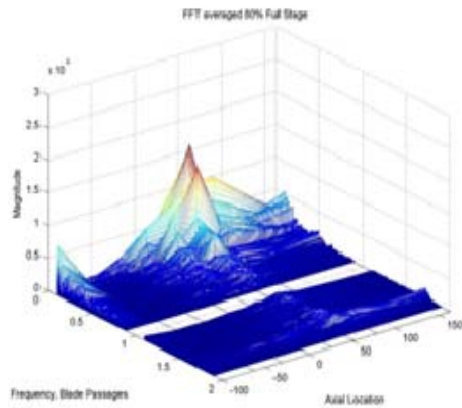
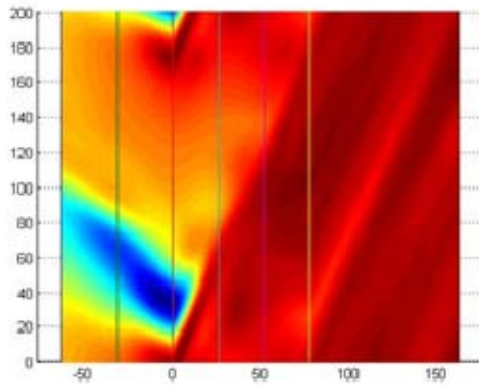


80% Rated Speed

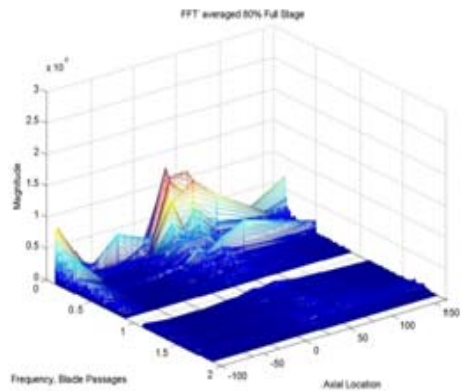
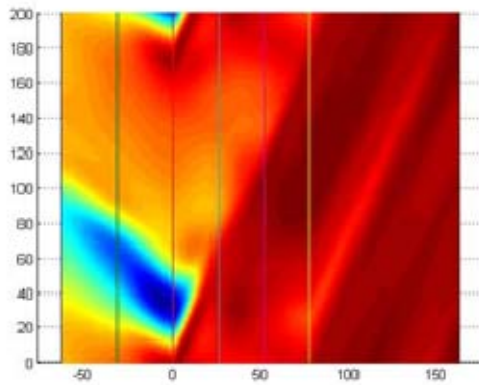




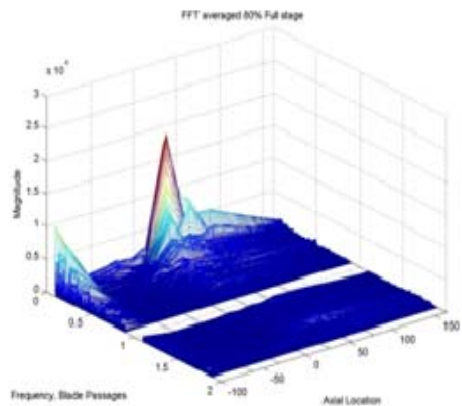
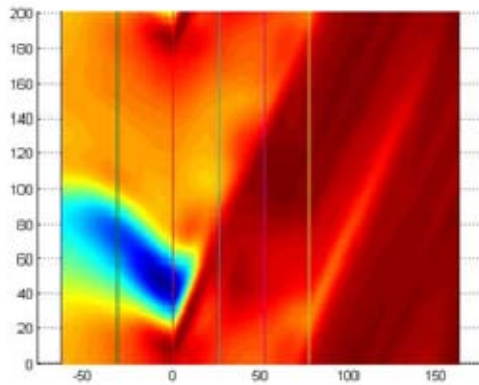
F

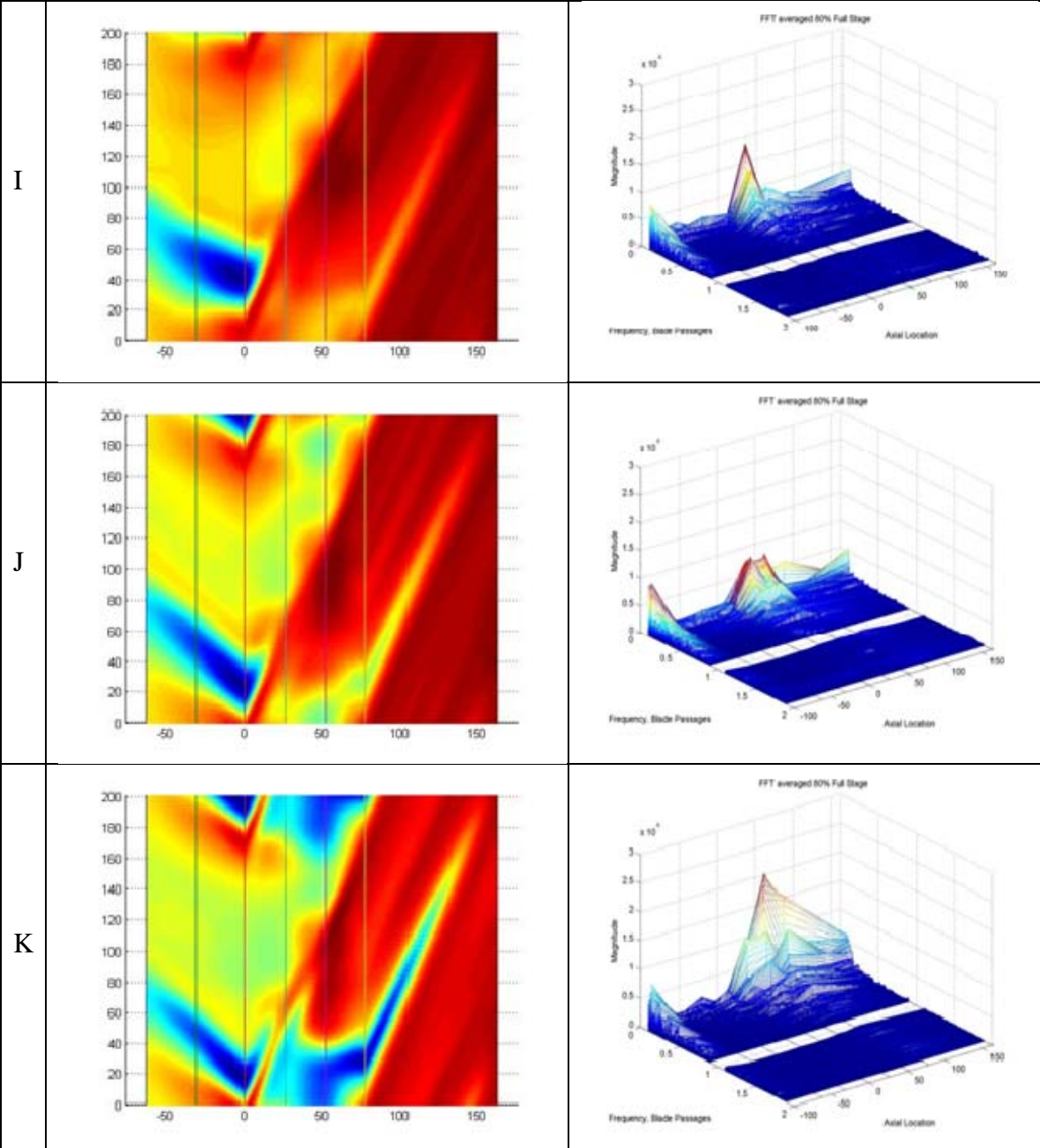


G

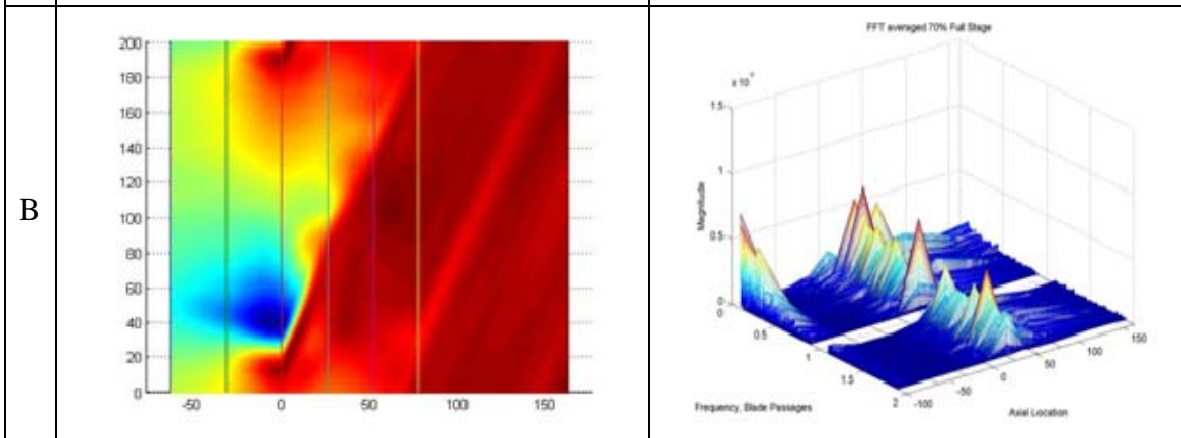
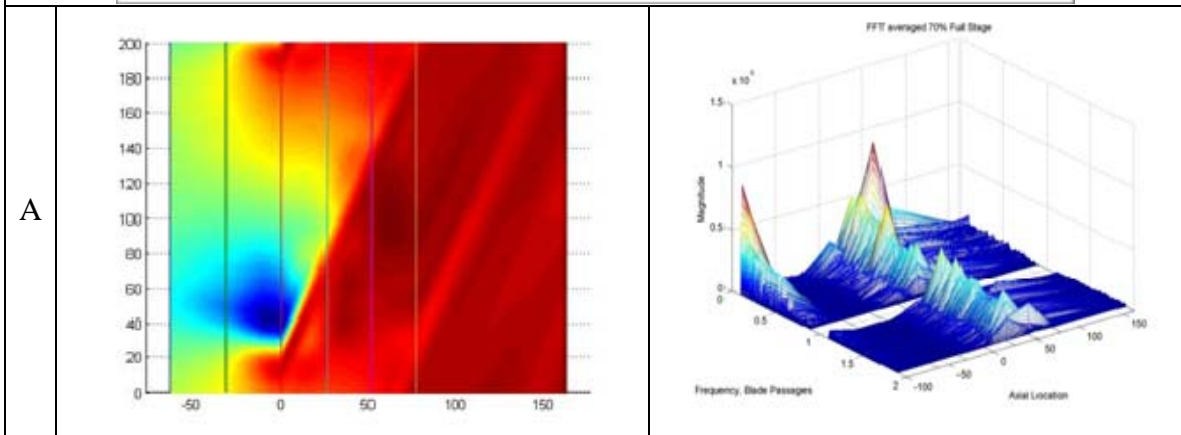
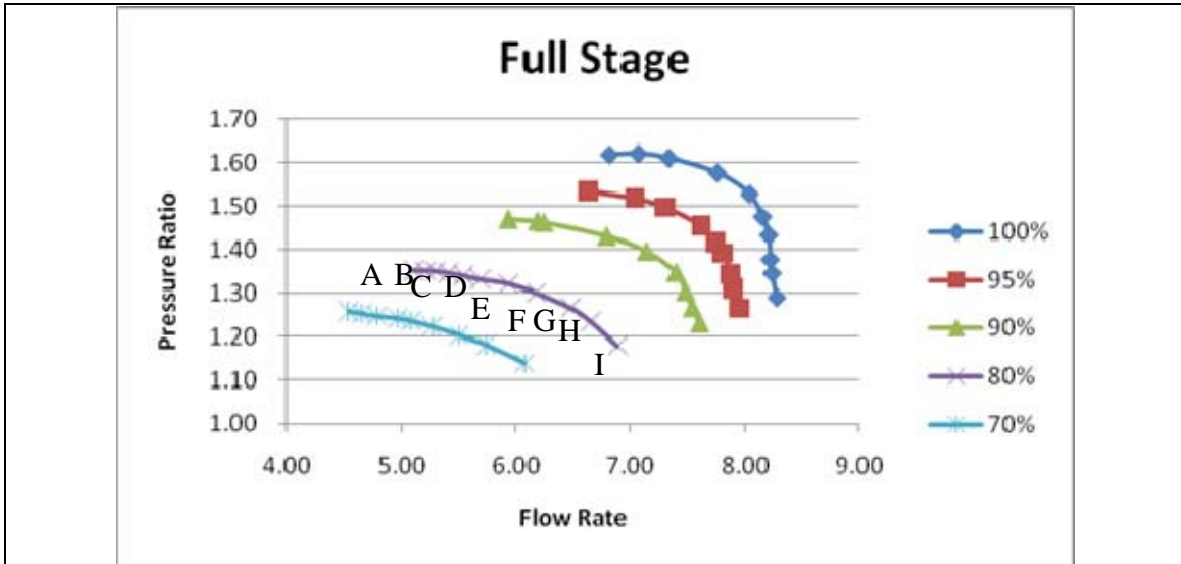


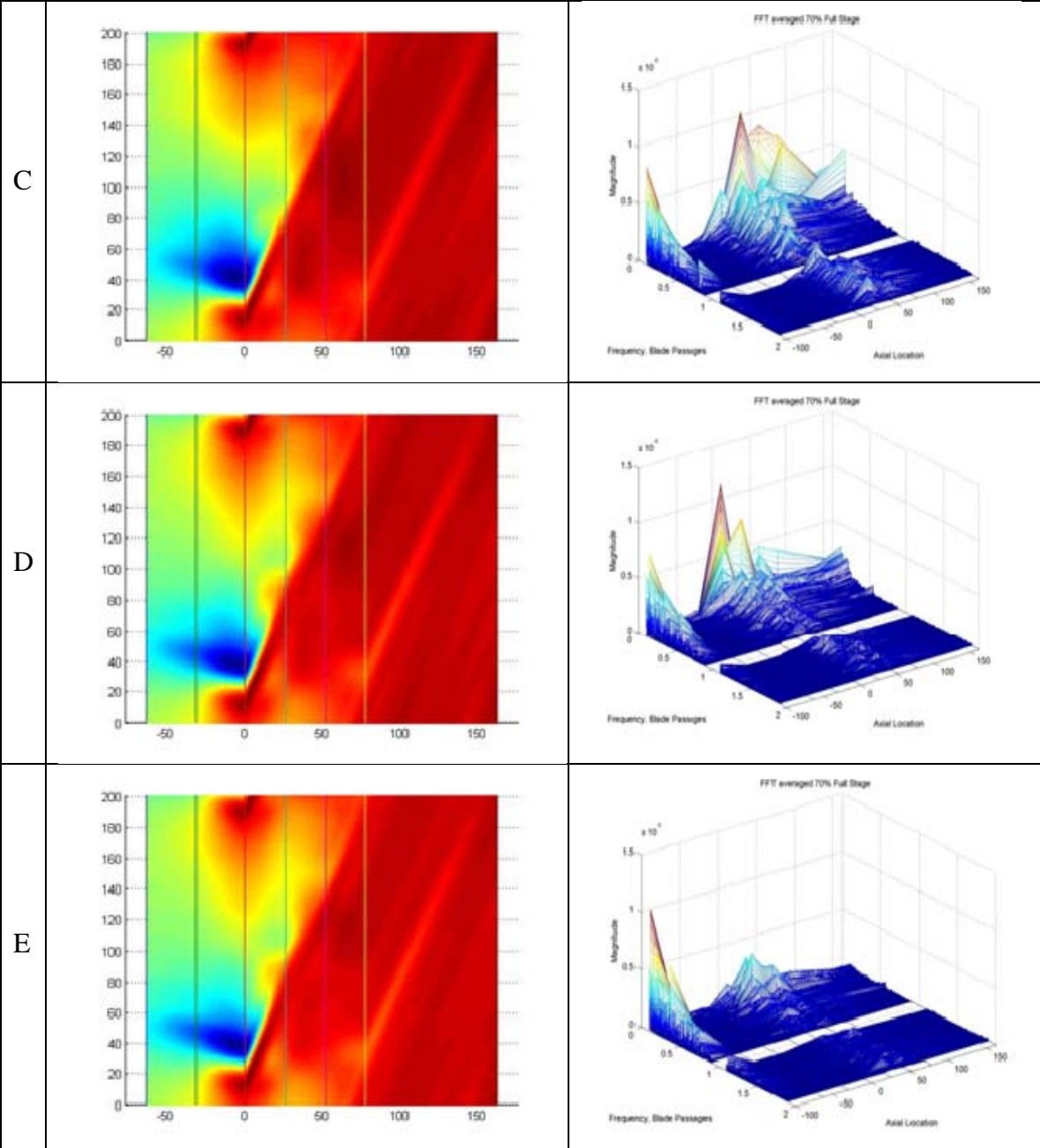
H



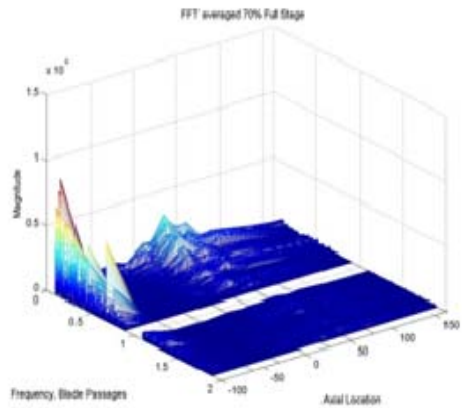
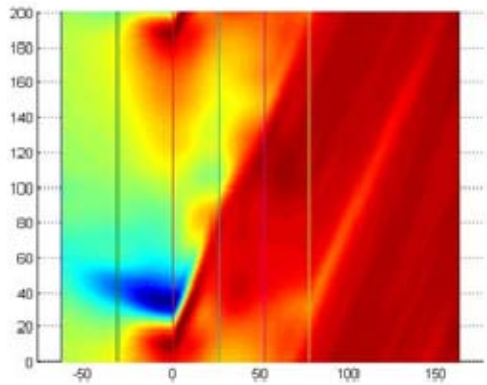


70% Rated Speed

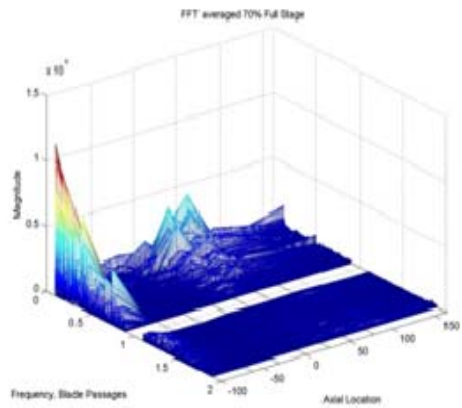
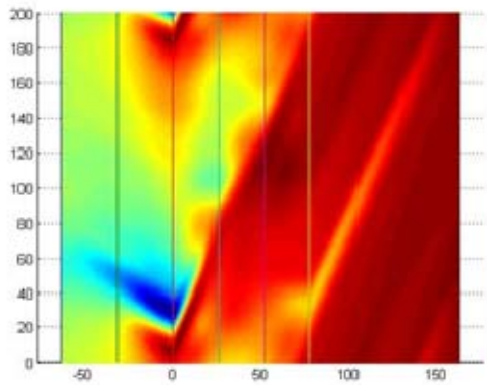




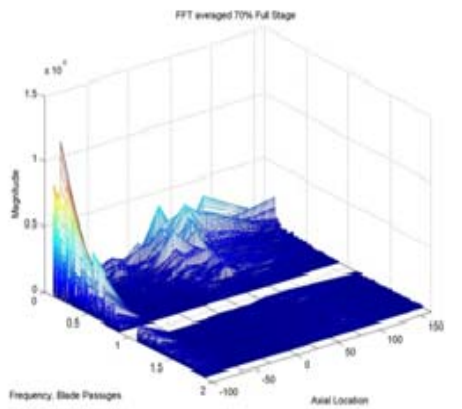
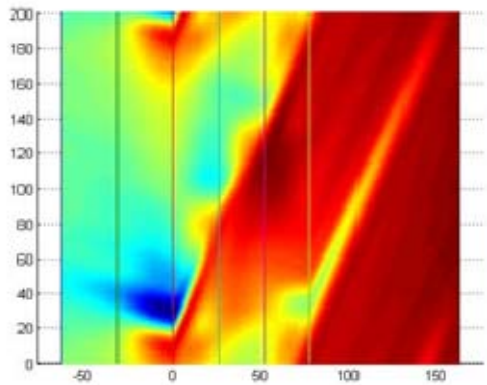
F



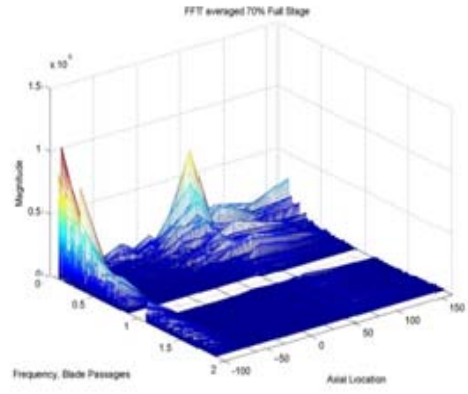
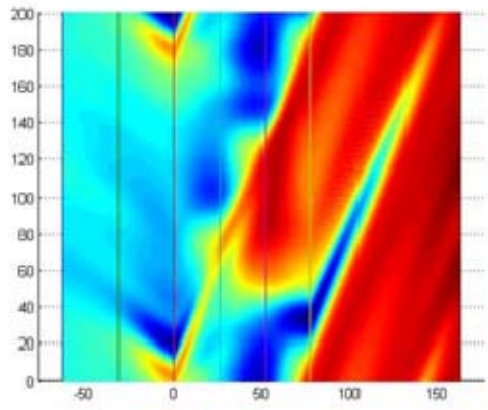
G



H

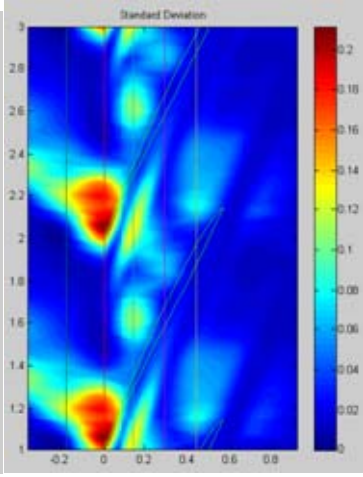
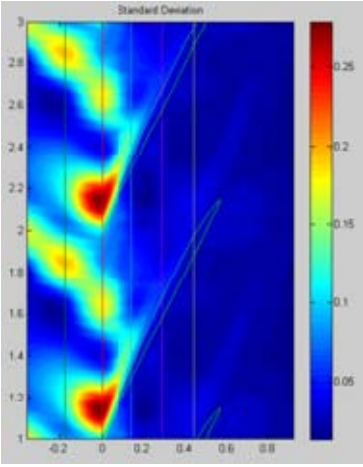


I

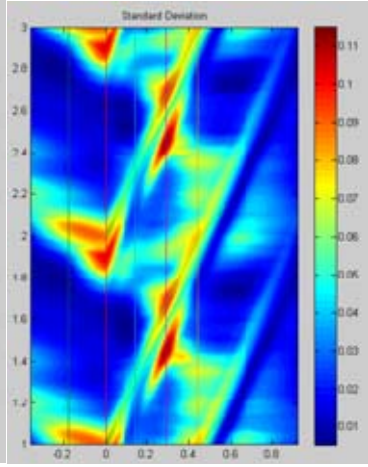


**Standard Deviation Plots
100% Rated Speed
Peak Efficiency**

Near Stall

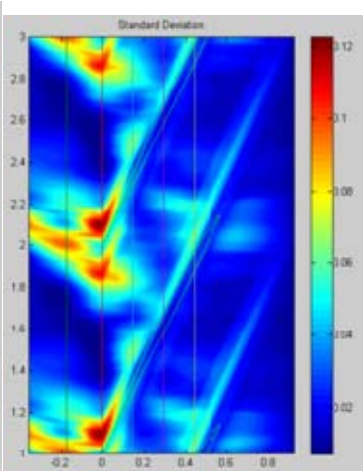
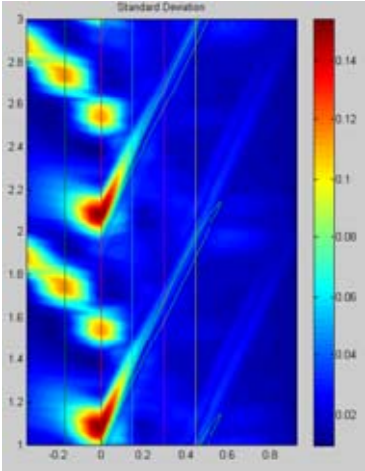


Choked

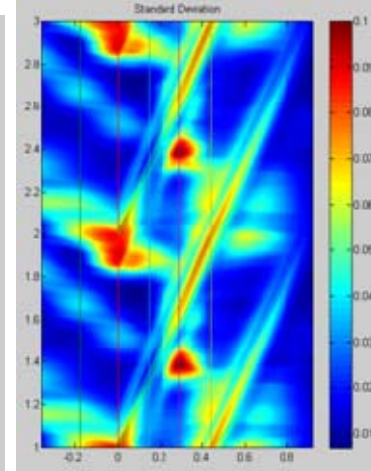


**95% Rated Speed
Peak Efficiency**

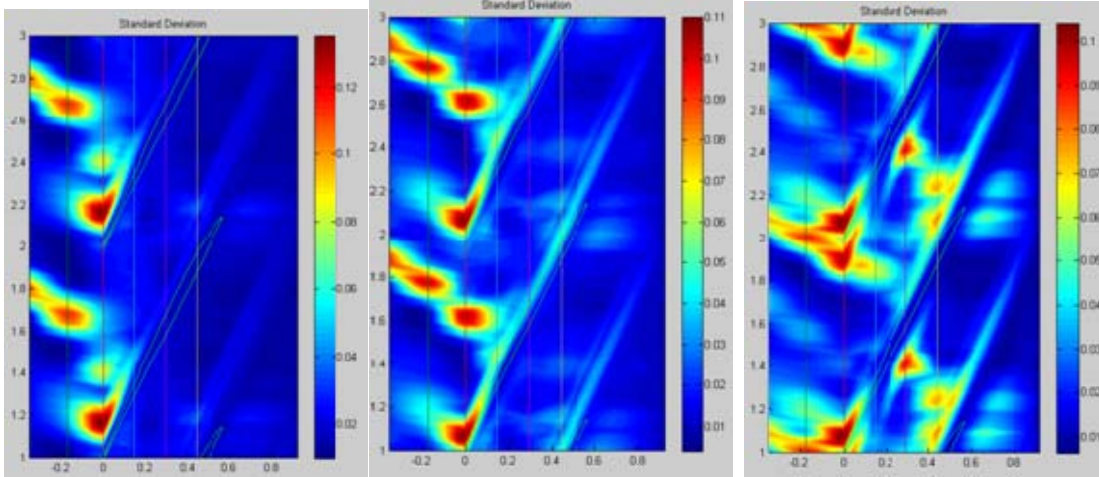
Near Stall



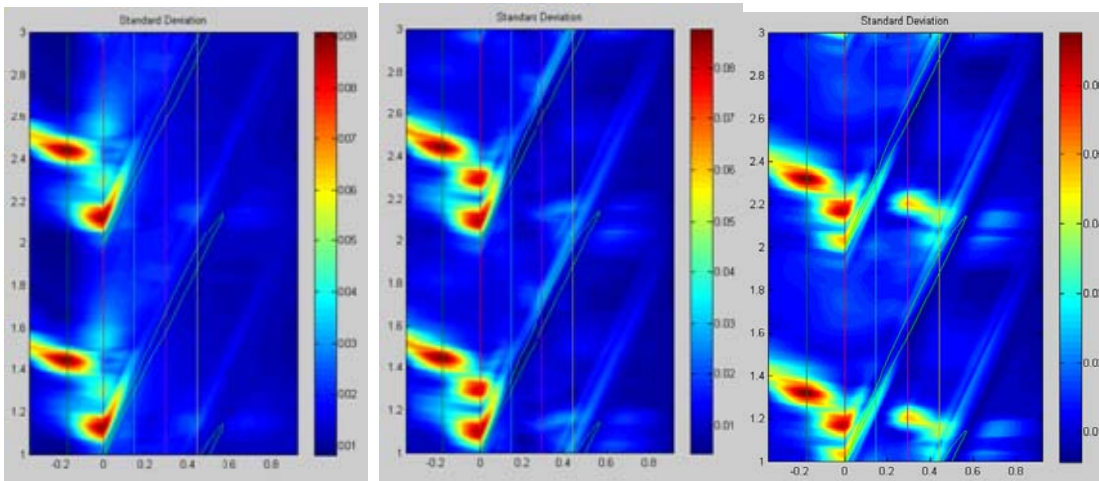
Choked



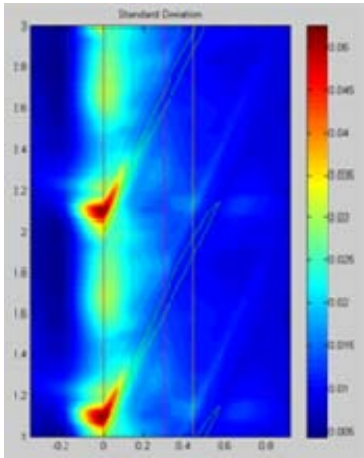
Near Stall **90% Rated Speed** **Choked**
Peak Efficiency



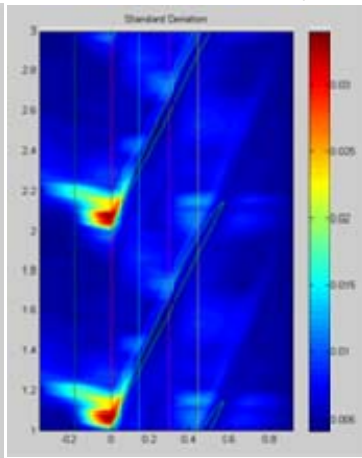
Near Stall **80% Rated Speed** **Choked**
Peak Efficiency



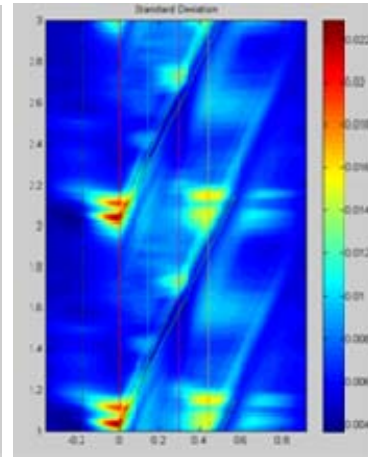
Near Stall



**70% Rated Speed
Peak Efficiency**



Choked



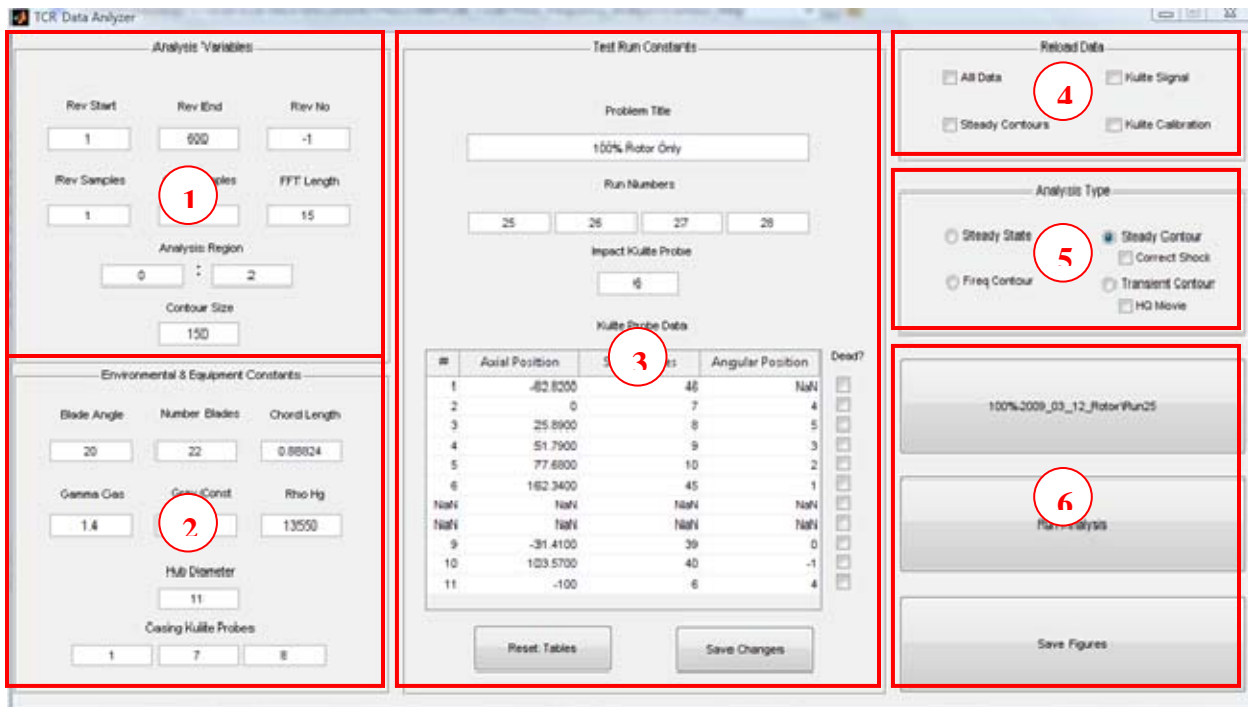
THIS PAGE INTENTIONALLY LEFT BLANK

APPENDIX C: MATLAB INTERFACE

To better integrate the analysis routines used in this research a MATLAB GUI was developed using the Guide GUI Builder so that new datasets could be quickly initialized and analyzed.

Overview of GUI Components

As shown below the TCR Data Analyzer GUI is separated into 6 sub windows. These sections control specific analysis variables (Window 1), Environmental and Equipment Constants (Window 2), Test Run Constants (Window 3), Subroutine Controls and Selectors (Windows 4 & 5), and analysis initiation and interface controls (Window 6). Each of these sections will be described below in the context of a full analysis cycle.

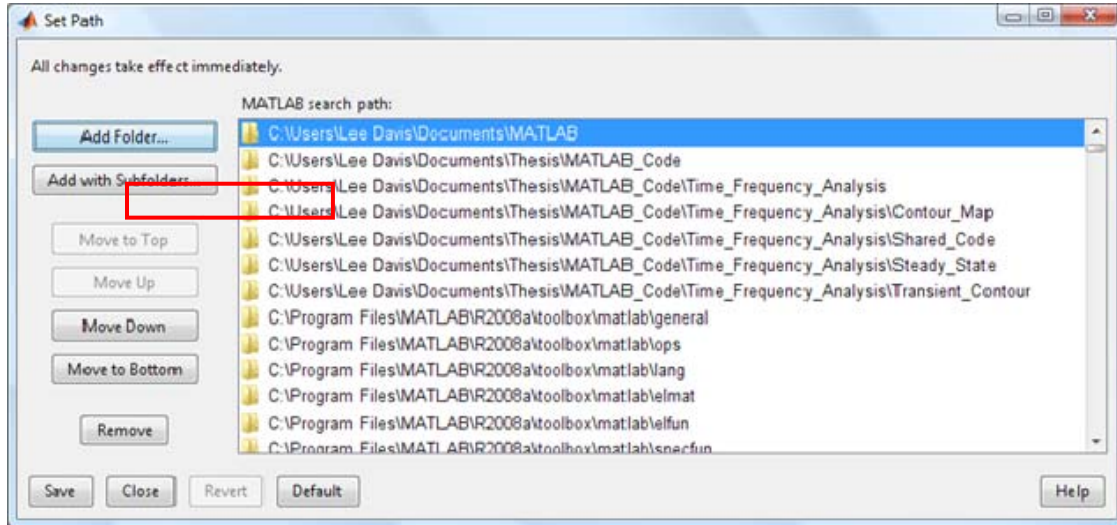


Setting up MATLAB Interface

To setup your specific MATLAB working environment to use the TCR Data Analyzer GUI you must first copy the m-files and GUI fig file to the directory of your choice and then add these directories to MATLABs path list.

To do this you should complete the following tasks:

1. Navigate to the **Set Path** Menu item under the **File** Menu.
2. In the new window you must choose to **Add with Subfolders...**



3. Navigate to the **directory** that you copied the GUI files to and select **OK**.
4. **Save** the changes and **Close** the Set Path window.
5. Start the program by typing **TCR_Data_Analyzer** in the MATLAB Command Window.

Initializing a Dataset

Prior to initiating a data analysis routine the GUI must first be given the test run specific parameters such as Run Numbers, Kulite Placement, and Test Run Title. This is accomplished through the use of the Test Run Constants window, below.

To use this interface you must first use the Select Data Set Directory Button from Window 6 and navigate to the directory where the Test Run CSV files are located.

A description of the input parameters is included below:

Test Run Constants

Problem Title

95% Rotor Only

Run Numbers

1 2 3 4

Impact Kulite Probe

6

Kulite Probe Data

#	Axial Position	Static Probes	Angular Position	Dead?
1	-62.8200	46	NaN	<input type="checkbox"/>
2	0	7	4	<input type="checkbox"/>
3	25.8900	8	5	<input type="checkbox"/>
4	51.7900	9	3	<input type="checkbox"/>
5	77.6800	10	2	<input type="checkbox"/>
6	162.3400	45	1	<input type="checkbox"/>
7	-62.8200	46	NaN	<input type="checkbox"/>
8	-62.8200	46	NaN	<input type="checkbox"/>
9	-31.4100	39	0	<input type="checkbox"/>
10	103.5700	40	-1	<input type="checkbox"/>
11	-100	6	4	<input type="checkbox"/>

Reset Tables Save Changes

- Problem Title – This is a matter of convenience. Usually a title includes the rotor speed and configuration although notes regarding peak efficiency or throttle setting may also be included.

An example Title for a 100% speed run in the Rotor only configuration might be “95% Rotor Only.”

- Run Numbers – These values come from the sequence of the test run and usually consist of four numbers although some early runs had three. The exact run numbers can be located in a text file in the root of the test run that is named after the date of the testing.
- Impact Kulite Probe – This value is always “6.” The ability to choose a different Channel Number is to allow easier upgrade of equipment in future testing.
- Kulite Probe Data – This table contains details regarding the number of Kulites (For plotting purposes) the axial and radial location of the Kulite Probes and identifies the Static Pressure probe that should be used for calibration. Default values for this window are automatically populated although changes can be made as needed to accommodate changes in sensors for a particular series of test runs. This window contains the functionality to tell MATLAB what channels are being recorded and if any of the recorded channels should be excluded from the analysis. As shown below, a sample test run is recording channels 1 thru 6 and 10 to 11. This window also shows that Channel 10 is a dead channel and should be excluded from the analysis.

#	Axial Position	Static Probes	Angular Position	Dead?
1	-62.8200	46	NaN	<input type="checkbox"/>
2	0	7	4	<input type="checkbox"/>
3	25.8900	8	5	<input type="checkbox"/>
4	51.7900	9	3	<input type="checkbox"/>
5	77.6800	10	2	<input type="checkbox"/>
6	162.3400	45	1	<input type="checkbox"/>
7	NaN	NaN	NaN	<input type="checkbox"/>
8	NaN	NaN	NaN	<input type="checkbox"/>
9	-31.4100	39	0	<input type="checkbox"/>
10	103.5700	40	-1	<input checked="" type="checkbox"/>
11	-100	6	4	<input type="checkbox"/>

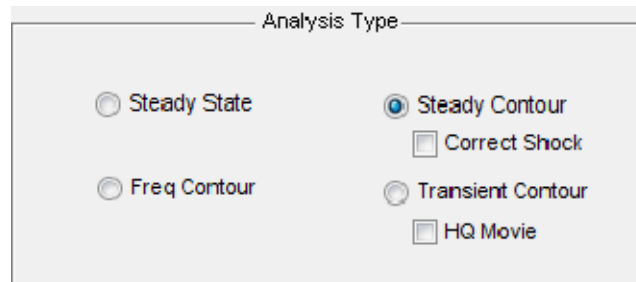
- If mistakes are made in entering the data the tables can be reset using the **Reset Tables** Button located at the bottom corner of the window.

- Once all changes have been made you should then **Save** the changes to the dataset directory. While saving changes in not strictly required to run the GUI it allows MATLAB to call up this file and read in the values directly if further analysis is required on a particular dataset.

Data Analysis

A steady state analysis consists of Frequency and time domain analysis of the Kulite and Hotwire signals. To initiate a steady state analysis the following procedure should be used:

1. The dataset should be initialized using the initialization procedure described above.
2. Select the Analysis from the Analysis Type Window.



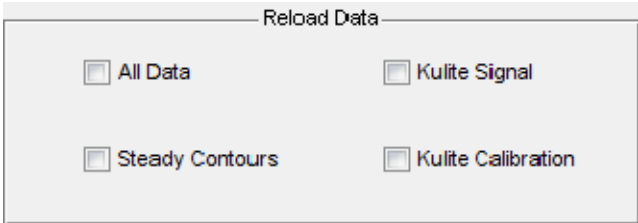
There are 4 primary analysis methods available and two analysis modifiers that only operate on their parent analysis. These 4 modes are:

- **Steady State** – Includes a series of time and frequency analysis that include output plots of pressure, inlet bulk properties, and water fall plots of Kulite Signal FFTs.
- **Steady Contour** – Produces a time averaged plot of a single passage. Can be modified with the Correct Shock switch in the event that the shock angle is not calculated properly.
- **Transient Contour** – Produces a pressure contour plot over an entire rotation, or series of rotations, similar to above but without the time averaging. Also

produces a movie of the pressure contour over time. Can be modified with the HQ Movie switch to ensure video is saved without compression (Useful for presentation purposes).

- Frequency Contour – Provides a time-averaged plot similar to the Steady Contour options but also includes the standard deviation and frequency response of each data point.

3. Select the data types to be reevaluated.



The image shows a dialog box titled "Reload Data". It contains four checkboxes arranged in a 2x2 grid:

<input type="checkbox"/> All Data	<input type="checkbox"/> Kulite Signal
<input type="checkbox"/> Steady Contours	<input type="checkbox"/> Kulite Calibration

- This is an optional choice in the event that data needs to be reloaded or recalibrated. Usually only necessary if changes in the code is changed or bad Kulites are discovered and need to be eliminated from the analysis.

4. Modify any of the variables in the Analysis Variables window as needed. The shown values are the default and usually don't require adjustment.

Analysis Variables

Rev Start	Rev End	Rev No
<input type="text" value="-1"/>	<input type="text" value="-1"/>	<input type="text" value="-1"/>
Rev Samples	Over Samples	FFT Length
<input type="text" value="1"/>	<input type="text" value="1"/>	<input type="text" value="15"/>
Analysis Region		
<input type="text" value="0"/>	:	<input type="text" value="2"/>
Contour Size		
<input type="text" value="150"/>		

- Rev Start and Rev End – Allows a targeted analysis of a specific segment of the sample. For analysis of data sets that don't include stall run out test this should be left alone. The range of revolution should be approximately 1000 for best results.
 - FFT Length – related to the resolution of the frequency analysis plots.
 - Analysis Region – Specifies beginning and end integer locations for signal filtering and waterfall plot range.
 - Contour Size – Specifies interpolation size for all pressure contour plots.
5. Adjust any equipment or environmental variables as needed. These are self-explanatory and should not require any adjustment unless there are geometry changes to equipment.

Environmental & Equipment Constants

Blade Angle	Number Blades	Chord_Length
<input type="text" value="20"/>	<input type="text" value="22"/>	<input type="text" value="0.88824"/>
Gamma Gas	Grav Const	Rho Hg
<input type="text" value="1.4"/>	<input type="text" value="9.81"/>	<input type="text" value="13550"/>
Hub Diameter		
<input type="text" value="11"/>		
Casing Kulite Probes		
<input type="text" value="1"/>	<input type="text" value="7"/>	<input type="text" value="8"/>

6. Initiate Analysis by pressing the **Run Analysis** Button.
7. If desired all the generated figures can be saved to a directory of your choice by selecting the **Save Figures** button.

INITIAL DISTRIBUTION LIST

1. Defense Technical Information Center
Ft. Belvoir, Virginia
2. Dudley Knox Library
Naval Postgraduate School
Monterey, California
3. Professor and Chairman Knox T. Millsaps
Department of Mechanical and Aeronautical Engineering
Naval Postgraduate School
Monterey, California
4. Professor Anthony Gannon
Department of Mechanical and Aeronautical Engineering
Naval Postgraduate School
Monterey, California
5. Professor Garth Hobson
Department of Mechanical and Aeronautical Engineering
Naval Postgraduate School
Monterey, California
6. LT William Davis
Monterey, California